Centre for Geo-Information
Thesis Report GIRS-2006-27

RETRIEVING LEAF AREA INDEX OF A MATURE NORWAY SPRUCE FOREST STAND FROM AIRBORE HYPERSPECTRAL IMAGE BY INVERSION OF THE DART MODEL

Abebe Mohammed Ali

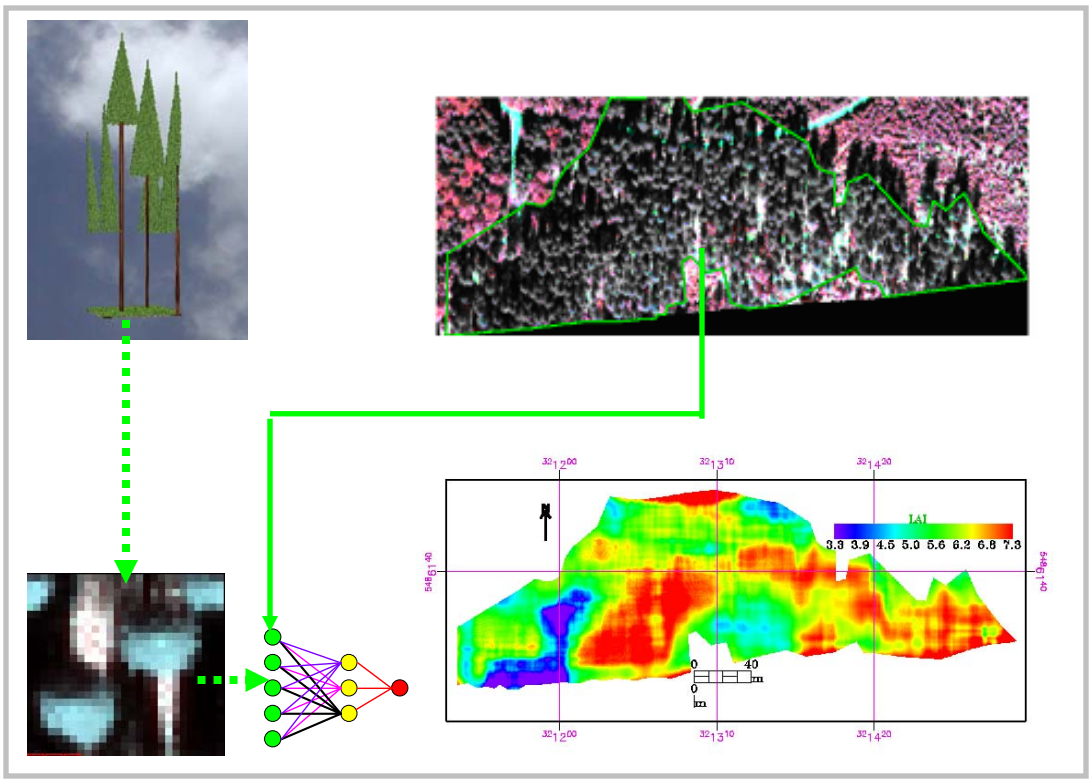

May/ 2006

WAGENINGEN UNIVERSITY
WAGENINGEN UR

Retrieving Leaf Area Index of a Mature Norway Spruce Forest Stand from Airborne Hyperspectral Image by Inversion of the DART Model

By
Abebe Mohammed Ali

Registration number: 73 02 23 011 050

Supervisors:
Zbyněk Malenovský
Prof. Dr. Michael Schaepman

Thesis submitted in partial fulfillment of the degree of Master of Science in Geo-Information Science at Wageningen University and Research Centre, The Netherlands

May, 2006
Wageningen, The Netherlands

Thesis code number: GRS-80436
Wageningen University and Research Centre
Laboratory of Geo-Information Science and Remote Sensing
Thesis Report: GIRS-2006-27

Abstract

Leaf Area Index (LAI) is a key canopy descriptor that is used to determine foliage cover, and predict photosynthesis and evapotranspiration and is an input to many ecological models. Its estimation from remote sensing data has been the focus of many investigations in recent years. In this context, we have used a three dimensional Discrate Anisotropic Radiative Transfer (DART) model to invert LAI of a mature Norway spruce forest stand from Airborne Imagining Spectroradiometer (AISA) image data. The AISA image was acquired on September 18th 2004 while the Ground truth LAI measurements and DART input parameters were collected in September 2004 and 2005 in a study area at Bily Kriz near Beskydy Mountains in Czech Republic. The DART model has been run to simulate the BRF of the forest stand under different canopy closures, which was used to build Look-up table. An Artificial Neural Network (ANN) was trained with the look-up table and employed to retrieve the LAI of the forest stand from the hyperspectral image. The retrieved LAI was validated against the ground truth LAI estimated by combination of the Hemispherical photography (HP) and TRAC (Tracing Radiation and Architecture Canopies) optical instruments.

The inversion of the model showed that the mean LAI of the stand is 5.62 with RMSE of 1.84. Overestimation in lower LAI values and underestimation at high LAI values were generally observed most probably due to the influence of scene size, crown shape, Understory, saturation, limited sample size and error in ground truth LAI measurements. This indicates a need for improvements in the parameterization of the model and selection of model out puts to be used for inversion. The addition of noise to the look up table as prior information improved the RMSE of the estimate. Evaluation of predictions revealed certain level of agreement with ground based LAI estimation (r^2 = 0.44 and 0.54 for ANN trained with and with out noise respectively): The ground based LAI estimation by combination of hemispherical photography and TRAC optical instruments reduced the gap fraction saturation problem and enabled better estimation.

Keywords: LAI; DART; ANN; AISA; Norway spruce

Acknowledgement

This thesis work would not have been done without the technical support and guidance of my supervisor Zbyněk Malenovský. I would like to thank him for his day to day guidance and provision of all the data used in this study. I am very grateful to Lucie Homolová from Academy of Sciences of the Czech Republic for her contribution in collecting the data and preparing the DART input parameters. I would also like to thank Prof. Dr. Michael Schaepman and Willy Ten Haaf from the department of GIS at Wageningen University for their useful advice.

I am indebted to the Netherlands organization for international cooperation in higher education (nuffic) for providing me a financial support to pursue my MSc study. Also my special thanks go to my family in Ethiopia for their motivation and encouragement during my stay here in wageningen.

Thanks are conveyed to my friends particularly Demeke Nigussie, Ernesto Bastidas Obando and Alemu Gonsamo who encouraged me and gave me friendly advices.

Table of Contents

List of Figures

Figure page

LIST OF TABLES

Table page

Acronyms

AISA	Airborne Imagining Spectroradiometer
ACRIM	Active Cavity Radiometer Irradiance Monitor
ANN	Artificial Neural Networks
ASTER	Advanced Spaceborne Thermal Emission and Reflection Radiometer
AVHRR	Advanced Very High Resolution Radiometer
AVIRIS	Airborne Visible/Infrared Imaging Spectrometer
b	bias
BRDF	Bidirectional Reflectance Distribution Function
BRF	Bidirectional Reflectance Factor
c	current age class of needles (first age class)
c+1	needles of one year old (second age class)
c+2	needles of two years old (third age class)
c+3	needles of three years old (fourth age class)
CC	Canopy Closure
CV	Coefficient of Variation
DART	Discrete Anisotropic Radiative Transfer
DBH	Diameter at Breast Height (diameter of tree stem in the height of 1.3m)
DN	Digital Number
FAI	Foliage Area Index
fAPAR	fraction of Absorbed Photosynthetically Active Radiation
FOV	Field Of View
FWHM	Full Width Half Maximum
GA	Genetic Algorithm
GI	Gitelson green Index
GMT	Greenwich Mean Time
HDRF	Hemispherical Directional Reflectance Function
HP	Hemispherical photography
IC	Illuminated Crown
IIR	Imaging Infrared Radiometer
IU	Illuminated Understory
LAD	Leaf Angle Distribution
LAI	Leaf Area Index
LAIe	Effective Leaf Area Index
LIDF	leaf Inclination Distribution Function
LUT	Look-up table
m	Linear line slope
MERIS	MEdium Resolution Imaging Spectrometer
MLH	Maximum Likelihood (classification)
MODIS	Moderate Resolution Imaging Spectroradiometer
MSE	Mean Square Error
NDVI	Normalized Difference Vegetation Index
NIR	Near Infrared
PAI	Plant Area Index

POLDER	POLarization and Directionality of the Earth's Reflectances
PPR	Projection pursuit regression
R	Correlation coefficient
R^2 (r^2)	Coefficient of determination
r	needles older than four years
RMSE	Root Mean Square Error
RT	Radiative Transfer
SAM	Spectral Angle Mapper (classification)
SC	Shaded Crown
SR	simple ratio vegetation index
Std	Standard deviation
SU	Shaded Understory
SVI	Spectral Vegetation Indices
TIS	Total Sky Imager
TRAC	Tracing Radiation and Architecture Canopies
trainbr	Automated Regularization
trainlm	Training by Levenberg-Marquardit algorithm
trainrp	Training by Resilient Backpropagation algorithm
trainscg	Training by Scaled Conjugate Gradient algorithm
U_f	leaf volume density [m^2/m^3]
UTM	Universal Transverse Mercator
VAI	Vegetation Area Index
VI	Vegetation Index
VIS	Visible Bands
W	Foliage element size
WDVI	Weighted Difference Vegetation Index
α	Ratio of woody area index to plant area index
Ω	Total clumping Index
Ω_E	Clumping index larger than foliage size
Y_E	Needle to shoot ratio

1. Introduction and research objective

1.1. Background

Surface area of foliage is a useful measure which can be expressed as a quantity (e.g., m^2 or ft^2) or as a ratio of leaf area to crown projection area or stand area, commonly referred to as Leaf Area Index (LAI). LAI is defined as half the total leaves surface area per unit of horizontal ground area (Chen and Black 1991). For conifer needles with four sides, this definition includes two sides (Chen *et al.* 2002). For most applications the LAI refers to the green photosynthetic parts of plants (Weiss *et al.* 2004).

LAI is a critical variable in monitoring and modeling forest condition and growth and is therefore important for foresters and environmental scientists to measure routinely and accurately, principally because of the importance of LAI to a number of ecological processes such as photosynthesis, transpiration, evapotranspiration and net primary production (Pierce *et al.* 1990). Measurements of *LAI* have been used to predict future growth and can be indicative of canopy structure responses to competition, disease, climate change and factors present on a site, including soil water status, nutrition and temperature (Battaglia *et al.* 1998). Leaf area index has also become a critical input or predicted variable in many ecosystem models that simulate carbon and hydrological cycles (Gower *et al.* 1999). Under certain assumptions, knowledge of canopy structure variables (LAI and leaf Inclination Distribution Function (LIDF)) allows the evaluation of the fraction of Absorbed Photosynthetically Active Radiation (fAPAR), which is required to model the canopy's photosynthetic activity in a straightforward way (Coops et al. 2004). *LAI is* therefore a valuable tool in forest management which is a variable that can be readily measured, often with widely varying levels of accuracy, using a variety of methods.

Methods of LAI estimation ranges from direct to more complex indirect methods. Direct techniques for estimating LAI include the point quadrate method, the stratified-clip method, the dispersed individual plant method and the litter fall collection method. All direct methods are similar in that they are difficult, extremely labor intensive, require many replicates to account for spatial variability in the canopy and are therefore costly in terms of time and money (Chason *et al.* 1991).

Accordingly, many indirect optical methods of measuring LAI that relate total leaf area to the radiation environment below the canopy have been developed. These techniques based on gap-fraction analysis assume that leaf area can be calculated from the canopy transmittance (Chason *et al.* 1991). In this approach Estimation of LAI is through the ground-based measurements of total, direct or diffuse radiation transmitted to the forest floor. A study by Chen (1996) publicized that optical methods can provide even more reliable LAI estimates than destructive sampling techniques if foliage elements are randomly distributed.

Remote sensing is the other powerful technique for describing and understanding Earth ecosystem functioning. The diverse information from Remote sensing allows for detailed and frequent observations of the vegetation to monitor the spatial and temporal variations of canopy characteristics (Koetz *et al.* 2005)**.** Various new satellite data are becoming available, which bring a new era of LAI mapping. It provides a unique way to obtain LAI over large areas (Chen and

Cihlar 1996). However, the results from these procedures vary by scale of observation, type of vegetation, spectral bands used, and the sophistication of the models, image calibration and atmospheric correction (walthall *et al.* 2004).

Numerous studies have been done to estimate LAI from satellite and air born sensor measurements through: 1) statistical methods 2) physical model inversion or 3) hybrid algorithm (Weiss and Baret 1999; Liang 2004). The major constraints of the statistical methods are they require ground measurements and limited validity inversion procedures designed with only single acquisition configuration (Gascon *et al.* 2004). They are suffering from severe limitations due to the lack of physics introduce in the retrieval technique and the small amount of radiometric information they can exploit (Weiss 2000). The physical model inversion methods and hybrid algorithms are potentially a more effective and accurate methods than the use of empirical relationships. Because, they can use complex reflectance models, do not need to decrease the number of input parameters used to characterize earth surfaces, and do not require initial guesses to model parameters (Gastellu-Etchegorry et al. 2003). These approaches are more suitable to exploit richer data provided by the new generation of sensors such as Airborne Imagining Spectroradiometer (AISA) eagle, Polarization and Directionality of the Earth's Reflectances (POLDER), Medium Resolution Imaging Spectrometer (MERIS) and Moderate Resolution Imaging Spectroradiometer (MODIS) (Weiss 2000). The retrieval of LAI by these methods is based on information taken using various types of Radiative Transfer (RT) models. The models relate the fundamental surface parameters (e.g., LAI and leaf optical properties) to scene reflectance for a given sun-surface sensor geometry and an appropriate LUT is Created for the use of inversion algorithms to retrieve surface biophysical parameters.

LAI estimations in coniferous forests like Norway spruce (Picea abies (L.) Karst.), which is one of the most important tree species in Europe and the focus of this study, needs a robust retrieval method. This is because needles are clumped together and violate the rule of leaf random distribution assumption in in-situ LAI estimation methods (Chen 1996). Also retrieval from remotely sensed data for such forests needs a thorough investigation of the relationship between reflectance and LAI as the clumped structure of conifers causes the relationships between LAI with absorbed, transmitted, and reflected solar radiation to behave differently in coniferous forests than in broadleaved forests (Smolander 2001).

Since RT models are mostly oriented towards their use with relatively high-resolution satellite images (Nilson *et al.* 2003), they are more appropriate to create quantitative relations between remotely sensed data and various forest variables. Particularly, the Discrete Anisotropic Radiative Transfer (DART) model is designed to simulate radiative transfer in heterogeneous 3D landscape scenes to address the entire Radiative transfer problem and could be the most suitable model for retrieval of LAI from the AISA hyspectral image data of the mature Norway spruce forest stand.

1.2. Research objective

General objective is to:

to retrieve LAI from high spatial resolution AISA Eagle airborne hyperspectral image of mature Norway spruce forest by inverting complex canopy radiative transfer simulation of the DART model using Artificial Neural Network (ANN). And evaluate the result with Ground truth LAI estimated by combination of Hemispherical Photography (HP) and Tracing Radiation and Architecture Canopies (TRAC) optical instruments.

Specific objective is to:

- ♠ Analyze and compare the ground truth LAI of the mature Norway spruce stand from HP and TRAC measurements
- ♠ Combine ground-based LAI determination methods for more accurate estimation of LAI
- ♠ Simulating the AISA Eagle image data of the stand by DART model
- ♠ Design ANN architecture for retrieving LAI of the mature Norway spruce stand from the DART model bidirectional reflectance and AISA Eagle hyperspectral image data.

Hypothesis:

- ♠ The LAI of the mature Norway spruce stand can be accurately estimated by inverting radiative transfer model simulating the AISA Eagle airborne hyperspectral image data.
- ♠ Combination of the HP and TRAC optical instruments measurement improves the ground based LAI estimation

Research questions:

1/ How reliable are values of LAI retrieved from the AISA Eagle airborne hyperspectral images using radiative transfer modeling?
2/ How significant is the difference of the leaf area index values from ground based measurements and AISA Eagle airborne hyperspectral image?
3/ What is the suitable ANN structure and training algorithm for LAI retrieval of the study area?

1.3. Thesis overview

We began the report by introducing the definition of the topic, the importance of leaf area index as a key biophysical parameter and problem statement in the first chapter. The objectives of this study and research questions are also covered in this chapter. This is followed in chapter two by review of the relevant studies conducted in the field of biophysical variables estimation. The third chapter describes the methodologies implemented in order to achieve the research objectives. The results of this study are presented and discussed in chapter four. Finally, in the fifth chapter we quickly look at conclusion and recommendations made about the study.

2. Literature review

2.1. Conifers canopy and LAI retrieval

The LAI of vegetation depends on species composition, developmental stage, prevailing site conditions, seasonality, and the management practices. LAI is a dynamic parameter: it changes from day to day (mostly in spring and autumn), and, driven by forest dynamics, from year to year (Welles and Norman 1991).

Studies in coniferous forest plantations showed the ranges in LAI are usually lower and relationships between LAI and vegetation indices (VI) may be disturbed as other biophysical stand characteristics (such as stem density, canopy closure, tree height, etc.) influence the reflectance signal (Treitz and Howarth 1999). Since conifer canopies are highly clumped, they do not cover as much ground surface as agricultural crops and grasses with the same LAI (Chen and Cihlar 1996). Hence, unlike broad leave forests for calculating LAI in conifer stands (Chen et al. 2002), needles should be grouped first in to shoots, which are often dense and allow little penetration by light. Shoots of conifer needles are therefore treated as foliage elements and a correction for this leaf grouping effect is made using the needle-to-shoot area ratio. For broad leaf stands, individual leaves are considered as the element, and no such correction is necessary.

Conifer needles often do not conform to a uniform and flat projection, as do some type of deciduous leaves (Mesarch *et al.* 1999). Conifer needles exhibit a species-specific cross-sectional shape, with thickness varying across the needle's width, as well as a characteristic three-dimensional shape (Brand 1987). Additionally, the widths and lengths of needles of many species and other canopy elements (such as twigs and some grass species) are relatively small, requiring the inclusion of multiple samples to provide adequate material for measurements. In the course of compositing a single layer of needles or other slender canopy elements, inter-needle gaps are unavoidable, producing a variable gap fraction per sample (Mesarch *et al.* 1999).

When LAI is retrieved from remote sensing data, consideration must be given also to the canopy shape. The three-dimensional structure of a coniferous shoot gives rise to multiple scattering of light between the needles of the shoot, causing the shoot spectral reflectance to differ from that of a flat leaf (Smolandera and Stenbergb 2003), At higher values of LAI, stands with conical crowns have much smaller reflectance than ellipsoidal crowns where larger crown volume is seen to result in higher single scattering from crowns (Rautiainena *et al.* 2004). For estimating canopy-related variables, this means that understanding the role of crown shape in forming the components of the stand Hemispherical Directional Reflectance Function (HDRF) is crucial. The openness of the overstory and spatial and temporal variations of the Understory vegetation pose special challenges to the extraction of LAI and other biophysical parameters of the overstory canopies from remotely sensed data (Hu *et al.* 2000).

2.2. Methods of LAI estimation

2.2.1. Ground based LAI estimation methods

Direct methods

LAI can be assessed directly by using harvesting methods such as destructive sampling and the model tree method or by non-harvesting litter traps during autumn leaf-fall period in deciduous forests. In these methods after leaf collection, leaf area can be calculated by means of either by correlating the individual leaf area and the number of area units covered by that leaf in a horizontal plane or by correlating dry weight of leaves and leaf area using predetermined green-leaf area to-dry-weight ratios (Jonckheere 2004).These direct Leaf sampling methods are extremely labor intensive and require many replicates to reduce sampling errors (Chason *et al.* 1991).

Jonckheere (2004) reviewed that since the leaf area is determined through repeated area measurements on single leaves and area accumulation, these methods are hence considered the most accurate, but they have the disadvantage of being extremely time-consuming and as a consequence making large-scale implementation only marginally feasible. However, the need for validation of indirect methods remains, so the direct techniques can be considered important as calibration methods.

Ground based indirect methods of LAI estimation

Indirect methods, in which leaf area is inferred from observations of another variable, are generally faster, amendable to automation, and thereby allow for a larger spatial sample to be obtained (Jonckheere *et al.* 2005). For reasons of convenience when compared to the direct methods, they are becoming more and more important. Indirect methods of estimating LAI in situ can be divided in two categories: (1) indirect contact LAI measurements; and (2) indirect non-contact measurements.

1). Indirect contact LAI measurement

This method includes:

- **inclined point quadrate**: consists of piercing a vegetation canopy with a long thin needle (point quadrate) under known elevation (i.e. the angle between the needle and the horizontal plane when vertically projected) and azimuth angles (i.e. the bearing of the needle from north when horizontally projected) and counting the number of hits or contacts of the point quadrate with "green" canopy elements. LAI is then determined using equations based on radiation penetration model. This method is impractical in forest stands because of the tall structure of trees and the high density of conifer leaves (Chen *et al.* 1997).
- **Allometric techniques for forests:** rely on relationships between leaf areas as such and any dimension(s) of the woody plant element carrying the green leaf biomass, i.e. stem diameter, tree height, crown base height etc. Allometric relationships between a dependent variable such as size, shape or area and an independent variable, is commonly used as a tool to directly estimate the area of tree parts. The leaf area determined via destructive sampling and the basal area of the physiologically active sapwood area have been proposed. Such sapwood-to-leaf-area conversions are based on the pipe model theory that stems and branches are considered an assemblage of pipes supporting a given amount of

foliage (for detail see the review by Jonckheere (2004). It has the advantage to quantify stem, branch and foliage areas separately. However, if generalized algorithm is used the method can lead to large errors and it is also affected by abiotic and biotic factors (Chen *et al.* 1997).

2). Indirect non-contact LAI measurement methods

The use of light to probe the canopy from different angles provides useful information on the structure of the canopy, given an adequate model to interpret the data (Chason *et al.* 1991). Optical methods are indirect non-contact methods based on the measurement of light transmission through canopies. They have great potential to obtain quick and low cost measurements over large areas and are more commonly implemented because of their convenience compared with direct methods, especially for forest stands (Chen and Black 1992a).

The general principle behind these optical instruments is in canopies where foliage is randomly distributed, LAI can be derived based on the probability that a beam of direct radiation will pass through a canopy unobstructed (Coops et al. 2004). Measurements of the below-canopy radiation interception then provide data to estimate LAI. The methods can become very complicated when the spatial distribution of foliage elements is not random (Chen and Black 1992b). The success, therefore, of any indirect method to estimate L is related to how accurately the simple model mimics the true canopy architecture (Welles and Cohen 1996).

There are a number of approaches for estimating LAI from gap fraction measurements. They can be divided into two main categories: a first group contains instruments that are based on gap size distribution analysis (TRAC and hemispherical photography) while a second group contains instruments based on gap fraction analysis (Accupar, Demon and Licor LAI-2000 Plant Canopy Analyzer).

A characteristic of the gap fraction-based approach is that it does not distinguish photosynthetically active leaf tissue from other plant elements such as stem, branches or flowers. Alternative terms for leaf area index have therefore been proposed, among them "Vegetation Area Index (VAI)" (Fassnacht *et al.* 1994), "Plant Area Index (PAI)" (Neumann *et al.* 1989), and "Foliage Area Index (FAI)" (Welles and Norman 1991) are the most common. Chen and Black (1992b) used the term "effective LAI (LAIe)" to describe LAI estimates derived optically and we also used this term in this study.

Tracing Radiation and Architecture of Canopies (TRAC)

The TRAC instrument accounts not only for canopy gap fraction but also canopy gap size distribution (the physical dimensions of a gap) (Leblanc 2002). The canopy gap size distribution or clumping index quantifies the effects of non-random spatial distribution of foliage that often occurs in mixed-stands with broad-leaved and conifer species. Using the solar beam as a probe, it records by means of three photosensitive sensors the transmitted direct light at high frequency (Leblanc 2002). The TRAC technology has been used in several LAI estimation studies (Fassnacht *et al.* 1994; Chen and Cihlar 1995; Chen 1996; Chen *et al.* 1997; Kucharik *et al.* 1998; Chen *et al.* 2005).

In this approach LAI is estimated as:

$$LAI = (1- \alpha) LAIe \Omega \quad \text{Eqn. 1}$$

Where α is the ratio of woody area index to plant area index to avoid the effect of non leaf materials. Chen (1996) evaluated α from intensive destructive measurements. Barclay *et al.* (2000) also proposed correcting LAI effective using a "bole area index" directly measured using a map of the stand (position of the stems, diameter, height, etc.). Both of these methods are quite tedious, and one solution could be a classification method applied on digital imagery (Chen *et al.* 1997).

$$LAIe = 2 \int_0^{\Pi/2} \ln\left[\frac{1}{P(\theta)}\right] \cos(\theta) \sin\theta d\theta \quad \text{Eqn. 2}$$

Where $P(\theta)$ is the gap fraction at the view zenith angle and expressed as:

$$P(\theta) = \exp(\left[-G(\theta)\Omega PAIe / \cos(\theta)\right] \quad \text{Eqn. 3}$$

Where G (θ) is the projection coefficient characterizing the foliage angle distribution, It represents the mean projection of a unit leaf area in the direction of the beam and onto a plane normal to the beam. G is a function of both θ and the leaf inclination distribution, but at θ = 57 °, G ≈ 0.5 for any distribution of leaf (Fassnecht *et al.* 1994).

A simple method to correct for the clumping of needles in shoots is derived from the assumption that individual shoots (instead of needles) are randomly distributed in the canopy (Leblanc *et al.* 2002).

$$\Omega = \Omega_E / Y_E \quad \text{Eqn. 4}$$

where Y_E is defined as the needle-to-shoot hemisurface area ratio, which approximates the amount of clumping that occurs within a typical shoot, and has been measured in many other studies for a variety of species (Gower and Norman 1991; Deblonde *et al.* 1994; Fassnacht *et al.* 1994; Chen *et al.* 1997a). Ω_E is measured with the TRAC and includes clumping at scales larger than the average element size; in deciduous forests this is a leaf, and in conifers, shoots are the primary foliage elements.

The TRAC quantifies the clumping effect by measuring the canopy gap size distribution. For deciduous stands the clumping index measured from TRAC includes the clumping effect at all scales, but in conifer stands it only resolves the clumping effect at scales larger than the shoot (Leblanc 2002). The instrument is unable to account for within shoot clumping in conifers because small gaps (less than a few mill meters in some cases) between needles disappear in shadows within the sun fleck gap-size distribution projected onto the ground. Chen *et al.* (1997) have recommended integrating the effective LAI measurement at several zenith angles of LAI-2000 or hemispherical canopy photography with the clumping index (gap size) of the TRAC, to produce a more accurate estimate of LAI that accounts for both gap fraction and gap size distribution.

Hemispherical canopy photography

Hemispherical canopy photography is a technique for studying plant canopies via photographs acquired through a hemispherical (fisheye) lens from beneath the canopy oriented towards zenith or placed above the canopy looking downward. A hemispherical photograph provides a permanent record and is therefore a valuable information source for position, size, density, and distribution of canopy gaps. It is able to capture the species-, site- and age-related differences in canopy

architecture, based on light attenuation and contrast between features within the photo (sky versus canopy). Hemispherical photographs generally provide an extreme angle of view, generally with an 180^0 field of view.

Digital cameras are available now with a very large number of pixels that provides a spatial resolution close to that of classical photographic films (Hale and Edwards 2002). In comparison to analogue cameras, these digital sensors have better radiometric image quality (linear response, greater dynamic range, wider spectral sensitivity range (King *et al.* 1994). One of the main problems of hemispherical photography for determination of LAI is the selection of the optimal brightness threshold in order to distinguish leaf area from sky area thus producing a binary image. A series of software packages for hemispherical images processing have been developed (e.g. Hemiview (Delta-T Device), SCANOPY, GLA, CAN-EYE (Weiss *et al.* 2002) and DHP (Leblanc *et al.* 2005). Previous researches demonstrated that with a high resolution digital camera, the choice of the threshold level would be less critical, because the frequency of mixed pixels is reduced in comparison to the aggregation of pixels in cameras with lower resolution.

Hemispherical photographs provide simple means to correct for clumping at the tree/canopy level for improved LAI estimates (Soudani *et al.* 2002). Gower *et al.* (1999) indicates woody material can comprise from 5% to 35% of the total Plant area in hemispherical photography. However, if leaves or shoots preferentially musk branches, Kucharik *et al.* (1998) suggest that branches may be neglected during the processing of the photographs.

LAI-2000 canopy analyzer

The LAI-2000 captures the light-dark contrast of a canopy against diffusely lit sky to give an estimate of VAI. The fisheye lens and internal optics direct diffuse sky light < 490 nm from a conical region approximately three-and-one-half tree heights in radius to a detector of five concentric silicon rings where data are recorded from regions centered on 7, 23, 38, 53, and 68 degrees zenith (LI-COR 1992). The instrument's microprocessor combines above and below canopy measurements to calculate VAI using the equation

$$\mathrm{VAI} = -2\int_0^{\Pi/2} \ln(T(\theta))\cos\theta\sin\theta d\theta \qquad \text{eqn.5}$$

For the best results, measurements should be made under a uniformly overcast sky (LI-COR 1992); otherwise, the scattered light beneath the canopy is assumed to be additional diffuse light resulting in an underestimate of VAI. Measurements under non-overcast skies have resulted in estimates of VAI as much as 50% lower than the estimates obtained for the same stands but under overcast skies (Welles and Norman 1991).

It has been used with success to estimate LAI in continuous and homogeneous canopies, such as millet and grasslands, validated by direct estimates of LAI based on harvesting (Levy and Jarvis 1999). In discontinuous and heterogeneous canopies, the potential of this instrument is restricted by a general tendency towards underestimating LAI (Chason *et al.* 1991).

2.2.2. LAI estimation methods from remote sensing data

Various new remote sensing data are becoming available, which bring a new era of LAI mapping (Fang *et al.* 2003). It provides a unique way to obtain LAI over large areas (Chen and Cihlar

1996). Although LAI can be directly or indirectly measured by several methods its spatial and temporal distribution is usually investigated using remotely sensed data and the results from these procedures vary by scale of observation, type of vegetation, spectral bands used, and the sophistication of the models. Image calibration and atmospheric correction can also affect results (Colombo *et al.* 2003). Remote sensing data involved in the inversion are critical to the accuracy of LAI estimates. There are a variety of cases that can affect the collection of target spectral reflectance data, such as the reflectance characteristics of background and adjacent materials, as well as variations associated with changing solar zenith and azimuth angles, sensor look angle, and atmospheric conditions (Williams 1991). A selection of bands to be used in the inversion process is recommended since highly correlated bands would get artificially more weight and bias the retrieval (Meroni *et al.* 2004).

The spatial resolution of an image also greatly influences the accuracy of the biophysical variable that can be retrieved. For example the relative error between retrieved and ground measured LAI could be reduced on average by 17%, if the image resolution is changed from 20m to 1m (Gascon *et al.* 2004).

Sensors of remote sensing data are divided in to two broad categories (CSC_NOAA 1999):

Active sensors: provide their own source of energy to illuminate the objects they observe. An active sensor emits radiation in the direction of the target to be investigated. The sensor then detects and measures the radiation that is reflected or backscattered from the target. RADAR and lidar are the most common sensor types of this kind.

Passive sensors: detect natural energy (radiation) that is emitted or reflected by the object or scene being observed. Reflected sunlight is the most common source of radiation measured by passive sensors. It includes radiometric instruments like:

- single channel (Active Cavity Radiometer Irradiance Monitor (ACRIM) and Total Sky Imager (TIS))
- multispectral (Advanced Spaceborne Thermal Emission and Reflection Radiometer (ASTER), Advanced Very High Resolution Radiometer (AVHRR), Imaging Infrared Radiometer (IIR), MODIS),
- hyperspectral (AISA, Airborne Visible/Infrared Imaging Spectrometer (AVIRIS))
- Polarimetric instruments (POLDER, Polarimetric Scanning Radiometer (PSR)). The focus of this study is on passive remote sensing data. Therefore, the major LAI retrieval methods from passive remote sensing data are briefly discussed as follows.

1. Statistical methods

Among the various Vegetation Indices the ratio-based Normalized Difference Vegetation Index (NDVI) and the simple ratio vegetation index (SR) are the most frequently used to correlate with LAI and other canopy structure parameters from airborne and Spaceborne remote sensing data (Gong *et al.* 2003). These and other ratio-based indices, although important, utilize only a fraction of the spectral information available in many image datasets(Cohen and Justice 1999) and thus may limit the power of predictive relationships. The ordinary least squares regression with the NDVI, the Weighted Difference vegetation Index (WDVI), the Gitelson green index (GI) spectral vegetation indices (SVI) and geostatistical approach that uses ground-based LAI measurements and image-derived kriging parameters to predict LAI are also grouped under this approach. The

VI-based models have various mathematical forms such as linear, power, exponential, etc. (Walthall *et al.* 2004).

Even though Retrieval of LAI using empirical approaches, is simple and easy, they tends to be site-specific, relationships are valid only under conditions similar to those at the time the correlation was established and the relationship may breakdown if the solar and viewing geometries, soil background, chlorophyll concentrations, or moisture conditions are different (Jacquemoud *et al.* 1995). Additionally, in situ calibration measurements of LAI over regional or global scales are impractical (Walthall et al, 2004). The other limitation of these approaches is there is no universal LAI–SVI equation re-applicable to diverse vegetation types; it is difficult to use this approach with large-scale remote-sensing images (Qi *et al.* 2000).The study by Baret and Guyot (1991) showed that identification of the specific crop (or dominant crop) and a priori knowledge of the corresponding set of parameters of the semi empirical models, will significantly improve the accuracy of determination of vegetation characteristics.

2. Physical model inversion methods

An alternative to empirical relationships is a modeling approach based on a set of radiative transfer equations or models. It involves inverting a model. Model inversion is a process in which the model is run in a reverse mode, that is, the inputs to the inversion procedure are the reflectance (*r*) and the output is a set of the parameters. The technique commonly used to invert a model is to adjust the model parameters in such a way that the model-predicted values closely match the measured values. Most commonly used models are bidirectional reflectance (Qi *et al.* 2000). These methods use a model **M** (a functional relation between variables and Bidirectional Reflectance factor (BRF)) to compute some cost function **C** which is expressed as:

$$\mathbf{C} = \sum_{i=1}^{nmeans}\left(\frac{R_i - R_{i,sim}}{R_i}\right)^2 + \sum_{j=1}^{n\,\mathrm{var}}\left(\frac{\alpha_j V_j - V_{j,priori}}{V_{\sup} - V_{\inf}}\right)^2 \qquad \text{Eqn. 6}$$

Optimization inversion method

This approach finds the value of a variable that maximizes or minimizes the objective function while satisfying constraints. Many types of optimization methods are available. The simplex method requires a geometric figure consisting of N + 1 vertex in N dimensions. The method starts with an initial simplex of N + 1 points, which expands and contracts to adapt to the functional surface and attempts to surround the optimum point. This is achieved through a series of geometric transformations where the current worst point is discarded and replaced by a better one. Once one simplex has terminated, the procedure is repeated with a new simplex. The process is repeated until the simplex collapses onto the same solution, which increases the likelihood of finding the global optimum (Kimes *et al.* 2002).

The conjugate direction set method begins from a single initial position and conducts single line minimizations, accurate to within a user defined tolerance, in each of the current N conjugate directions in order to arrive at the minimum for a given iteration (Liang 2004).

This optimization approach has been used in many studies for bidirectional Reflectance Distribution Function (BRDF) inversion and the result showed that LAI is retrieved with fair degree of accuracy (Liang 2004). Kimes et al. (2002) had made a comparison between the simplex

method and neural network method for retrieving LAI from DART model and found that at moderate noise levels, the simplex method was equal to the ANN method in RMSE values where as at high noise levels, the simplex method had significantly lower RMSE values than the ANN method.

In the minimization of nonlinear functions, one of the common problems is that the merit function **F** does not change, even though there is another set of values of the parameters for which **F** takes on a lower value. In other words, the minimization process gets trapped in a local minimum. For such cases, the calculated values of the parameters will depend upon the initial guess and may be quite erroneous if one does not reach a global minimum (Goel and Strebel 1983). Therefore, they may not be appropriate for many operational applications on a per-pixel basis for regional and global data (Kimes *et al.* 2002)

Genetic Algorithm (GA)

The fundamental concept of GA is based on the concept of natural selection in the evolutionary process, which is accomplished by genetic recombination and mutation (Fang *et al.* 2003) . Genetic algorithms have been developed for retrieval of land surface roughness and soil moisture (Jin and Wang 2001). Lin and Sarabandi (1999) used GA as a global search routine to characterize the input parameters (such as tree density, tree height, and trunk diameter and soil moisture) of a forest stand with measured single-polarized data.

The GA optimization method provides an alternative to invert the RT models in remote sensing. The advantage of GA is twofold (Fang et al, 2003). First, it scans all the initial conditions and provides several possible solutions for the detailed examination of the global optimum solution, thus it avoids the inaccuracies introduced by traditional minimization algorithms. Second, it only runs the forward RT model with constrained parameter space and is straightforward in the optimization process. However, in their study of retrieving LAI with a canopy radiative transfer model using all six bands of thematic mapper, GA is likely to overestimate when field LAI>4.

Lookup Table Method (LUT)

The LUT method like other physical approaches solves the inverse problem by searching canopy variables values leading to the closest match between model simulations and radiance measurements. LUT algorithms offer an advantage over other physical models because it is a global search and thus is not sensitive to a local minimum. Further, it is performed on pre-computed data, and the search can easily be parallelized. Similarly to iterative minimization algorithms, the LUT algorithm is based on a cost function that can incorporate prior information. The principle of a LUT consists of generating a table of canopy variables by sampling the space of canopy realization. Then a radiative transfer model is used to generate the corresponding table of reflectance values.

To select the solution of the inverse problem, the LUT is sorted according to a cost function, which is a simple Root Mean Square Error (RMSE):

$$\text{RMSE} = \sqrt{\frac{1}{Nmean}\sum_{i=1}^{nmean}(R_i - R_{i,LUT})}^{2} \qquad \text{Eqn. 7}$$

Where R_i is the BRF measured for the wavelength i and $R_{i,LUT}$ is the BRF simulated. The solution is considered as being the distribution of the set of variables providing the smallest RMSE and can be simply represented by its median value to prevent widely spread solutions (Combal *et al.* 2002).

Gastellu-Etchegorry et al (2003) generalize a look-up table to any view-sun direction with the inversion of a series of SPOT images for determining the LAI and tree cover of a temperate forest. This led to LAI maps that are as accurate as LAI maps that are derived from classical relationships which are calibrated with LAI in situ measurements. If prior information is known as a function of species, LUT would be both a fast and an economic approach to estimate vegetation properties (Combal *et al.* 2003).

3. Hybrid inversion methods

A hybrid inversion algorithm is a combination of extensive simulation using a canopy radiative transfer model (physical) and a non parametric statistical inversion model (Liang 2004). As a result it takes the advantage of both the physical and statistical approaches. They require little a priori information as opposed to LUT method. There are various hybrid inversion algorithms. The most commonly used in the remote sensing field are the neural network and Projection pursuit regression and discussed as follows.

Neural network

In the field of remote sensing, neural networks have been used for classification (and other spatiotemporal relationships), predicting vegetation and soil parameters, and for fast and stable inversions of relatively complex physical models (Kimes *et al.* 1997; Kimes *et al.* 1998). Neural networks are composed of single neurons connected to each other and characterized by a transfer function, and associated weight and bias. Neural networks have the ability to learn patterns or relationships given training data, and to generalize or extract results from the data. They enable to relate a given set of input variables to a set of output variables, irrespective to any known functional relationship between input and output, provided an implicit relationship exists between these sets (Kavzoglu and Mather 2003). Detail review of ANN attributes for extracting vegetation variables from remote sensing data can be found in review article of Kimes *et al.* (1998).

The accuracy of the method depends on the number of layers and nodes, initial parameter values (weight, bias, momentum, etc.), number of training samples, input out put encoding and type of training algorithm as well the measurement and model uncertainties (Kimes *et al.* 1998; Kavzoglu and Mather 2002; Kavzoglu and Mather 2003). From the design perspective, the specification of the number and size of the hidden layer(s) is critical for the networks capability to learn and generalize (Kavzoglu and Mather 2003). The input and output nodes are usually equal to the number of input and out put variables. Consequently, it is the hidden layer nodes that are subject to adjustments in number. There is no universally accepted optimal number of hidden layer nodes for a particular problem. A trial-and-error strategy is frequently employed to determine appropriate values for Significant parameters like the range of the initial weights, the learning rate, the value of the momentum term, and the number of training iterations, all of which relate to the question of when and how to stop the training process (Kavzoglu and Mather 1999).

An appropriate number of training samples is required in order to define the nature of the inversion problem. This number is mainly dependent on the network structure and the level of complexity of the problem. In general, it is not known exactly how ANNs learn particular problems and apply the extracted rules to unseen cases, or how conclusions can be drawn from the trained networks. As a consequence, artificial neural networks are generally called 'black-box' methods (Kavzoglu and Mather 2002).

Combel *et al*. (2002) used a backpropagation neural network together with LUT and Quasi-Newton algorithm for retrieval of biophysical variables from a range of Radiative transfer models. In the case of 3D RT model inversion they found that ANN overpasses the other two methods in accuracy when model uncertainties are taken in to account. Weiss and Baret (1999) used a two layer backpropagation network with a learning rule based on the Levenberg–Marquardt algorithm for Evaluation of canopy biophysical variable retrieval performances from the accumulation of large swath satellite data. They suggested that ANN can accurately estimate biophysical variables if the optimum amount of radiometric information is used.

Gong (1999) employed a semi-linear feed-forward neural network program to invert LAI and leaf area density from a canopy reflectance model. The test results showed that a relative error between 1% and 5% or better was achievable for retrieving one parameter at a time or two parameters simultaneously. Fang *et al.* (2003) retrieve leaf area index using neural network. His result revealed that LAI can be best retrieved by neural network method from Landsat thematic mapper band 3 and 4. A study by Weiss *et al.* (2001) depicted ANN performance is much better than NDVI to estimate LAI from satellite data . The error is two times lower in ANN when compared to NDVI.

Projection Pursuit Regression (PPR)

PPR model approximates high dimensional functions by simpler functions that operate in low dimensional spaces-typically one-dimensional (Fang and Liang 2005). As its name indicates it pursue interesting projections in space and smooth them using simple regression techniques. It has the form:

$$Y = \alpha + \sum_{j=1}^{M} W_j \alpha^T X \qquad \text{Eqn. 8}$$

Where X and Y are the independent and dependent variables respectively and α is the transformation vector. The dimension (or term) M is to be chosen by the user, which depends on the number of variables and the training data. Wj is the weights for different terms. Eqn.8 uses an additive model on predictor variables, which are formed by projecting X in M carefully chosen directions. The results of PPR are not sensitive when the dimension 'M' is set between 15 and 25 (Liang 2004).

Fang and Liang (2005) used the PPR and ANN to estimate LAI from MODIS data and the result showed that both methods produce similar LAI results. This is because of their similar statistical mechanism. Li *et al.* (2005) compared PPR model with traditional multivariate linear statistical methods and found PPR much more accurate in estimating grassland yields.

2.3. Radiative transfer models

Reflectance modeling is a necessary component of scientific investigation that establishes diagnostic links between investigative conjecture and spectral data collected in the laboratory and field or through remote sensing (Ganapol *et al.* 1999). RT models serve as a basis for extracting vegetation variables using directional/spectral data from modern-borne sensors. The retrieval of LAI through inversion methods is based on information taken from remotely sensed data using RT models. Physically based models range in complexity from simple nonlinear models to complex numerical RT models in realistic three-dimensional (3D) vegetation canopies (Kimes et al. 2002)

Simple homogeneous targets may require only one-dimensional models for an accurate description of their radiation field, while more complex heterogeneous targets require complex three dimensional models (Meroni *et al.* 2004). The PROSPECT (Jacquemoud and Baret 1990) model simulating the leaf optical properties, KUUSK (Kuusk 1995) , IAPI (Iaquinta *et al.* 1997), and NADI (Gobron *et al.* 1997) canopy reflectance models are some of the 1D models. Whereas the DART (Gastellu-Etchegorry et al., 1996) and the K-K (Kimes and Kirchner 1982) models are among 3D radiative transfer models which, offers advanced functions to adjust structural parameters of heterogeneous forest stands.

To estimate the canopy reflectance using RT models, three important variables must be carefully formulated: the architecture of the canopy, the optical properties of foliage elements, and the background surface reflectance properties (Tian *et al.* 2002). A major limitation of one dimensional models is that they do not account for some canopy architecture variables such as tree crown closure, tree density, tree height, shape and dimension of crowns, which may imply wrong estimation of forest fAPAR and BRF (Gastellu-Etchegorry *et al.* 1999). The K-K model provide an interesting means for taking into account the architecture of covers with some series drawbacks due to simplifying assumptions (Myneni 1991).

In RT models the fundamental quantity that characterizes the reflectance property of a surface is BRDF, defined as the ratio of the radiance scattered by a surface into a specified direction to the unidirectional irradiance incident on a surface (Di Girolamo 2003).

Each RT model has its own advantage and disadvantage. Parameters used greatly vary depending on the dimension of the model. Details about the capability, performance and agreement of the latest generation of RT models which could lead to model enhancements and further developments can be found in (RAMI 2005). Here we briefly reviewed the main findings about the RT model used in this study only.

The Discrete Anisotropic Radiative Transfer (DART) model

The DART model offers advanced functions to adjust structural parameters of the forest stands such as horizontal and vertical distribution of the leaves density, zones of total defoliation, and distribution of woody parts. The model was designed to simulate radiative transfer in heterogeneous 3D landscape scenes containing trees, shrubs, grass, soil, etc. The scene is divided into rectangular cells of variable dimension containing materials (e.g., leaf, wood, soil, water, etc.) (Figure1). Radiative scattering and propagation are simulated with the exact kernel and discrete

ordinate approaches. Topography, hotspot, leaf specular, and polarization mechanisms are also modeled. The model output predicts any specified directional sensor response. The volume and scattering properties of the materials in the cells are specified. This model represents one of the more complex 3D radiative transfer models (Kimes et al. 2002).

The simulation of bidirectional reflectance by the model encompasses two major steps (Bruniquel-Pinel and Gastellu-Etchegorry 1998): 1) illumination of the elementary cells by direct sun radiation and diffuse atmospheric radiation, possibly anisotropic; 2) interception and scattering of previously scattered radiation. In a first iteration all direct solar source vectors, and in a second step atmospheric source vectors, give rise to secondary source vectors in all illuminated cells with non nill scattering phase functions. In a second iteration all source vectors induced by secondary sources are processed. These give rise to tertiary source vectors that are further processed in a third iteration. Iterations are for all sources and for all directions. Radiation that escapes from the upper cells of the scene is stored at each iteration. Processing goes on until source vectors escape from the canopy or reach a zero threshold level of flux.

The model has been verified for its robustness of simulating biophysical variables in many studies (Esteve *et al.* 1998; Gastellu-Etchegorry *et al.* 1999; Pinty *et al.* 2000; Kimes et al. 2002; Martin *et al.* 2003; Gascon *et al.* 2004; Gastellu-Etchegorry *et al.* 2004). However, solving a 3D radiative transfer model is very time consuming. Moreover, the inversion of 3D reflectance models leads to high levels of complexity, a significant increase in required computer resources, a higher potential of ill-posed problems, and many method-specific problems such as sensitivity to noise and initial guesses at the solution (Gastellu-Etchegorry et al. 2003).

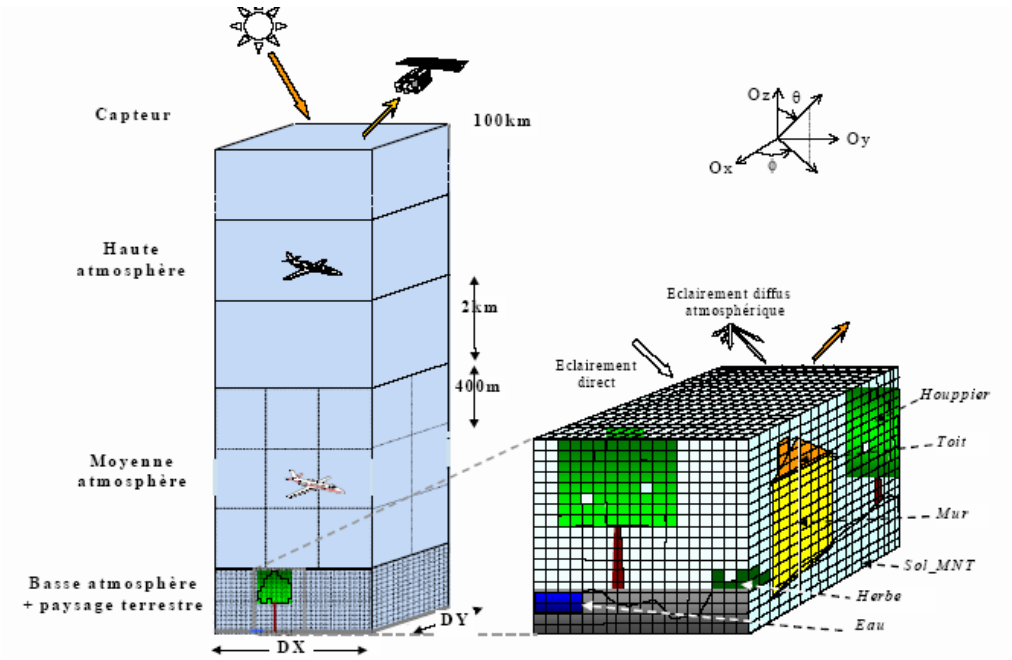

Figure1. Diagrammatic representation of the system landscape-atmosphere-sensor (Anonymous 2004)

3. Methodology

The LAI of the mature Norway spruce stand was retrieved as follows. First the field data were processed to determine the ground truth LAI and the DART inputs. Secondly the heterogeneous 3D scene radiative transfer of the mature Norway spruce stand was simulated using the DART model. Thirdly the selected method (ANN) to retrieve LAI from radiative transfer models was applied to estimate LAI at the stand level from the pre-processed AISA hyperspectral image. Finally, comparison with ground truth LAI had been performed to validate the LAI inverted by ANN (Figure2).

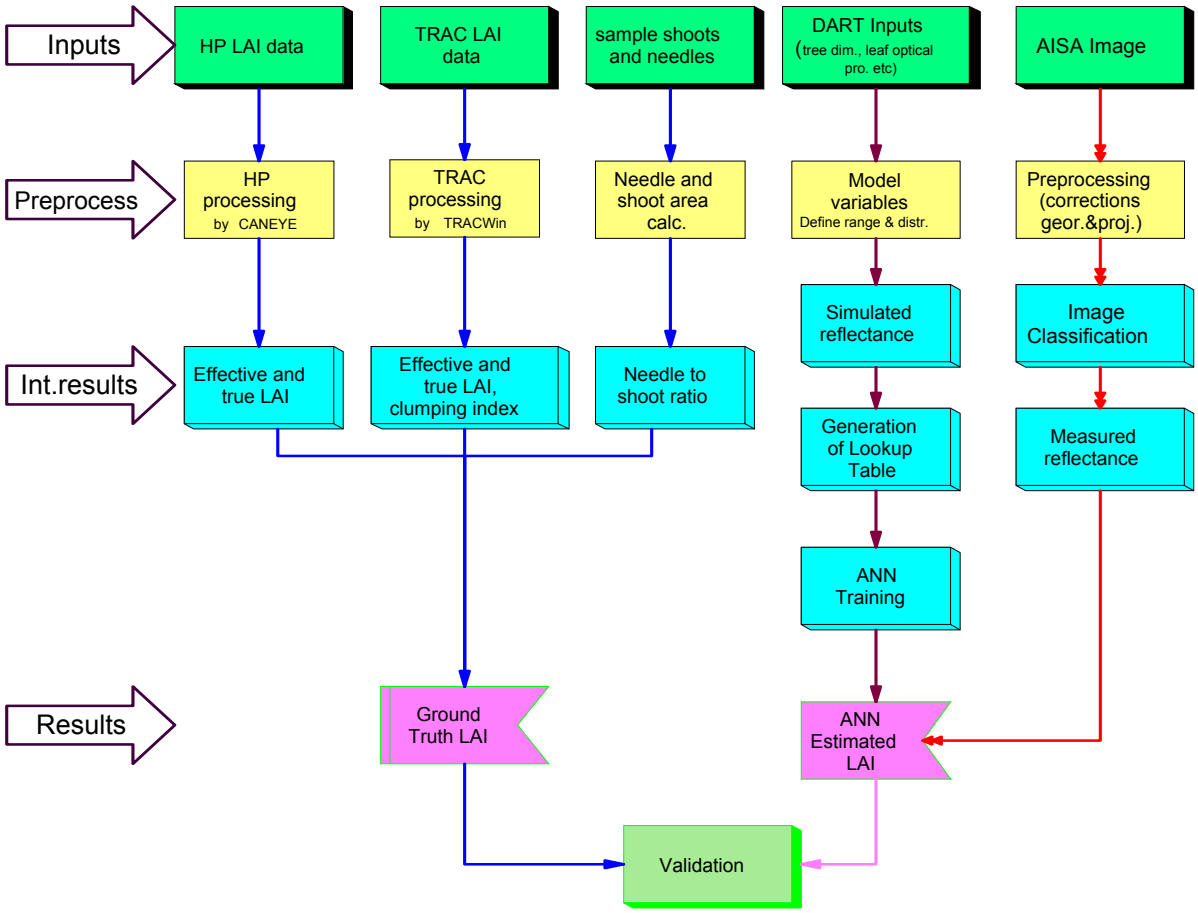

Figure 2. Conceptual model of canopy reflectance model (DART) inversion using ANN and validation with ground truth LAI computed from combination of HP and TRAC optical instruments.

3.1. Study area

The study area “Bily Kriz” (49°30´N, 18°32´E) is centered at the Beskydy Mts. in the eastern part of the Czech Republic at the borders with the Slovak Republic (Figure3). The mean elevation of the study area is 936 m above sea level. The soil type is humic podzol soil combined with loamy sand soil. The depth of the humic horizon is 60-80 cm with the gravel fraction of 30-40% and clay

fraction of 15-38%. The average annual air temperature is about 5.5 ºC, the average annual precipitation amount is between 1000 and 1400 mm. The mean number of days with snow cover is 160 days per year. The average slope gradient of the study site is 13% with the slope oriented towards south-west.

A mature Norway spruce **(***Picea abies* (L.) Karsten) forest stand with heterogeneous canopy structure was selected for this study. The stand has an average tree height of 37.96m and 0.51m Diameter at Breast Height (DBH). It is the oldest stand in the area (> 100 years).

Norway spruce is a fast growing evergreen needle leaf tree widely found in Europe. It is a conical shape very useful timber tree grows from 41 to 65 meters in height and as much as 60 centimeters in diameter on older ones (RFS 2001). Leaves (needles) are 4-sided (rectangular in section) and sharp or somewhat blunt at the tip (NCTA 1996)**.**

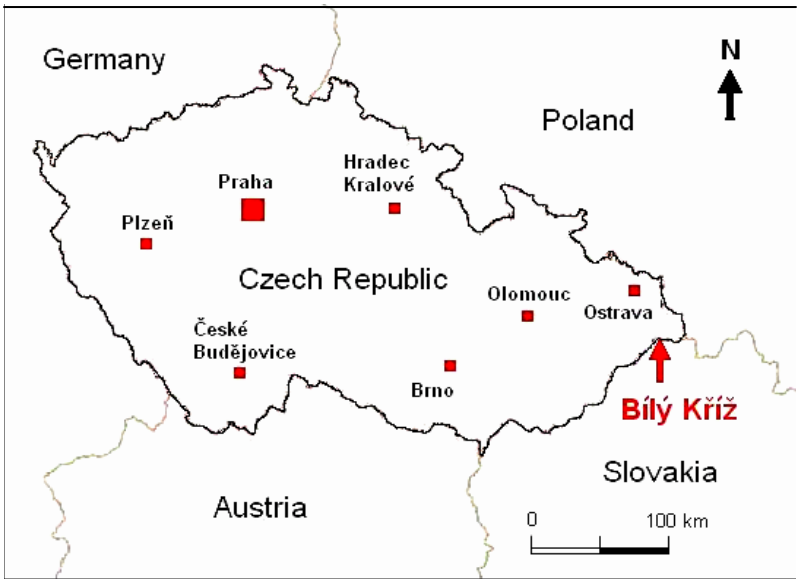

Figure 3. Location of the study area

3.2. Ground based data and pre-processing

Both the ground based LAI measurement and DART input data were collected by Lucie Homolová and Zbyněk Malenovský. Much of the data were collected during the field campaign in August-September 2004 and some in September 2005.

3.2.1. Ground based LAI data collection and pre-processing

A 60m by 60m plot was established in the middle of the study area (Figure 6) to take in-situ leaf area index estimates for validation of the method implemented to retrieve LAI from the AISA image. The validation data were collected by means of two indirect optically-based methods: TRAC and hemispherical digital camera. The hemispherical photos were taken during the field campaign in September 2004 while the TRAC measurements were made in September 2005.

3.2.1.1. TRAC measurement

The TRAC measures the transmitted direct photosynthetically active radiation along transects beneath a plant canopy using a high-frequency (32 Hz) sampling technique. Both the canopy gap fraction and gap size distribution were obtained along transects and element clumping index, true and effective LAI were driven using the appropriate equations.

TRAC measurements were made in three directions: west to East (A), Northeast to Southwest (B) and Southeast to Northwest (C) as shown in Figure 4 on the sample plot keeping the perpendicularity of each transect to the sun. The measurements were made in seven transects in 'A' during noon time and in nine transects in each of the 'B' and 'C' directions during morning and afternoon times respectively. The measurements were made two times in 'A' and 'B' and once in 'C' on 31stAugest and 1st September 2005. The distance between markers was 10m for 'A' and 14.14 for 'B' and 'C'. All the TRAC measurements were made under clear sky conditions or in large gaps between clouds.

The needle to shoot area ratio and element width (W) were calculated from previously collected data of Norway spruce stand near the study area (Kykulka site). A total of 107 shoots and their corresponding needles were used to determine the ratio. The projected area of each shoot and the needles were measured through scanning, then the needle to shoot ratio was averaged for the 107 samples.

The element width was determined by Eqn.9 (Leblanc *et al.* 2002). It is one of the inputs in the estimation of LAI using this method.

$$W = \sqrt{G(\theta)A} \qquad \text{Eqn. 9}$$

Where: W is element width

G (θ) is projection coefficient ≈ 0.5

'A' is average projected shoot area

The woody to total area ratio (α) of black spruce by Chen *et al* (1996) was taken for this study assuming the two species have much similarity and determining α is a time consuming activity that requires destructive sampling.

The Foliage clumping larger than the shoots (Ω_E), effective and true LAI were calculated in the program TRACWin 3.7.1 for each transect. See appendix 1 for general procedures in calculating LAI using TRACWin. The average Ω_E is considered to be the clumping index of the stand and used as input parameter in other LAI calculation methods.

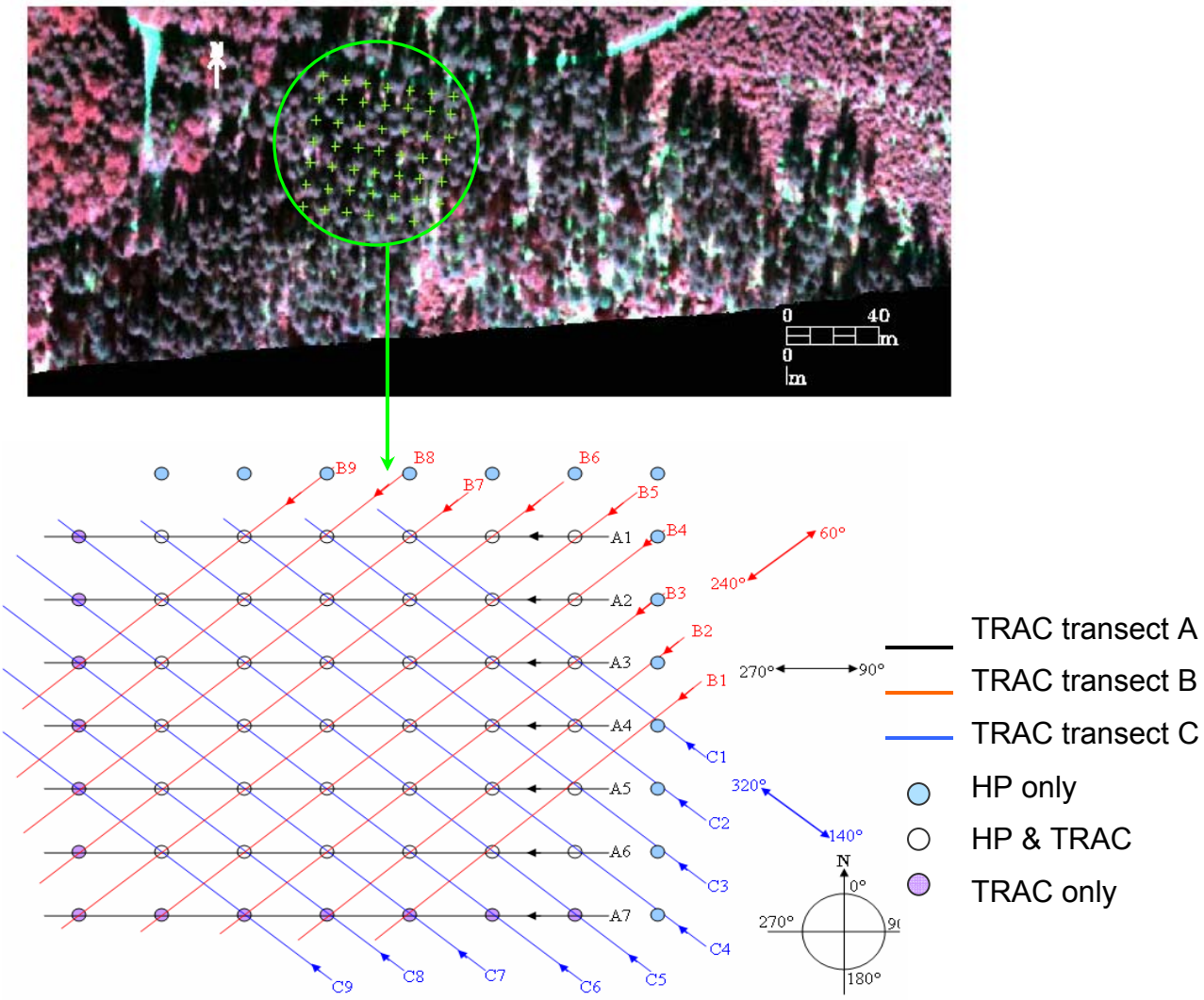

Figure 4. Lay out of the sample plot and its position in the AISA hyperspectral image of the study area

3.2.1.2. Hemispherical photography method

The developments of high-resolution digital cameras and advances in image processing software have made hemispherical photographs suitable for canopy parameter calculation. As shown on Figure 4 the hemispherical photographs were acquired at 10m interval in the sample plot. The photos have been taken using a digital camera Nikon Coolpix 8700 with fish-eye lens placed on it to offer 180º's field of view (FOV). All photos were taken at 1.5 m height from the ground surface.

For each sample point a set of 4 photos were taken one upward and one downward looking and two photos of oblique views (one upward and one downward at zenith angle 57.5°) (Figure 5). A total of 196 hemispherical photographs were taken during the field campaign in September 2004. However, only the 49 upward photos were used in this study. The photographs have been first pre-processed in adobe Photoshop for noise reduction and better contrast.

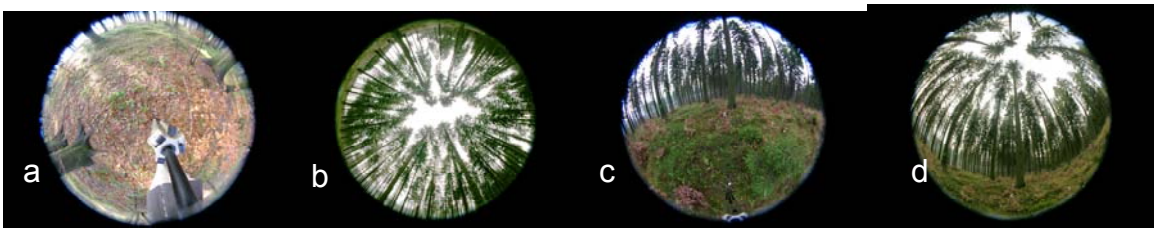

Figure 5. A Set of Hemispherical photographs taken at a sample point: downward (a), upward (b), oblique downward (c), and oblique upward (d).

The pre-processed hemispherical photographs have been organized in two fashions. On one hand the sample photos were organized into a subplot using a 3 by3 moving window going one step at a time. As a result 25 subplots with 9 photos (Figure 6) in each were created. On the other hand to make comparison between the two optical methods (TRAC and HP), the photos were organized using a window size equals to each TRAC transect foot print.

Then the CAN-EYE software was used to obtain effective LAI, true LAI and other canopy indices value. To keep the foot print of the photos within the chosen subplot the CAN-EYE software was parameterized at circle of interest 15.5^0 so that each photo has a foot print of 10m radius (eqn.10) (Baret and Weiss 2004). The analysis was made at 2.5^0 and 5^0 zenith and azimuth angular resolution respectively.

$$Ft = \pi \times [H \times \tan(\theta]^2 \qquad \text{Eqn. 10}$$

Where: Ft is foot print of hemispherical photograph
H is the average tree height (37.96m) in the stand and
θ is circle of interest

Each group of photo was classified in to leaves and none leave parts (sky) and, LAI and other indices were automatically computed and stored by the software. Trunks and big branches were carefully selected and assigned to sky to avoid their effect on LAI computation (Figure 6).

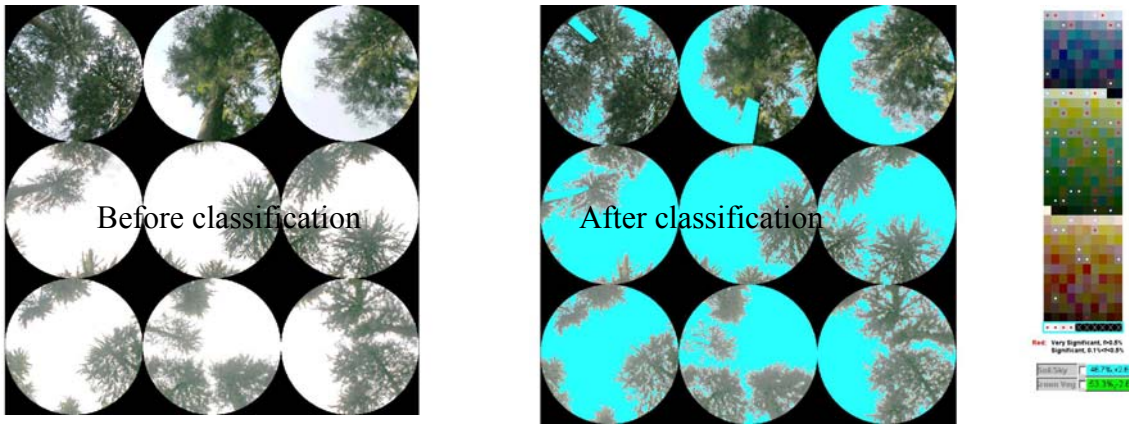

Figure 6. The set up of the hemispherical photos and classification into leaf and non leaf (sky) in CAN-EYE software

3.2.2. DART inputs

In order to describe the structure of the Norway spruce crown and the whole forest stand in the DART model, the structural data were collected during the August and September 2004 field campaign. A total of 24 trees which were considered representative of the stand were selected from Suppressed, average, co-dominant and dominant canopy parts. The basic parameters such as position of the trees (X, Y coordinate), total tree height, DBH, height of live and dead crown and crown projection area were measured for each mature tree of interest. Out of the 24 sample trees only three trees (one suppressed, one co-dominant and one dominant) were used for a simple forest representation in the DART model to minimize the computation time.

The three functional (Saturation, production and juvenile) parts of crown, the ratio of needle age classes, horizontal distribution of leaf density from a branch base towards crown periphery, and foliage clumping index were determined based on the destructive sampling made on 8 trees in the near by Kykulka site mature Norway spruce stand. The starting points of each functional part of the 8 trees were defined relative to the total tree height. Proportions of height where the functional parts start were averaged for the 8 trees. Then the averaged proportion values were applied to determine the saturation, productive and juvenile zone of our sample trees.

The results of laboratory analysis through distractive sampling of three branches, each from the three functional parts of crown taken from the near by stand, were used to specify the percentage ratio of needle age classes (current year (**c**), one year old (**c+1**), two years old (**c+2**), three years old (**c+3**) and the rest age classes (**r**). Details of the laboratory analysis procedures can be found in Homolova (2005) and Ufer (2004).

The hemispherical reflectance and transmittance of spruce needles and background elements (spruce bark, species of under story, etc.) were measured by FieldSpec spectrometer in combination with integrating sphere 1800-12. A weighted average of all spectral signatures of functional growing parts and needle age classes has been calculated to obtain a representative sample.

3.3. Image acquisition and post processing

A set of nadir hyperspectral images of very high spatial resolution (0.4m) was acquired over the study area on September 18th, 2004. The images were taken by the AISA Eagle (Airborne Imagining Spectroradiometer) sensor. AISA Eagle is one of the AISA hyperspectral systems which are complete, pushbroom imaging systems, consisting of a hyperspectral sensor head, a miniature GPS/INS sensor, and a data acquisition unit in a rugged PC easily installable/ removable on/from any aircraft. The AISA Eagle is operating within the visible and near infrared spectra (400 – 970 nm). The sensor is capable to acquire any spectral band combination up to datasets of 244 bands and boasts a 1000 pixel swath width (SPECIM 2004). The description of the airborne hyperspectral images acquisition flight campaign over the study area is shown in Table 1 below.

Table 1. Specifications of the September 18th 2004 airborne flight campaign over the study area

Parameters	
Spatial resolution /Ground pixel size [m]	0.4
Band widths [nm]	8.6-10,0
Number of bands	60
Flight speed [m/s]	50
FPS (Frames per second)	125
Swath width [m]	204.8
Altitude [m]	384
Focal length of lens [mm]	23
FOV (Field of view) [º]	29.9
Binning of pixels (spectral x spatial)	8x2

3.3.2. Image post processing

The post processing has been already done prior to the start of this study by Zbyněk Malenovský. The images were radiometrically calibrated (i.e. the sensor recorded digital numbers (DN) have been converted in to radiance value). Then the radiance values were changed in to reflectance values through atmospheric correction. The images were also geo-referenced and projected for Universal Transverse Mercator (UTM zone 34N).

3.3.3. Image classification

Two sets of images which differ only in their flight directions were cut out and exploited for their potential for classification of the study area. The very high resolution images were classified into Illuminated tree Crown (IC), Shadowed tree Crown (SC), Illuminated Understory (IU) and Shadowed Understory (SU) to use the reflectance of the IC and SC as reflectance of tree crown and the IU and SU as lambertian in the inversion procedure according to Gascon et al (2004). Two methods of classification, Spectral Angle Mapper (SAM) and Maximum likelihood (MLH) were applied and evaluated for their performance on both images. Eventually, the best performing image was used for the LAI retrieval.

The first step in the classification process was collecting endmembers for the four classes from region of interest (ROI). To improve the spectral separation, an Hourglass procedure consisting of MNF transforms was applied. The selected endmembers were displayed using N-Dimensional visualization technique and edited for better separation. Separability of ROI were also computed and checked for Jeffries-Matusita and Transformed Divergence separability measures. Then the selected classification methods were applied and evaluated by means of confusion matrix.

3.4. Simulation of forest canopy by DART model

All available information was used as DART input parameters. This information consisted of (1) structural characteristics such as tree dimensions (height, crown diameter, etc.), and (2) optical characteristics such as the leaf reflectance, the leaf transmittance, etc. Simulations were made for selected spectral bands suitable for the LAI retrieval. Other input variables were solar zenith angle,

tree cover, Crown architecture, leaf density, and Understory vegetation property and soil reflectance. Each of these input parameters are described in the following sub sections:

3.4.1. Directional parameters

The first step in DART parameterization is approximating the number of propagation directions (N_{dir}) that sample the 4ð space of directions and defining the sun Zenital and Azimutal angles. N_{dir} is approximated by the formula (Gastellu-Etchegorry *et al.* 1996):

$$N_{dir} = \sum_{u=1}^{u} \cdot \sum_{v=1}^{v(u)} \quad \text{Eqn. 11}$$

where u is the discretizing level of coordinate μ that is the cosine of zenith angle θ, and v is the discretizing level of coordinate φ, which is the azimuth angle.

A total of 95 propagation directions were used based on eqn.11. These directions are the only possible directions of incident and scattered radiant fluxes.

In the DART model the angles has to be set from 90^0 t0 180^0 for zenith and from 0^0 to 360^0 for azimuth. Therefore, the zenithal and azimutal position of the sun over the research area was calculated for the particular location and exact time of the flight and transformed to fit the DART definition. Consequently, DART sun zenith angle of 137.8°, and azimuth angle of 183.5° were applied.

3.4.2. Selection of spectral bands and RT parameters

The forest canopy BRF was studied with simulations conducted in the visible (VIS) and near infrared (NIR) spectral regions. Different wavelength regions are sensitive to different vegetation variables. The spectral information captured by the AISA sensor for the wavelength higher than 900 nm is noisy. On the other hand many of the bands within VIS and NIR region are closely related. Therefore, only those bands that have the largest information content were selected. The commonly used bands are green, red, and NIR. The four spectral bands selected for the RT simulations and building the look-up-table (LUT) database in this study were band No 13, 27, 35 and 48. Their position in the AISA hyperspectral image is shown in Table 2.

The multispectral mode of DART was used for RT simulations. A threshold value of 0.000010 for albido change and 10 for Number of iterations were set to stop the iteration when either of the threshold values first reached. Output images were requested for each of the iterations. The Gauss-Seidel approach (Gastellu-Etchegorry et al., 1996) was used to extrapolate the multiple scattered radiations in the last iteration.

Table 2. Description of the spectral bands selected for DART simulation.

Band No.	Band center (nm)	FWHM
13	540.8	9
27	670.74	9
35	745.45	9.35
48	868.99	9.49

3.4.3. DART 3D scene

As noted by Gastellu-Etchegorry et al. (2003), the accuracy of inversion procedures strongly depends on the scene simulations (i.e., computer representations) of the earth landscapes that are used by the reflectance model. Scene simulations imply many compromises. The simulation should be done at wide land range as possible and it has to be small enough to reduce the computation time. Here forest is simulated as the repetition of a basic pattern made of three representative trees each from suppressed, co-dominant and dominant canopy part of the stand over a square surface (Figure 7).

Figure 7. A 3D computer Scene of the three trees selected for DART simulation at 50% canopy closure**.**

3.4.4. Canopy closure

Numerical experiments by means of the reflectance model and sensitivity analyses have shown that the most important variables that determine the reflectance of a forest stand are canopy closure (CC), leaf area index, tree species composition, Understory type and abundance (Nilson *et al.* 2003b). To control the effect of canopy closure on LAI retrieval, eight canopy closures (50%, 60%, 70%, 75%, 80%, 85%, 90% and 95%) which are abundant in the stand were considered. These canopy closures were represented in the scene by three trees over a square surface area. The area of the scene has been varied to achieve the required canopy closure. One tree is always kept at a corner and the other two trees were located in such a way that the canopy closure is as specified and canopy reflectance is very close to BRF simulated with money trees (Figure 8).

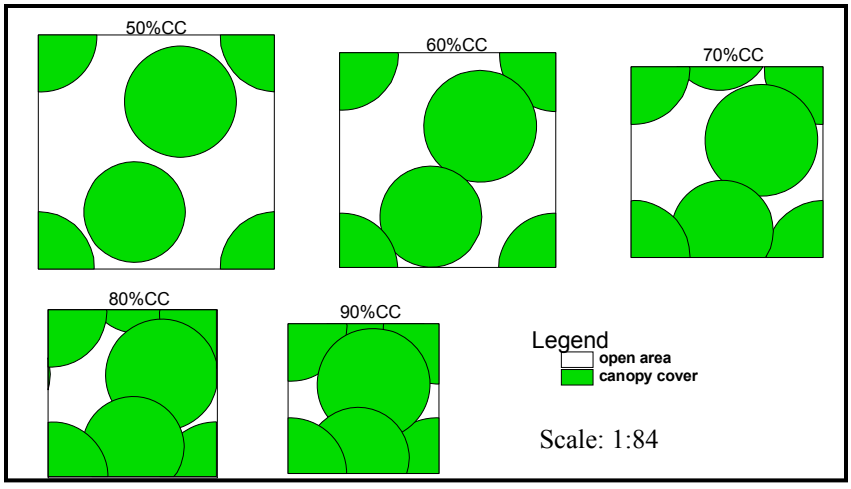

Figure 8. Schematic presentation of canopy closure starting from the more open upper left to more closed lower right.

3.4.5. Tree structural and optical properties

There are three options for simulation of trees in DART: i) random location and dimension, ii) exact location and random dimension and iii) exact location and dimension. For this study the third option (i.e. exact location and dimension) has been selected so that each tree was defined exactly by its X and Y coordinate and tree characteristics were assigned accordingly based on field measurements. The three trees were considered as separate species and tree characteristics such as location, trunk height, trunk diameter, crown radius, crown height, crown shape and optical properties where applied for each species.

3.4.6. Crown architecture

a) Crown shape: Once the option for simulating trees in DART has been decided the next step is to select the appropriate crown shape. There are several tree crown shapes in the DART model. However none of them exactly fit to the Norway spruce tree. Among the available shapes the truncated cone with zero upper radius more resembles our trees and used in this study.

b) Crown vertical levels: Parameters such as trunk diameter, vertical and horizontal distribution of leaves and optical properties vary within a tree. The possibility of creating as many levels as one wish in DART enables to attribute those parameters per level separately so that the heterogeneity within crown can be maintained. The number of tree levels was defined according to the length of live crown and normalized in such a way that the total sum of relative heights' of all levels is equal to one. In our case the suppressed tree has the longest live crown part. Therefore, the suppressed tree crown was divided into 11 levels and the co-dominant and dominant trees in to 9 and 7 levels respectively.

c) Trunk definition: Trunk height and diameters of each "DART tree species" are defined separately inside and outside of crown. The trunk height within a crown was reduced by 6% in order to avoid unrealistic influence of a trunk at the crown top. The diameter of trunk for each crown level has been calculated using eqn. 12. For the trunk below crown the average diameter was employed.

$$D_i = TAN(\theta)*(H-L))^2 \qquad \text{Eqn. 12}$$

Where: D_i is diameter at a given crown level
θ is the apex angle[1]
H is total tree height and
L is cumulative tree height up to the given crown level

d) Vertical distribution of leaf within a crown: Leaves are not equally distributed vertically along the tree crown. They have a positively skewed distribution. The Maximum weight for leaves is at 71% of each tree height. It gradually increased from the base of the crown and drops drastically after this maximum point (Figure 9). The vertical weights of leaf distribution for each crown level were introduced as weight of leaf volume density (U_f [m^2/m^3]). The weights for U_f were derived from the graph of vertical distribution of needles for each of the trees (Figure 9). The leaf volume density of a cell at any location can be described by the following equation:

[1] Apex is the pointed tip of a cone. The apex *angle* is the angle between the lines that define the apex.

$u_f[j,x,y,z] = u_f[j].w[j,l].w[j,x(l),y(l)]$ Eqn. 13

Where u_f [j, x, y, z] is leaf volume density of tree species j in particular location (x, y, z) and u_f[j] is unit leaf volume density of tree species j. The vertical weight of u_f at tree level l of tree species j is denoted as w [j, l] and w [j, x (l), y (l)] is horizontal weight of u_f

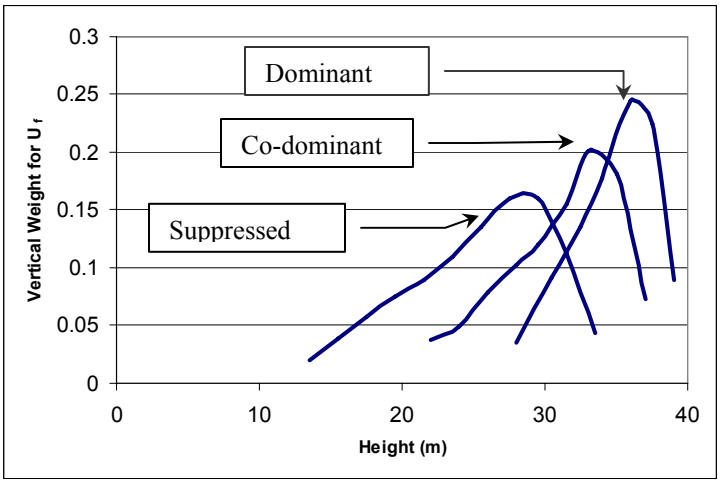

Figure 9. Vertical distribution of the suppressed, co-dominant and dominant tree foliage depicted in terms of weight for the leaf volume density.

e) Horizontal distribution of leaf area and empty cells: The horizontal distribution of crown structural features is defined in the model by varying leaf volume density in the horizontal direction. Parameters **α**, **β**, **γ** and **κ** were used to specify the horizontal distribution of full leaf and parameters **a** and **b** to determine empty (air) cells within each tree level **l**. Function of the horizontal distribution of leaf volume density is indicated in Figure 10 . The position of each leaf cell can be expressed as the relative ratio r(x,y,z)/Max r(x,y,z), where r(x,y,z) is current position of a leaf cell and Max r(x,y,z) is the position at the crown periphery. Depending on the position of the level in the crown the horizontal parameters **α**, **β**, **γ** and **κ** were specified for each crown level, so that the leaf volume density of each leaf cell is defined in the following manner as described in the manual of the Model:

- If ratio ∈ ⟨0, α) then u_f [j, x, y, z] = 0
- If ratio ∈ ⟨α,β) then u_f[j].w[j,l].w[j,x(l),y(l)], where w[j,x(l),y(l)] = (ratio–α)/(β-α)
- If ratio ∈ ⟨β, γ) then u_f [j, x, y, z] = uf[j].w [j, l]
- If ratio ∈ ⟨γ,κ) then u_f[j].w[j,l].w[j,x(l),y(l)], where w[j,x(l),y(l)] = (κ-ratio)/(κ- γ)
- If ratio ∈ ⟨κ, 1) then u_f [j, x, y, z] = 0

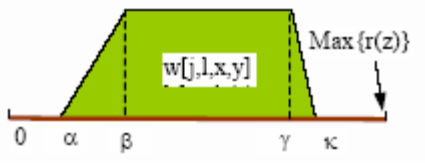

Figure 10. Horizontal distribution w[j,l,x,y] of U_f in crown (Anonymous 2004)

The horizontal parameters **a** and **b** determine zones of total (100%) inner and peripheral crown defoliation. if ratio ∈ ⟨0, a) or ⟨b, 1) then 100% of empty cells is defined automatically. Percentage of full leaf cells were specified to define the amount of hole if ratio ∈ ⟨a, b).

Parameters **κ** and **b** were assumed to be equal to 1 and **α** was taken to be equal to zero. The horizontal parameters determined from destructive sampling were **β**, **γ** and **a** (Table 3). The derivation of the parameters is based on the reconstruction of sample branches collected from Sumava 2003 and Bily Kriz 2004 field campaigns. The branch analyses were done by Pavel Rejnek from 16 trees (eight trees from each site). Representative branches were taken from the juvenile, productive and saturation part of the crown functional parts and the parameters were computed as follows.

i. **Horizontal structural parameters β and γ of leaf volume density**: First of all percentage of total branch segment area per each sector ring was calculated. The result of the total needle area per segment was used to compute the total needle area [m2] within each sector ring and in final step recomputed into the percentage of the half of total needle area per sector ring. The average values of these percentages for juvenile and first productive branches were plotted in cumulative way. The cumulative curve was fitted by a sigmoid function: The first and second derivative of the sigmoid function was calculated. Finally, the parameter **β** was estimated as the maximum and the parameter **γ** as the minimum of the second derivative function.

ii. **Horizontal parameter 'a' of inner zone of defoliation:** Only first productive branches were taken into account for calculation of the parameter '**a'**. The length of non-leaf part for each examined branch was determined, averaged and converted into the percentage of total branch length.

iii. **Percentage of full leaf cells:** Percentage of full leaf cells per functional crown part is another main input parameter for the DART model which determines the distribution of holes in the DART scene canopy. Unfortunately, there were no data that can be used to calculate this parameter in our study area. The percentages calculated by (Ufer 2004) on matured Norway spruce stand in Sumava Mountains National park were used. He calculated the percentage of full leaf cells based on the assumption that percentage of full leaf cells is equal to the total clumping index (Ω) of the crown. He analyzed clumping index for stressed and non stressed trees separately and take average Ω values for each functional part. The clumping index (Ω) was made at one level in the saturation and juvenile and at two levels in the productive crown functional parts. Thus, the values for the remaining levels were computed by means of simple linear interpolation.

Table 3. Parameters of leaf and foliage gaps horizontal distribution used for representative trees of DART simulations.

Crown functional part	Parameter			
	β	γ	a	Full leaf cells
Saturation	0.299	0.594	0.28	0.2
Productive	0.033	0.494	0.22	0.6
Juvenile	0.016	0.425	0.1	0.85

* The estimates presented in this table correspond with first level of each functional crown part. The estimates for others levels were linearly interpolated and are not shown in this report.

3.4.7. Simulation of the first order branches

As branch has significant influence on the optical property of the crown the first order branches has been incorporated in the DART parameterization process. The construction was done by Lucie Homolová. Each branch has to be defined by a relative height of its branch base on a trunk. The orientation of a branch is defined by its zenith and azimuth angle. In average two branch whorls per a crown level were created along the trunk each assembled from four to six branches. The branch zenith angle linearly decreased from 90° to 60° with growing tree height.

3.4.8. Tree optical properties

As one goes from the lower part of the crown up wards to the juvenile the needles optical property is changing because of age difference among needles. To incorporate this variability to DART, first the directional hemispherical reflectance and transmittance of needles of juvenile, primary and secondary shoots of different age classes were computed. Directional hemispherical reflectance and transmittance of needles of age class **c** and **c+1** were simulated in PROSPECT model by Zbyněk Malenovský while for the rest age classes the field measured directional hemispherical reflectance and transmittance were used. Then the directional hemispherical reflectance and transmittance of the juvenile shoot was used to determine the hemispherical reflectance and transmittance of the juvenile crown functional part while primary and secondary shoots reflectance and transmittance were mixed proportionately to determine the optical property of the productive and saturation crown functional parts. Leaf optical properties for each crown functional part were calculated as a weighted average of hemispherical optical characteristics of four needle age classes (**c**, **c+1**, **c+2** and **r**). Because of the absence of enough information about the vertical distribution of needle age classes of the study area forest stand, the needle age distribution obtained from destructive sampling of Kykulka site were used. To avoid complexity only three leaf optical properties one for each functional part were applied weighted by the average needle age class in each functional crown part. The optical properties of Norway spruce bark of trunks and branches measured during the field campaign at Sumava Mts. in 2003 were used.

3.4.9. Leaf area index in DART

LAI is a free input variable which can be expressed directly as LAI or indirectly in terms of leaf volume density in DART. The maximum and minimum LAI expected in the stand were estimated from the ground LAI measurements and simulations were made at 0.5 LAI value intervals. This interval is chosen because of time constraint as well the sensitivity of the model is low when the difference in LAI value is minimal. In this study LAI was expressed as U_f using eqn. 14.

$$U_f = \frac{LAI * scene\ \dim. \big/ cell\ volume}{total\ number\ of\ leaf\ cells} \qquad \text{eqn. 14}$$

Where U_f is leaf volume density expressed as m^2/m^3

LAI is intended Leaf Area Index to be simulated

3.4.10. Background structural and optical properties

One of the interesting features of DART is that it allows creation of plots which enable simulation of varied landscape. The most common understories of the stand were represented by plots. There are different grass species in the Understory. However, due to absence of information the Understory is considered as homogeneous vegetation layer and represented by the most frequently observed grass in mature Norway spruce forest stands (i.e. Calamagrostis villosa) (Ufer 2004) A constant mean height (0.3m), standard deviation (0.1m), LAI (2.5 for canopy closure > 80% and 3 for others), optical and structural properties were assigned. 2m by 2m square Plots were also established around each tree to represent litter fall and the optical property of senescent needles was used (Figure 11). The average soil optical property of the stand was applied as background of the scene.

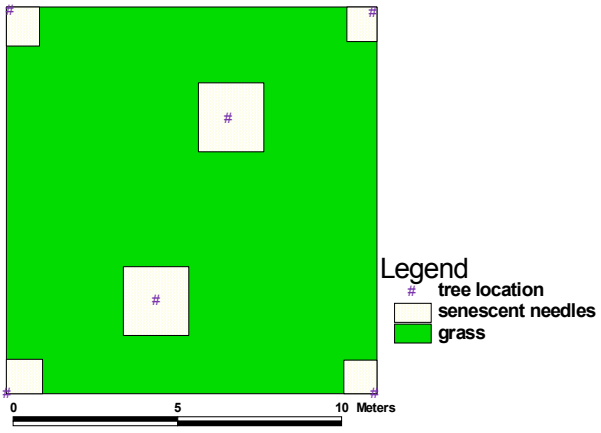

Figure 11. Schematic representation of the Understory vegetation in a 50% canopy closure DART scene

3.4.11. Building the spectral look-up table

LAI was simulated under eight canopy closures (see section 3.4.4) starting from LAI of 3.0 up to 15.0 at 0.5 intervals. Accordingly, 25 simulations were made for each canopy closure. In total 200 simulations were carried out under the eight canopy closures to build the Look-Up Table (LUT) database.

The nadir view output images from DART have been aggregated from 0.2m resolution to 0.4m to fit the resolution of the AISA hyperspectral image. Masks were prepared to separate shaded and sunlit crown part from Understory. Then, the average spectral signatures of shaded and sunlit pixels were extracted separately from each image and used to build the spectral LUT together with LAI value and canopy closure. All the information has been stored in one LUT.

3.5. Method of LAI retrieval

To propose appropriate methods of LAI retrieval using inversion of the DART model, several biophysical variables estimation methods of remote sensing were reviewed. In many literatures the physical and hybrid inversion methods are recommended because of their efficiency and applicability on a per pixel basis. Although, the merit function, neural network and projection

pursuit regression were first selected to retrieve LAI from the hyperspectral image of the matured Norway spruce stand because of time limitation we have decided to use only neural network method. As discussed in previous sections the images were classified into IC, SC, IU and SU. Based on the average reflectance of IC and SC of the AISA hyperspectral image and that of the LUT of DART simulated reflectance of the same class, LAI was retrieved. All computations were performed in neural network tool box 4.0.3 in Matlab (ver.7.1).

Artificial Neural Network (ANN)

A feed forward back-propagation neural network with three layers (input, hidden, and output layers) was used for the purpose of this study (Figure 12). The general process of a ANN inversion is: 1) given a set of empirical environmental, leaf, canopy, and soil parameters, determine the set of canopy reflectance with a forward RT model; 2) initiate the ANN training (or learning) process with part of the lookup table obtained in the first step, and establish the relationship between the input data and the output LAI; 3) check the ANN training with the other part of the LUT data or ground measurements; and 4) apply the trained and checked ANN model to a new scenario to predict output parameters.

Combal *et al.* (2003) showed that the inversion of RT models is by nature an ill-posed problem and needs regularization techniques to obtain stable and reliable solution of the ill-posed inverse problem. Their study revealed introduction of prior information on uncertainties in the system provides more robustness to the neural network training rather than solving the ill-posed problem.

Therefore, for the purpose of introducing prior information to the data set we had calculated the variance of the noise level of each band from the AISA hyperspectral image and added to the DART simulated crown reflectance values through a random noise addition function. As a result the retrieval was made on two LUTs one with noise and the other without noise added to it. Although, it is better to train the ANN using different band combinations to identify the best band combination for LAI retrieval because of time limitation we did not exhaust all possible band combinations, but did evaluate the most commonly used bands.

Each LUT data set was divided in to three parts with the proportion of 2:1:1 for training, validation and testing respectively. To eliminate the possibility of reaching the saturation regions of the sigmoid transfer function during training both the input and the out put values were linearly scaled to ensure they lie within the range [-1 1].

Since the network has to be first trained in order to retrieve LAI the training set of reflectance and the corresponding LAI were used for this purpose under the selected CCs. After a series of preliminary tests the architecture of the neural network has been defined to be a single hidden layer with 11 nodes and tan-sigmoid transfer function along with one out put layer with linear (purelin) transfer function. The initial values of the weights and biases were set to a random value between -1 and +1.

One of the problems that occur during neural network training is overtraining. The error on the training set is driven to a very small value, but when new data is presented to the network the error is large. The network has memorized the training examples, but it has not learned to generalize to new situations(Demuth and Beale 2005). To improve the generalization of the network we used earlystopping with the Scaled Conjugate Gradient (trainscg) optimization algorithm, which

combine the model-trust region approach (used in the Levenberg-Marquardt algorithm), with the conjugate gradient approach for fast computation. To protect the convergence of the learning algorithm before it reaches the global minimum error, the learning rate was set to 0.1, 'momentum' term to 0.9, momentum decrease and momentum increase to 0.8 and 1.5 respectively. Besides, the network has been initialized many times to start from different error surfaces and to take the best one.

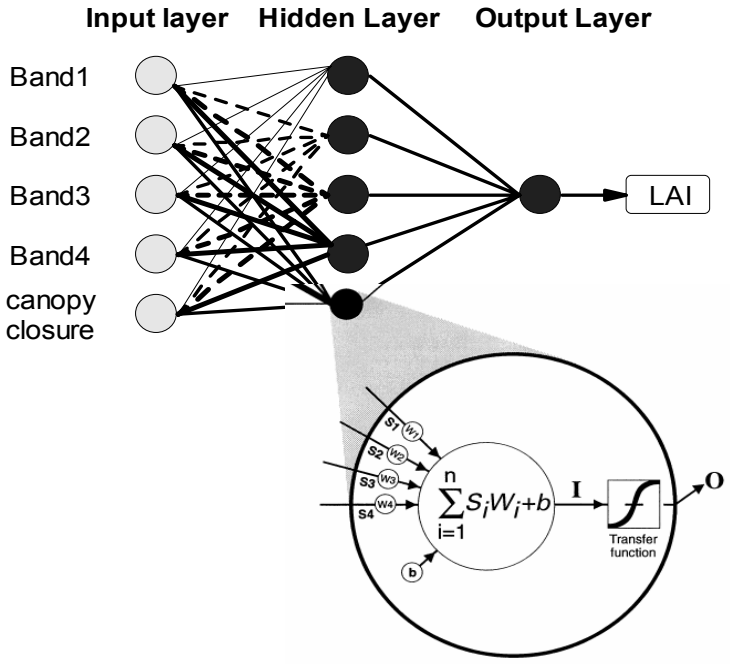

Figure 12. Model of multilayer neural network showing the structure and detail of processing nodes. The network consists of multiple inputs, a single layer of hidden nodes, and output nodes. The inputs are fully connected to the nodes in the hidden layer(s) which in turn are fully connected to output nodes. All processing of signals flows from the input nodes through the hidden layer(s) to the output nodes (feed-forward). Each hidden node (denoted as circles) is a nonlinear processor of its input signals [adapted from Danson *et al.* (2003)].

3.6. Validation of the retrieved LAI

To keep the foot print of the validation data and the estimated LAI same, the inversion was done approximately at the same window size as that of the field LAI measurements processing (i.e. 39.6m by 39.6m).Then the estimated values for those validation points were extracted from the LAI map by considering four neighboring pixels and compared to the ground truth data. The root mean square error in LAI estimation was determined against ground truth measurements in order to evaluate the performance of the inversion method on the LAI retrieval accuracy. A simple linear regression was also applied to establish relationships between the result of the inversion method and field LAI measurements.

4. Results and discussion

4.1. Ground based leaf area index measurements

4.1.1. TRAC measurement

The estimation of LAI using TRAC needs the determination of clumping index (Ω) and proportion of woody materials (α) in the TRAC measurement. Needle to shoot area ratio (Y_E) and clumping index of the leaves at the scale larger than shoot (Ω_E) are the two parameters required to compute Ω. Therefore, the needle to shoot area ratio was calculated for 107 sample shoots and their needles giving an average ratio of 1.466 with 0.069 RMSE. The maximum and minimum needle to shoot ratio was 2.46 and 1.11, respectively. The slope of the regression line for the ratio across sample shoots (Figure 13) was not significantly different from zero (-0.0011), which indicates that the ratio is close to a constant value. The needle to shoot area ratio of several plant species was presented by Gower *et al.* (1999). This ratio was varying from 1.3 to 1.4 for black spruce trees. Our calculation of the ratio revealed a slightly higher value. This can be attributed to the clumping difference due to age of sampled trees and difference in species.

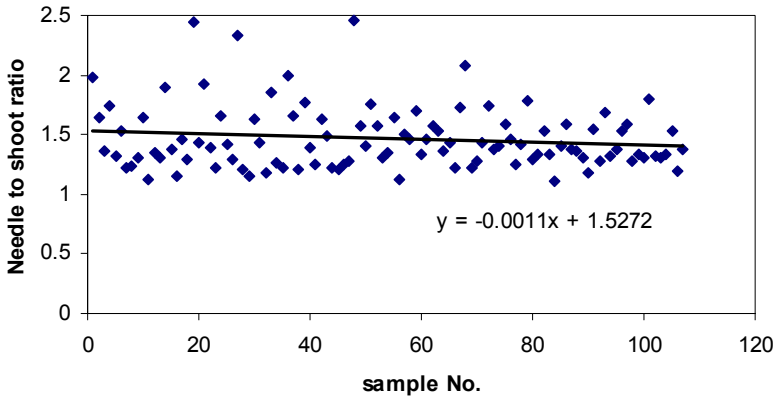

Figure 13. The needle to shoot area ratio for the 107 sampled Norway spruce shoots.

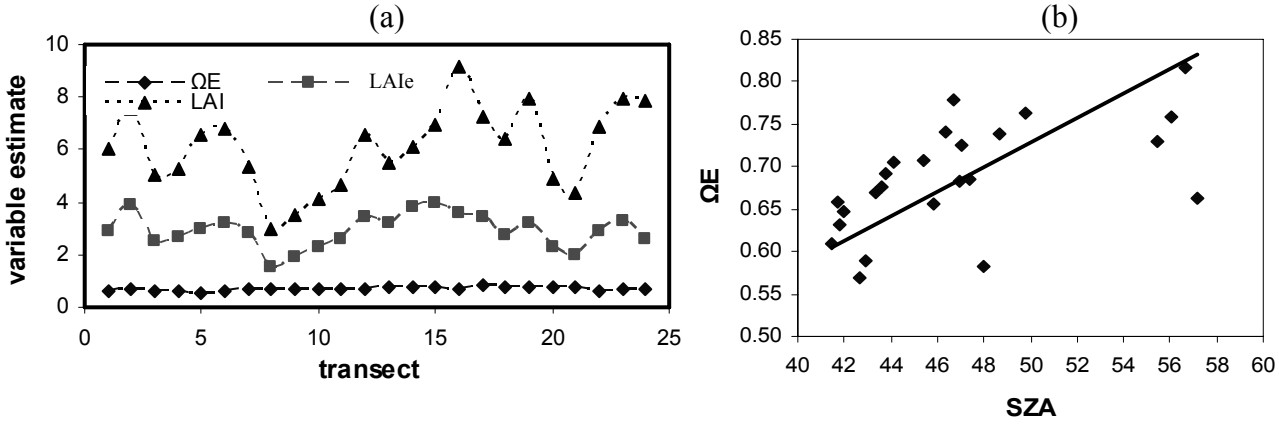

Figure 14. Spatial distributions of clumping index of the leaves at the scale larger than shoot (Ω_E) , effective Leaf area index (LAIe) and true leaf area index (LAI) estimated values from TRAC device (a) and relationship between solar zenith angle (SZA) and Clumping index at the scale larger than shoot (Ω_E) (b).

The estimation of Ω_E in the TRACWin software is stored for different foliage element sizes. In order to obtain the corresponding Ω_E value, the average element width (W) has to be known. Hence, we calculated the leaf element (shoot) width of the investigated trees using eq.9 and its average value was found to be 8.11mm.

Table 4 is summarizing the result of Ω_E, LAIe and LAI estimated using the TRACWin 3.7.1 software from the TRAC measurements of 25 transects acquired within the sample plot. Figure 14a illustrates the spatial distribution of the variables per transect. The average Ω_E, LAIe and LAI were equal to 0.6918, 2.82 and 5.88, respectively. More detail result about each transect can be found in appendix 2.

Assuming the α equal to 0.14, the LAI values obtained from eq.1 were ranging between 1.35 and 9.17. The lowest LAI was recorded on transect which has the shortest segment length. This could be an erroneous result indicating the need to make longer transects in order to characterize the architecture of a canopy properly as noted by Leblanc (2002). Ω_E varied between 0.5697 and 0.8197.

Table 4. Summary statistics of clumping index of the leaves at the scale larger than shoot (Ω_E) , effective Leaf area index (LAIe) and true leaf area index (LAI) from TRAC measurement.

	SZA	**Ω_E**	**LAIe**	**LAI**
Transects	25	25	25	25
Mean	46.72	0.691	2	5.9
Minimum	41.47	0.5697	0.9	1.4
Maximum	57.15	0.8197	4	9.2
Std	4.7701	0.0664	0.729	1.745

Leblanc (2002) pointed out that LAI measurements using TRAC can suffer from considerable errors if the solar zenith angle is not kept within range of 30 to 60 degree. Although the SZA was kept within the suggested range, the clumping factor (Ω_E) was large for higher SZA and reduced for decreasing SZA (Figure 14b). Hence, our results approve that the TRAC measurement method tends to produce outcomes of high variability and a larger number of erroneous estimates if the SZA is not kept constant. As suggested by Chen et al. (1997) another possible source of error for this technique is the large proportion of foliage concentrated at the top conical part of the tree crown making, the core of the cone impermeable to the solar beam. The TRAC device is capable to quantify the effect of foliage clumping on LAI measurements only under the condition that all foliage clumps larger than the shoot are penetrable by light. This assumption is necessary for calculation of the clumping index, because it is impossible to estimate the foliage area inside a clump without foliage gaps. The dense top of Norway spruce crowns may limit the light penetration and hence violates this assumption, so that the TRAC underestimates the shoot clumping effect and consequently LAI values.

4.1.2. Hemispherical photography

The effective and true LAI values estimated from hemispherical photographs are overviewed in Table 5 and fully presented in appendix 3. The true leaf area index has been calculated in two

ways. First, the $LAI_{combined}$ was computed from eq.1[2]., using values of LAIe as estimated from CAN-EYE and Ω_E estimated from TRAC. This method yielded the highest and presumably better accurate LAI estimates, with an average of 7.6.

In the second approach, using only inputs generated by CAN-EYE (Weiss *et al*. 2002), the average LAIe was estimated to be 3.6 and the true LAI was equal to 6.4. Figure 15b illustrates that comparing to the former approach this method generally underestimates the average true leaf area index by means of 16%. The mean LAI estimate of 6.4 is statistically lower than the LAI_{comb} estimate (P = 0.05).This can be attributed to higher real clumping of shoots than assumed in the method. LAI of both cases varies among the subplots more than LAIe (figure 15a).

Table 5. True and effective leaf area indices estimated from hemispherical photography. (LAIe and LAI are computed by the CAN-EYE software, while $LAI_{combined}$ is the true leaf area index calculated from LAIe of CAN-EYE and average Ω_E of TRAC using eq.1).

	LAIe	LAI	$LAI_{combined}$
Mean	3.6	6.4	7.6
Minimum	1.7	3.7	3.6
Maximum	5.3	8.3	11.23
Std	0.83	1.13	1.75

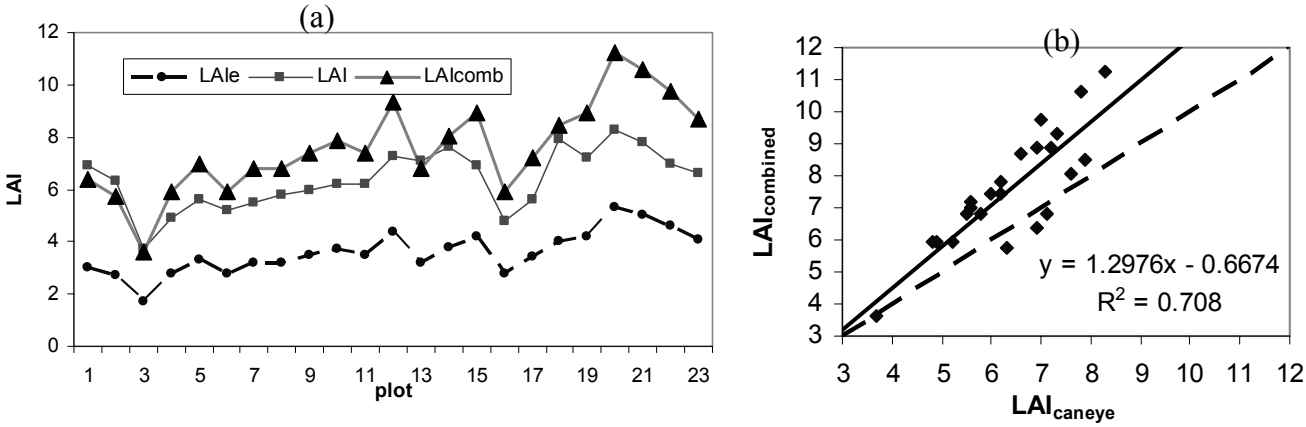

Figure 15. The distribution of CAN-EYE effective leaf area index (LAIe), CAN-EYE true leaf area index (LAI) and true LAI computed using eq.1 (LAI_{comb}) from hemispherical photographs across the 23 examined subplots[3] (a) and comparison of the two LAI computation methods (b).

The CAN-EYE method has both advantages and disadvantages. On one hand, it provides a permanent image of the forest canopy that can be reanalyzed later if required, which is beneficial. On the other hand, the CAN-EYE image analysis software had to be used interactively to classify the hemispherical photographs to sky/ green vegetation. The manual selection of sky and green vegetation colors, and manual removal of woody materials (trunks and branches) introduces an element of subjectivity, which rises potential of operator error in the estimates of canopy variables.

[2] Woody materials have been removed during the hemispherical photograph processing, therefore 'α' is considered to be 0 in this case.
[3] Two of the subplots result were found outlier and discarded from the sample

4.1.3. Comparison between the two optical methods of LAI estimation

Both the hemispherical photography and TRAC methods provide plant canopy structure information based on the measurements of gap fraction within canopy. The hemispherical photography method provides canopy structure measurements with Leaf Angle Distribution (LAD) and clear sky fraction automatically predicted for a series of azimuth and zenith increments over the 360^{o} field of view. Whereas, the TRAC relies on software to predict the LAI and foliage clumping index from two sets of observations: 1) gap fraction and 2) gap size distribution.

Because of the difference in foot print of both devices, it is not possible to conclude on the best method based on the results described so far. The hemispherical photographs need to be adjusted and organized in such a way that the foot prints of both instruments cover the same area. Only seven common subplots were found which allow comparing the LAI measurements of the two optical instruments.

Mean LAI values are shown in Table 6. Hemispherical photograph LAI estimates are higher, estimated as 6.6 using CAN-EYE and 8.2 using combined approach (eq.1), respectively. LAI from TRAC measurement (5.9) was by 28% lower compared to LAI estimated using eq.1.

Table 6. Statistical summary of leaf area index computed from hemispherical photographs and TRAC records within seven subplots of the experimental Norway spruce stand.

	$LAI_{CAN-EYE}$	LAI_{TRAC}	LAI_{comb}
Mean	6.6	5.9	8.2
No. of Samples	7	7	7
Std	0.4192	0.7231	0.6170
*CV (%)	6.38	12.17	7.49
Min	6.0	5.1	7.6
Max	7.1	6.9	9.1

* CV stands for coefficient of variation

Variability in LAI produced by the two instruments within the subplots is illustrated in figure 16a. LAI values range from 5 through 6.9 for TRAC measurements and from 6 through 9.1 for the hemispherical photographs. CV is much higher for TRAC measurement (12.17%) than the hemispherical photos (6.38% and 7.49 %.). Still the average values of LAI obtained from TRAC measurement and hemispherical photography technique were well correlated with $r^2 = 0.73$ (figure 16b). Figure 16c and 16d shows the comparison between combined LAI computation using eq.1 with TRAC and hemispherical photography measurements. The correlation is relatively lower between TRAC measurement and combined approach, $r^2 = 0.57$. Results of the hemispherical photograph's analysis and the combined approach are still in good agreement ($r^2 = 0.76$). The relationships between the LAI values of all approaches are essentially linear. However, t-test analysis showed the significant difference among the average LAI value of all three methods at P = 0.01.

In general, comparison of the methods (i.e. CAN-EYE, eq.1, and TRACWin) used to derive the ground truth LAI from hemispherical photographs and TRAC measurements produced results with a good correlation. However, the average values showed statistically significant differences and

further examination of the results showed that the LAI calculated by TRACWin from TRAC measurement was lower for most of the sample plots. This suggests that TRACWin analysis most probably results in underestimation of LAI as described in section 4.1.1.

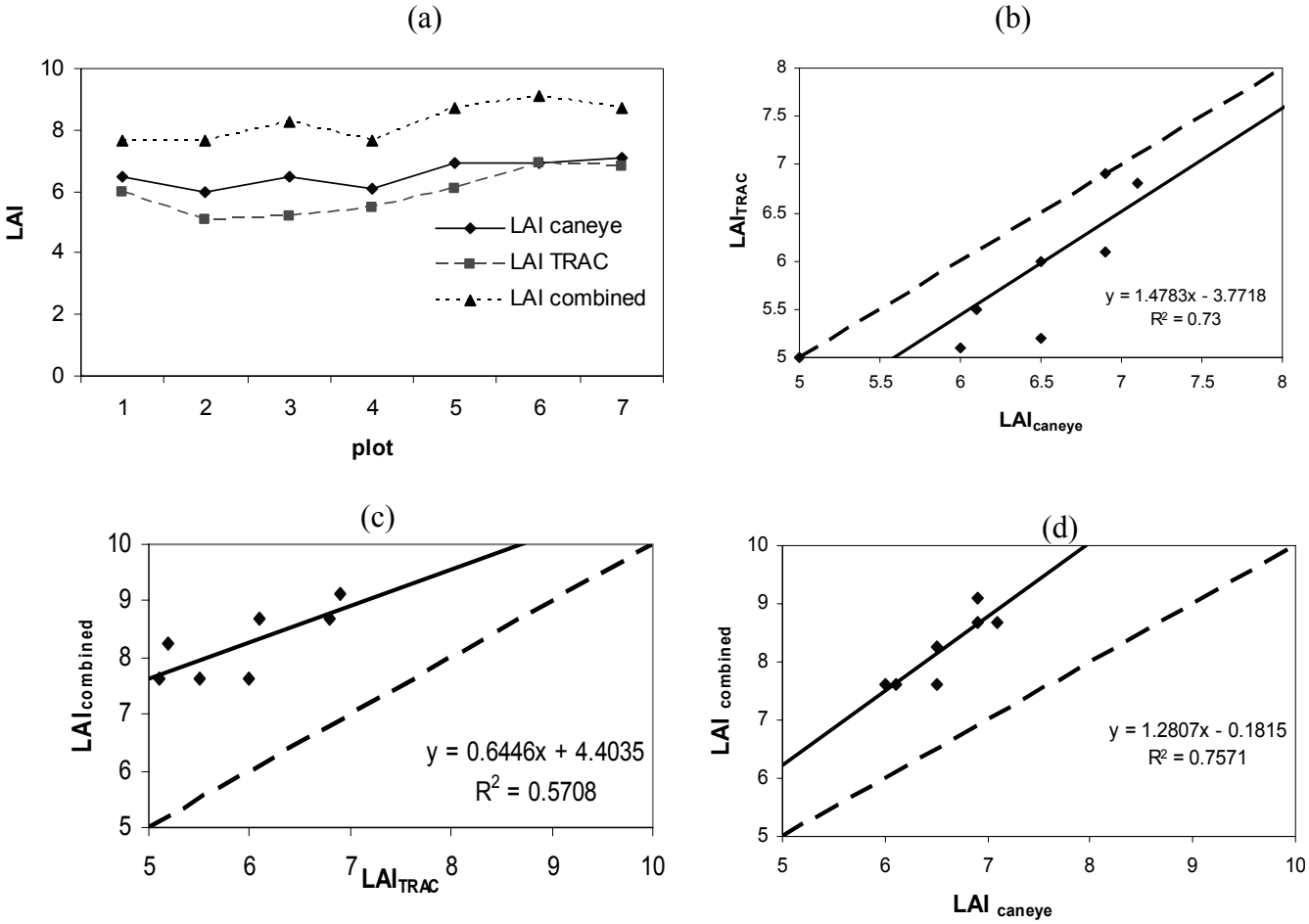

Figure 16. Variability of LAI estimates among methods (a), comparison between LAI computed from hemispherical photographs using CAN-EYE and TRAC measurement (b), and comparison of LAI computed using both optical instruments against the combined result (c) and (d).

Many studies have demonstrated that optical methods tend to underestimate true LAI (Chen *et al.* 1997; Kucharik *et al.* 1998; Gower *et al.* 1999; Soudani *et al.* 2002). Gower *et al.* (1999) noted that indirect estimates of LAI saturate around 5–6, while direct estimates reach 9. The likely cause is no change in gap fraction (i.e. gap saturation) as LAI approaches values of 5–6. The combined use of the optical instruments can reduce this problem. For this reason we considered the estimation of true LAI using the combined approach (eq.1) to be the most reliable out of the three used techniques. The uncertainty associated with this alternative approach is rising from two assumptions: 1) the clumping factor is expected to be constant between individual sampling locations within an experimental area, and 2) clumping is assumed to be uniform within a layer or area of the canopy. However, these assumptions may not be valid for more complex heterogeneous canopies (Gardingen *et al.* 1999).

4.2. Image classification

The AISA hyperspectral image subset of the study area (Figure 17) was cut out of the flight line and classified into four classes (IC, SC, IU and SU, see section 3.3.3) in order to separate the canopy pixels of interest from Understory. The classification was made over two subsets of AISA images which differed only in their flight direction (flight line 1 and line 5). Comparison of two classification methods (SAM and MLH) showed the results of MLH method more accurate. The confusion matrix of randomly selected pixels showed the overall accuracy of the SAM classification to be 78% and 82%, while MLH accuracy was 94% and 96.32% for flight line 1 and 5, respectively. Because of the highest accuracy, the image of flight line 5 classified by MLH was used for the LAI retrieval.

The accuracy assessment results for flight line 5 are presented in Table 7. The Kappa coefficient is close to one (0.95) indicating the good performance of the MLH classification method. The comparison showed a relatively higher confusion of pixels between illuminated crown and shaded crown classes than the others. As a result the illuminated crown class showed the highest error of commission (8.47%) while shaded Understory showed the lowest one (1.12%). This means that many pixels of other classes had been assigned into illuminated crown class, particularly shaded crown pixels. In contrast, almost all (98.80%) of illuminated crown pixels has been assigned correctly so that the error of omission of this class is the lowest (1.20%).

Table 7. Summary of accuracy assessment of AISA image classification using MLH. The values are in percent. The assessment was made using 2525 pixels taken randomly from the four classes.

Class	Illuminated crown	Shaded crown	Illuminated understory	Shaded understory	Total	Commission	Omission
Illuminated crown	98.8	6.25	1.45	2.33	28.51	8.47	1.2
Shaded crown	0.3	93.09	0.87	0	22.73	1.39	6.91
Illuminated understory	0	0.66	97.68	2.5	27.45	2.6	2.32
Shaded understory	0.9	0	0	95.17	21.31	1.12	4.83
Total	100	100	100	100	100		
					Overall accuracy		**96.32**
					Kappa coefficient		**0.9507**

The SAM algorithm should be the best choice for a hyperspectral image classification as it was designed for this data type. However, in this study MLH, a multispectral classifier, was found to perform better over the hyperspectral data. The low accuracy of SAM method could be caused by its insensitivity for illumination changes. The illuminated and shaded parts of one vegetation type can have a similar spectral angle. The difference may only be in reflectance magnitude driven by intensity of illumination. Design of the SAM is relatively insensitive to changes in pixel illumination, because increasing or decreasing illumination does not change direction of the vector, but its magnitude (i.e. a darker pixel will be plotted along the same vector, but closer to the origin) (Yuhas *et al.* 1992). For this reason, high confusion between shaded and illuminated parts decreased accuracy of the SAM classification.

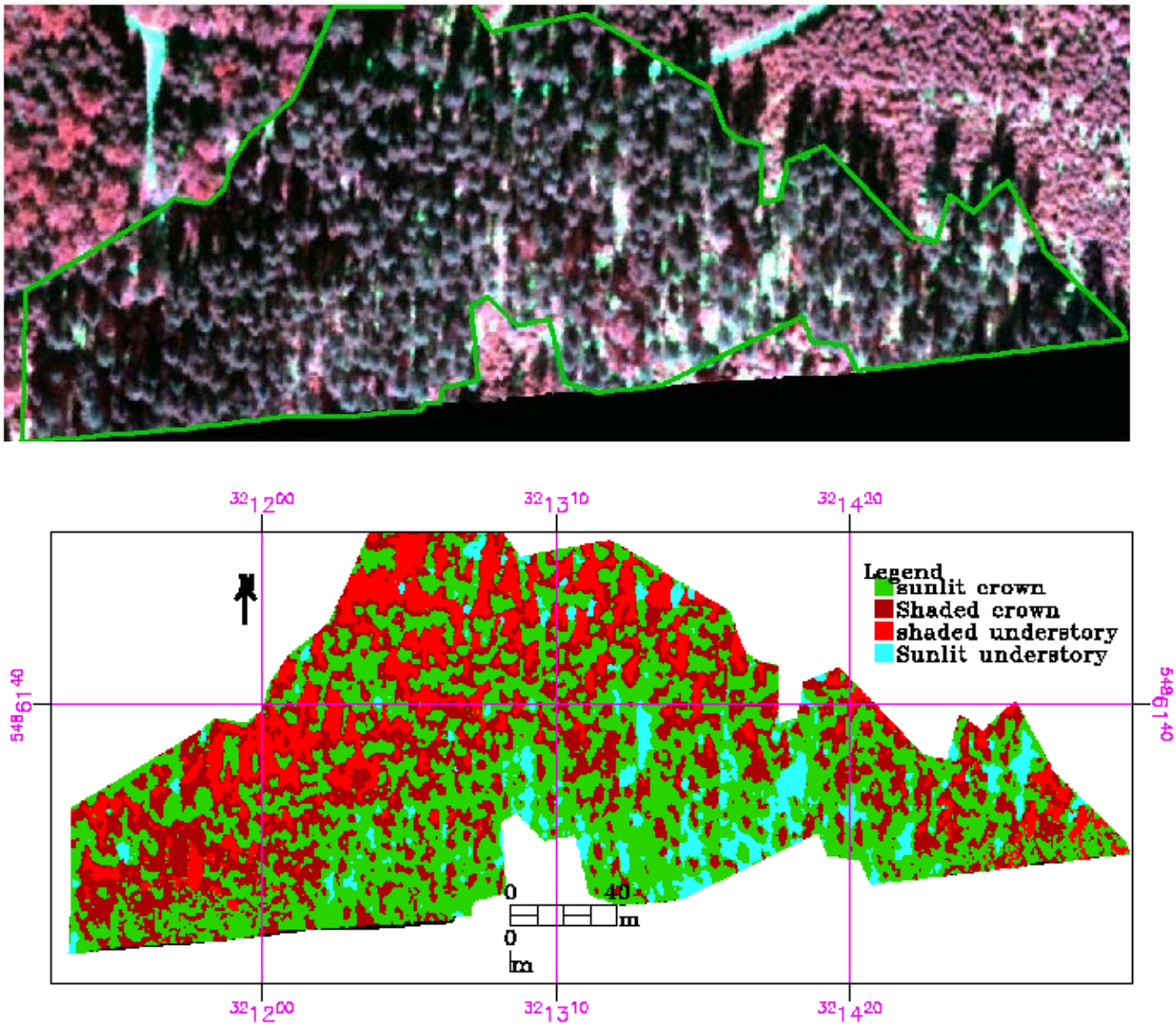

Figure 17. AISA image of the study area (experimental Norway spruce stand and its surrounding) (upper) and the best classified image (lower).

The best classification results obtained from flight line 5 can be attributed to the low shading effect in this direction. This flight was most probably done closer to noon time of the day when shading effect is minimal. Also the very high spatial resolution of 0.4m, minimizing number of mixed pixels, substantially strengthened the overall accuracy of the classification.

However, the error matrix could be insufficient to conclude about the accuracy of the classification due to bias in the selection of the reference pixels per class. Although enough number of sample pixels (2525) was randomly selected for the accuracy assessment, they were mainly taken from relatively homogenous areas to address properly the ground truth classes. This may lead to an

optimistic accuracy of classification since heterogeneous areas, which are more difficult to classify correctly, are excluded from reference data selection.

4.3. Canopy closure of the study area

Canopy closure, as it has an effect on reflectance of forest, was one of the inputs used for inversion of LAI by means of neural network. Therefore, the DART simulations were prepared according to representative canopy closures. The canopy closure of the stand has been calculated by dividing the sum of sunlit and shaded crown pixels to the total pixels of the sliding window throughout the AISA Eagle image using the classified image as a mask. The result is illustrated in Figure 18. The canopy closure of the stand varied from 20% up to 95.3%. Most of the stand area had a canopy closure of 60% and higher, with the highest frequency at 88% (Figure 19). The mean canopy closure of the forest was found to be 78.3% with standard deviation of 13.2%.

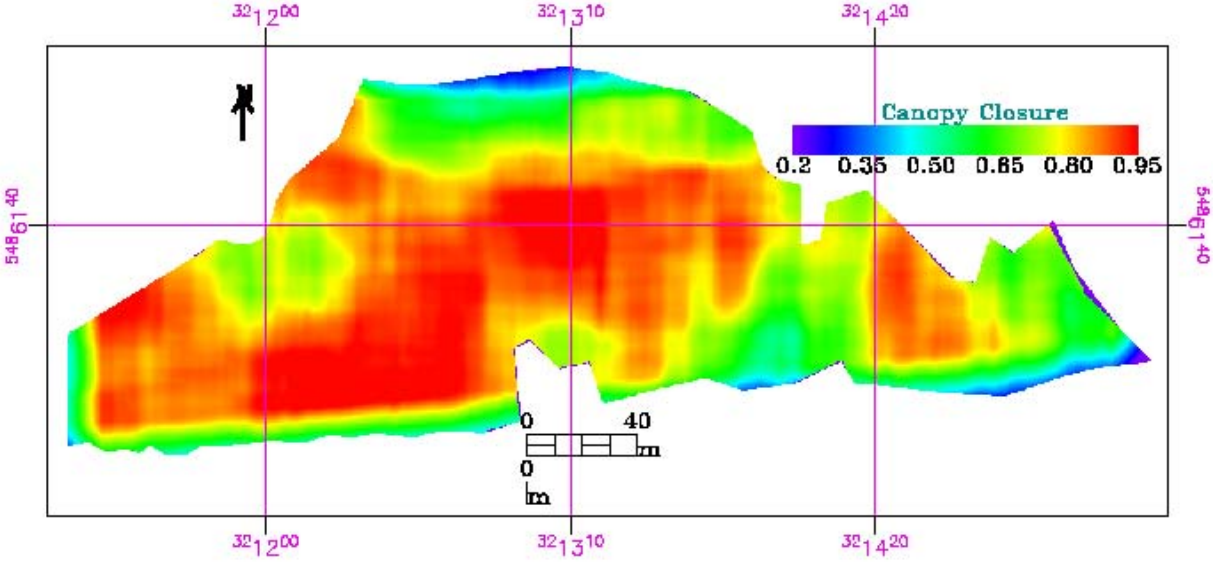

Figure 18. Map of the canopy closure of the mature experimental Norway spruce forest stand.

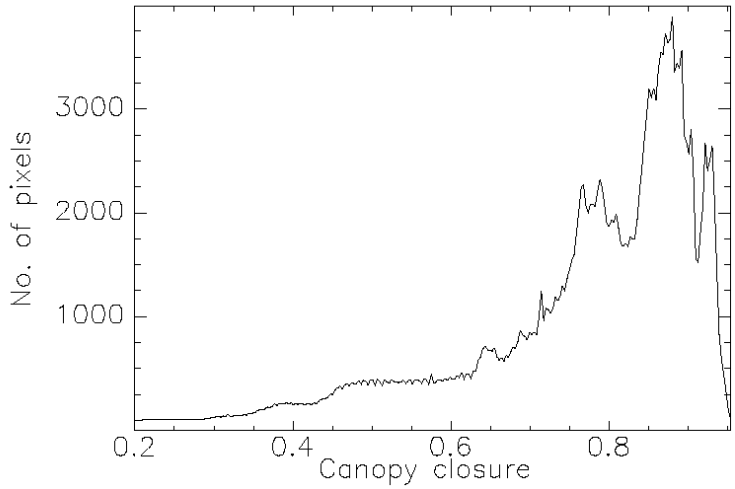

Figure 19. Canopy closure frequency distribution of the mature Norway spruce stand computed at a sliding window size of 99 by 99 pixels (pixel resolution = 0.4 m).

Almost all pixels of lower canopy closure value (Figure 18) were located around the periphery of the stand. This may be due to the edge effect of the processing using a zero-padding at the edges to move the sliding window through the image. This zero-padding, adding more zero values into the sliding window of the edge pixels, lowered proportion of crown pixels within the window and consequently introduced uncertainty into the inversion process for these edge pixels. The problem was exacerbated by the large size of the moving window. Reducing the window size can scale down the edge effect significantly.

4.4. DART parameterization and simulation

4.4.1. DART parameterization

Tree structural parameters

The DART parameterization needs compromise between the scene dimensions and computational time requirements. Our experimental area was represented by heterogeneous forest of many trees, however, due to limitation of computer capacity we were forced to build up a DART scene containing only three trees. To keep heterogeneity high as much as possible, the representatives were selected carefully to reproduce trees of three social positions. The basic information about the trees is illustrated in Table 8. Still, it is worth mentioning that representing such a heterogeneous forest stand with very small number of trees could strongly affect the inversion procedure by decreasing the accuracy of the simulated canopy reflectance (Gastellu-Etchegorry et al. 2003).

Table 8. Basic structural parameters of the three representative trees used for DART simulation (all units are in meter).

Tree type (social position)	Tree DBH	Total tree height	Stem length below crown	Stem length within crown	Diameter below crown	Diameter within crown	Live crown height	Live crown bottom radius
Suppressed	0.51	33.60	11.6	20.1	0.42	0.33	22.0	2.7
Co-dominant	0.45	36.80	20.0	14.6	0.36	0.26	16.8	2.7
Dominant	0.52	39.20	26.8	10.0	0.42	0.31	12.4	2.4

Certain modifications were made on stem length and crown top diameter, since no crown shape that would appropriately represent the mature Norway spruce crown was available in the DART model. As noted in section 3.4.5 the top crown diameter was set to zero and the stem length was reduced by 6 % to avoid the trunk from being too thick at the top. In spite of these adjustments the trunks were visible on DART simulated images. This can be explained by the truncated cone crown shape with thin elongated crown top created by few leaf turbid cells, which were not able to hide the top part of trunk. Therefore, the stem length was further shortened until its effect on the simulated image disappeared. The crown shape alteration obviously influenced the reflectance value of the simulated canopy. A study by Rautiainen *et al.* (2004) also pointed out the effect of crown shape on simulated reflectance. Their study confirmed that crown shape has influence on retrieval of LAI since it determines the portion of sunlit ground vegetation, and also the spatial distribution of foliage within the canopy. The change in crown shape may affect the most important geometric structural characteristics like the size, shape, 3D-distribution and orientation of foliage elements, which have equal importance to optical property of the canopy (Nilson et al. 2003).

Only live crown parts were simulated within DART simulation of this study. However the spruce trees have considerable parts of dead crown covered by lichens, dry twigs and branches that might affect the optical property of the canopy. For higher reliability of simulated canopy reflectance, the dead branches and twigs should be considered too.

Leaf optical properties

The optical properties of the needles in the DART scene were partially simulated by the PROSPECT model (**c**, and **c+1**) and partially measured (**c+2** and **c+3** age classes). The weighted average hemispherical reflectance and transmittance for each functional crown part was computed using the age class distribution, listed in Table 9 as weight.

Table 9. Age class distribution (%) of the needles used in DART simulation computed from destructive sampling of the branches from representative trees at Kykulka site (Beskydy Mts., Czech Republic).

Crown functional part	Age classes				
	c	c + 1	c+2	c+3	r
Saturation	20.7	26.7	17.9	10.8	24.0
Productive	22.7	31.8	19.9	11.0	14.6
Juvenile	46.3	31.4	12.3	5.9	4.1

Figure 20 illustrates the resulting hemispherical directional reflectance and transmittance of each functional crown part. The optical property of the saturation and the productive parts were quite similar, because the needle age difference in these crown parts was not significantly different. The highest difference between these two functional crown parts was found in the last age classes (Table 9). However, the output from the PROSPECT model adjusted to simulate age class **c+3** was used to simulate the age class **r**, which narrowed the difference in optical property among the functional crown parts. The juvenile needles have slightly higher reflectance and transmittance than the others across the whole wavelength.

It should be noted that merging of the last two age classes could reduce the heterogeneity among the crown functional parts and lead to a potential error in the LAI inversion process. Besides, the age class distributions were collected at another nearby Norway spruce forest stand. From figure 21 one can observe how optical properties varied among different age class from two mature Norway spruce tree shoot types. The difference is more pronounced in the first two age classes.

The optical properties of the Understory, represented by plots of grass Calamagrostis villosa over the bare soil as described in section 3.4.10, are illustrated in Figure 22. The leaf area of the Understory vegetation was made to vary between open and closed canopies. An Understory LAI of 3 was used for 50%, 60%, 70% and 80% canopy closures and LAI of 2.5 for the remaining since the density of Understory vegetation decreases when the canopy is more closed. The Understory should be carefully represented particularly in the scene with open canopy, since its effect is more enhanced there. A study by Erikssona *et al.* (2005) in Sweden, indicated that the influence of the ground cover on LAI retrieval of dense oak stands (LAI around 5) was minor (within 0.3 units) while it was major (within 2 units) in case of sparse stands (LAI around 2). However, due to time limitations and data constrains we used only one vegetation type for the Understorey, which could

be another uncertainty source in the process. To achieve a reasonable accuracy at least major Understory vegetation functional types should be represented in the scene.

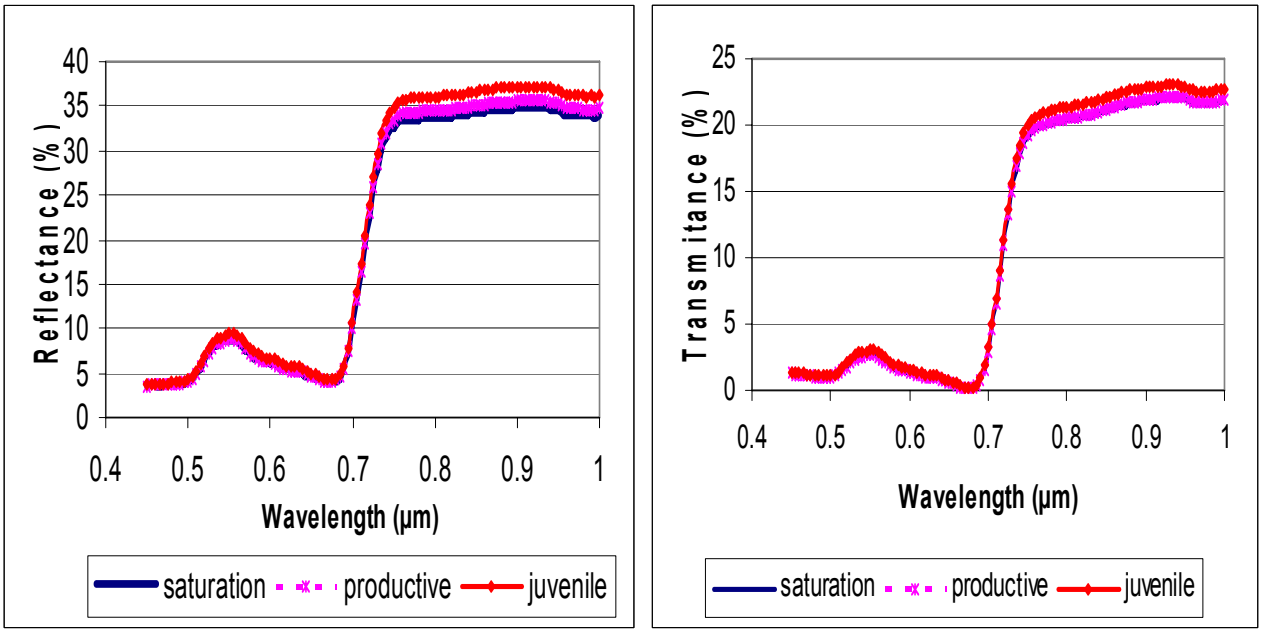

Figure 20. Hemispherical directional reflectance (left) and transmittance (right) of the saturation, productive and juvenile functional crown parts of mature Norway spruce trees as measured and computed by the PROSPECT model and used in DART simulations.

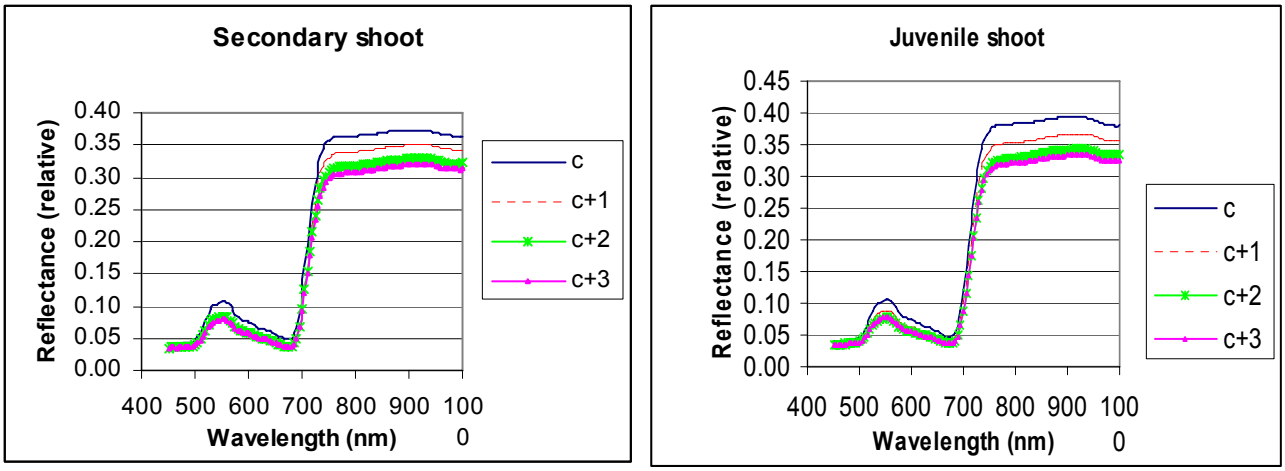

Figure 21. Hemispherical directional reflectance of needle of four age classes from juvenile and secondary shoots of mature Norway spruce trees as measured and simulated in PROSPECT model.

Due to the occurrence of senescent needles covering the stand floor, the reflectance values of this type of background was considered in the scene by constructing rectangular plots around each tree trunk. Although, the senescent needles were found in circular pattern, the current DART version allows only rectangular and/or triangular plot shapes. Trunk and branch bark optical properties were taken from measurements of these surfaces at the Sumava Mts. (2003), assuming no significant difference between the two sites. Their reflectance signatures are shown in Figure 23.

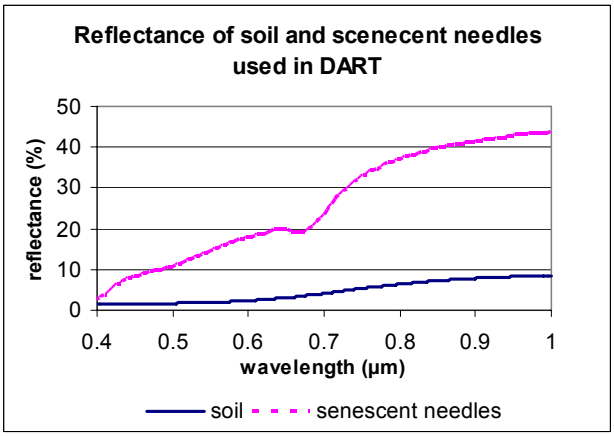

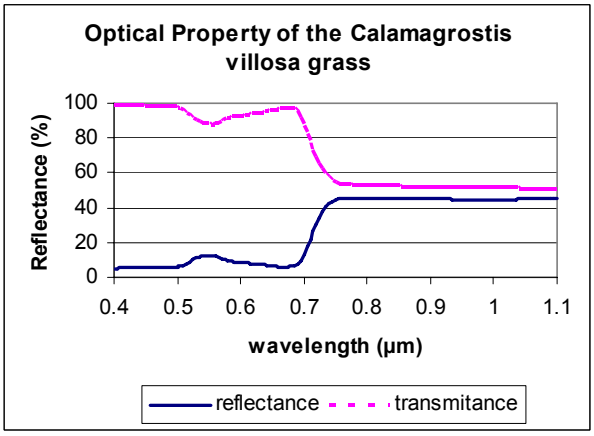

Figure 22. Optical properties of soil, senescent needles and Understory vegetation of the mature Norway spruce stand used as DART input.

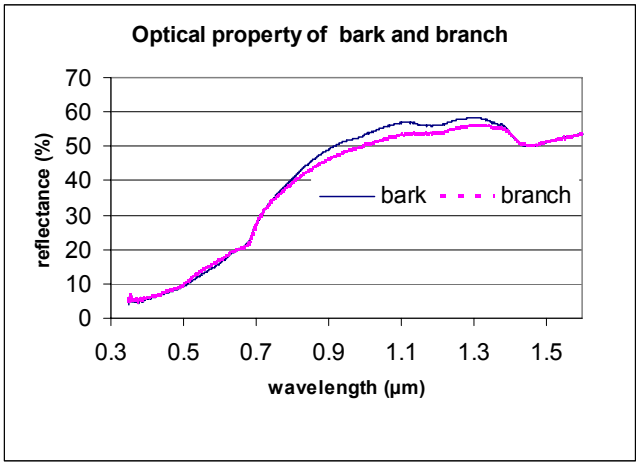

Figure 23. Optical properties of trunk and branch bark for mature Norway spruce trees used as input in DART.

4.4.2. DART simulations

Figure 24 illustrates two examples of the DART top of canopy reflectance images. The images resolution of 0.2m allows clear distinction of the spruce crowns from the Understory. The model provided a set of 11 nadir and different oblique images for each band of the given scenario. However, in this study we used for the LAI inversion only the nadir images. The nadir view images of four spectral bands for each defined LAI and eight canopy closures were used to build the spectral LUT.

This phase is the most time consuming part of the whole process. The images have to be thoroughly investigated to make sure that they have precisely fit the AISA image. It is also the crucial step that determines the accuracy of the inversion. It was proved that construction of the main branches improved the correlation between the DART simulated and AISA hyperspectral images to a large degree. Their presence increased the absorption within the canopy and reduced the proportion of the reflectance. Therefore, one can expect better results if the branches of lower

order and small twigs would be also included. To compensate the absorbance effect of these missing woody materials we applied the spherical LAD which lowered canopy reflectance compare to other LAD types. This way the canopy reflectance of the DART simulated images became comparable within the reflectance range of the AISA image data.

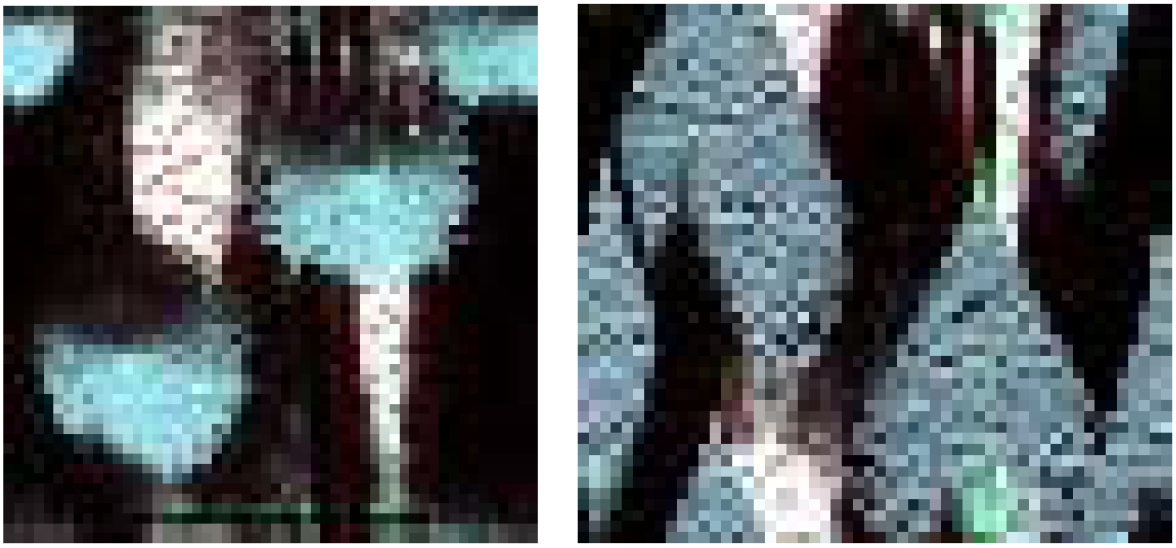

Figure 24. One of the 200 DART output image sets. Nadir view (left) and oblique view (right) of a 50% canopy closure with LAI = 5. Both images are RGB color composite of band 48, band 27 and band 13. The Glacier blue in the nadir view image represents the Norway spruce crowns, the Pearl white represent the sunlit ground cover and the dark color represents shaded area of the scene.

The simulated images were further aggregated from 0.2 m to 0.4 m pixel size in order to reproduce the spatial resolution of the AISA hyperspectral image. Unfortunately, this operation caused lost of information since certain pixels had to be dropped to bring the resampled images of odd matrix size to even numbers of rows and columns.

The extracted average reflectance signatures of shaded and sunlit crown pixels related to LAI per canopy closure are presented for the spectral band 13 (540.8nm) and band 35 (745.45nm) in figure 25. See appendix 4 for the signatures of two remaining bands. From these figures one can see that reflectance of crown parts decreases with increasing LAI in both the VIS and NIR region of the spectra. However, the rate of LAI decrease was smaller, especially for higher LAI values. In some cases of the shaded crown parts the difference in reflectance due to both canopy cover and LAI change became insignificant. This can be attributed to saturation. It is important to note that the extraction of the sunlit and shaded crown reflectance was made based on the masks created by visual classification over the false color RGB combination of three spectral bands. Therefore, the accuracy of this separation was greatly dependent on interpreter judgment. To some extent the deviations and overlaps between reflectance signatures for different canopy closures in figure 25 could be explained by the subjective errors of the operator. It would be more objective to use an automatic separating mechanism to avoid such biases.

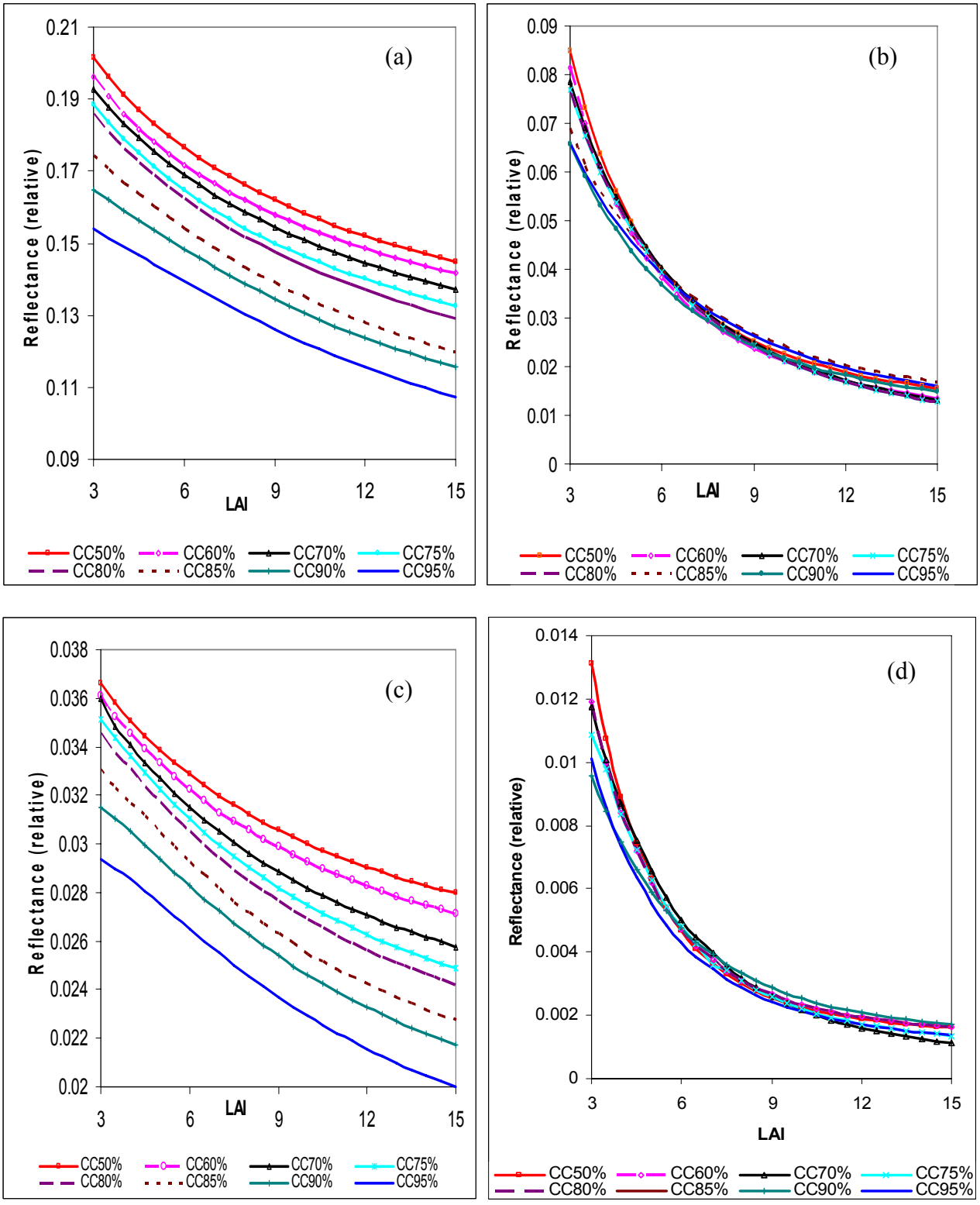

Figure 25. Sunlit and shaded DART simulated crown's reflectance. Graph (a) and (b) represent the sunlit and shaded crown spectral signature in the NIR region (band 35 (745.45nm)) and, (c) and (d) represent the sunlit and shaded crown spectra in the VIS part (band 13 (540.8nm)) of the AISA hyperspectral image).

All the extracted reflectance values of the shaded and sunlit crown parts were used to establish the spectral LUT. Also the canopy closure was considered as a variable and stored in the LUT. We have considered the sunlit and shaded crown reflectance as separate entities, because size of our sample set required for the next methodological step (training of the ANN) was limited. This increases the complexity of the input data so the ANN could get more time to generalize the input output relationships before it would be stopped forcefully to prevent the network overfitting. However, due to the time constrains we did not validate robustness of this method against the others (e.g. using ratio of the crown part's reflectance) which could help to choose better approach. According to Figure 25b and 25d the reflectance of shaded crown part did not show a clear trend for change in LAI across the different canopy closures. Therefore, it may be interesting to test the LAI inversion based on the reflectance value of the sunlit crown only, if sufficiently large dataset for the ANN training would be available.

4.5. LAI inversion using Artificial Neural Network (ANN)

Appropriately trained ANN enables mapping of the output variable if the apparent relationship exists between a set of inputs and corresponding outputs. Parallel to this the spectral LUT build in section 4.4 were organized in such a way it fits the data format of neural network. A feed forward backpropagation neural network method was applied on the two LUTs (one with noise and the other without noise) to create the relation between stand crown's reflectance and LAI. The results are presented and discussed in the following sections.

4.5.1. Training

Training of an ANN is the toughest step of the inversion process. If ANN is not trained correctly it could affect the accuracy strongly and may lead to wrong results. As described in section 3.5 we divided our LUT data into training, validation and testing datasets, which is very important to prevent overfitting of the ANN. The training error estimated per the dataset in the LUT with out noisy is depicted in Figure 26.The errors of the testing dataset are between the training and the validation errors. This indicates suitable division of the input data among the three sets. The major task of the training phase was to determine the number of hidden layers, the number of nodes in those layers and the optimum range for weights and bias.

A number of neural network training tests were done by alternating several possible parameter combinations. Several set-ups combining a number of hidden layers with number of their nodes, training algorithms, weight initialization combinations, as well as input and output encoding/normalization mechanisms and overfitting control methods were tested and validated for their performance. The mean square error (MSE) and linear regression correlation coefficients were used to compare performance of the different network architectures. In all cases the parameters were very close to the expected value, the correlation coefficient (R) and the linear line slope (m) were near to 1 and the MSE was close to zero. Figure 28b and 28c shows the scatter plot of the predicted LAI against the trained target LAI with/without regularization on noise added LUT, respectively. The ANN trained without regularization had the highest correlation coefficient with the regression line close to one (0.999) and bias term (b) near zero (0.0168). But the validation of estimations made by such networks showed a very poor correlation to the ground

truth data. This proved the presence of the ANN overtraining. Consequently, we applied the early stopping regularization method to reduce this overtraining problem.

After series of preliminary tests the architecture of the neural network was defined to be a single hidden layer with 11 nodes for both LUTs. Previous studies have also showed that a single hidden layer is enough for inversion of canopy biophysical variables (Combal *et al.* 2003; Danson *et al.* 2003; Fang and Liang 2003). The training was very fast and stopped before 100 iterations. Use of more hidden nodes is advisable to reduce the danger of the learning process stopping at the local minimum of the error function. That is why we used more hidden nodes. Besides, we set the learning rate and the momentum terms to relatively higher values, so that the training converges as slowly as possible.

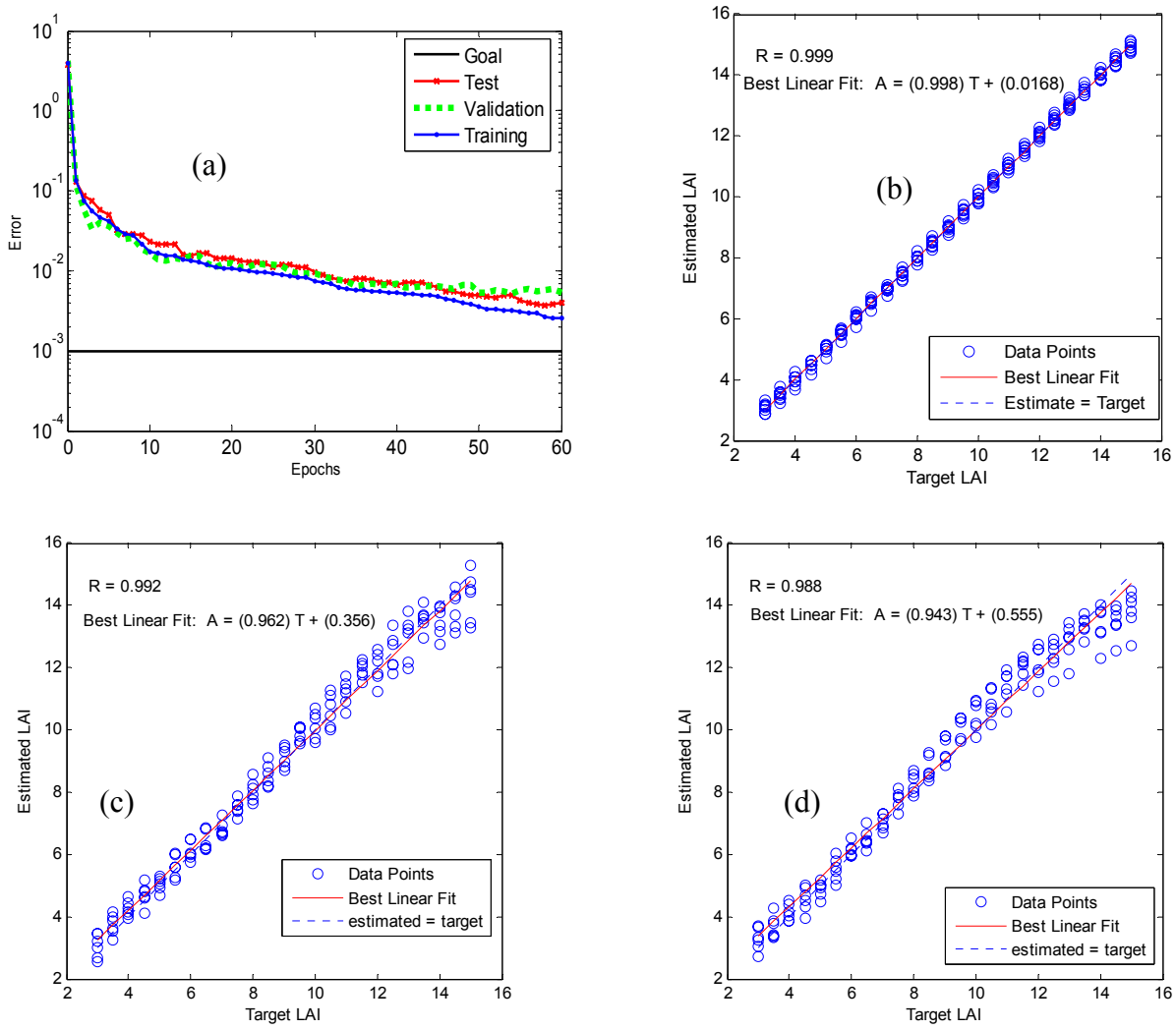

Figure 26. The error level of the training, validation and testing datasets during the training phase of a LUT with out noise (a), the scatter plot of the network estimation trained without early stopping (b) and scatter plot of estimates made on a network trained with early stopping method on data set with noise (c) and without noise (d) compared to the target LAI values.

Determination of the optimum numbers of hidden layer nodes, weight ranges, learning rate, and momentum terms was not an easy one. In our case the training problem was a matter of reducing the risk of overfitting. Even use of the early stopping method to reduce the risk of overfitting resulted finally in very poor results in some cases. We have observed variations in the results for each network initialization due to the randomness of the weights and biases. In each initialization the network starts from different error surfaces which can lead to different predictive accuracy (Kavzoglu and Mather 2003)

Unfortunately, there is no a straight forward way how to define the desirable range of weight and bias terms. It is always based on a trial/error approach. We initialized the ANN with different ranges for weight and bias starting from the wider [-3 3] up to the narrower [-0.01 to 0.01]. We have even tried weights of all positive [0 1] and all negative [-1 0] values. Finally, we found the range [-1 1] the most appropriate one for our case. This range was also used by Combal *et al.* (2003) for LAI , Chlorophyll content and fAPAR retrieval.

We also tested performance of many of the training algorithms available (e.g. Levenberg-Marquardit (trainlm), Scaled Conjugate Gradient (trainscg) and Resilient Backpropagation (trainrp) optimization algorithms and Automated Regularization (trainbr)). The previous studies (Combal *et al.* 2003; Danson *et al.* 2003) recommended trainlm as the best performing algorithm for LAI estimation. However it was not the case in our study, even if we increased the learning rate, the momentum, momentum increase and decrease terms to higher values as suggested by Demuth and Beale (2005). The ANN training stopped always after few iterations (< 50 epochs). This may not give the ANN enough time to create a proper relationship between the input and the target dataset. The reason of poor performance of this algorithm was most probably the early stopping. Therefore, we rather implemented the optimization algorithm trainscg, which converges slowly compared to others. It increases the number of the iteration and the error is relatively low.

In general, the training with noisy data showed better performance than training with out noise LUT (figure 26c and 26d). It converged slowly and runs for more iterations. The MSE (0.22306) is lower than the training without noise data (0.33019).The coefficient of correlation and bias are also better in this case. However, it is not possible to conclude about its accuracy before validation with ground truth data is made.

4.5.2. LAI retrieval using trained ANN

Once the training is completed the inversion by ANN is very fast and simple. The reflectance of sunlit and shaded canopies in four spectral bands (simulated also by DART) was extracted from the AISA hyperspectral image using the masks derived from the classification (see section 4.2). To facilitate the LAI inversion validation, the sunlit and shaded crown reflectance of the hyperspectral image was averaged within a sliding window of 39.6 by 39.6 m in size, which was approximately equal to the window of the hemispherical photography processing in CAN-EYE. The average canopy reflectance of selected bands and the canopy closure of the stand were organized in the same style as the training dataset. Afterwards they were feed into the ANN of the two cases: i) ANN trained without noise (case 1) and ii) ANN trained with noisy input dataset (case 2). The maps of the LAI inverted by both ANNs are presented in figure 27. Table 10 shows the summary

Table 10. Summary statistics of the mature Norway spruce stand LAI retrieved by the two ANN trainings.

Case	Min	Max	Mean	Std
1	3.34	7.3	5.52	0.602
2	3.44	8	5.62	0.77

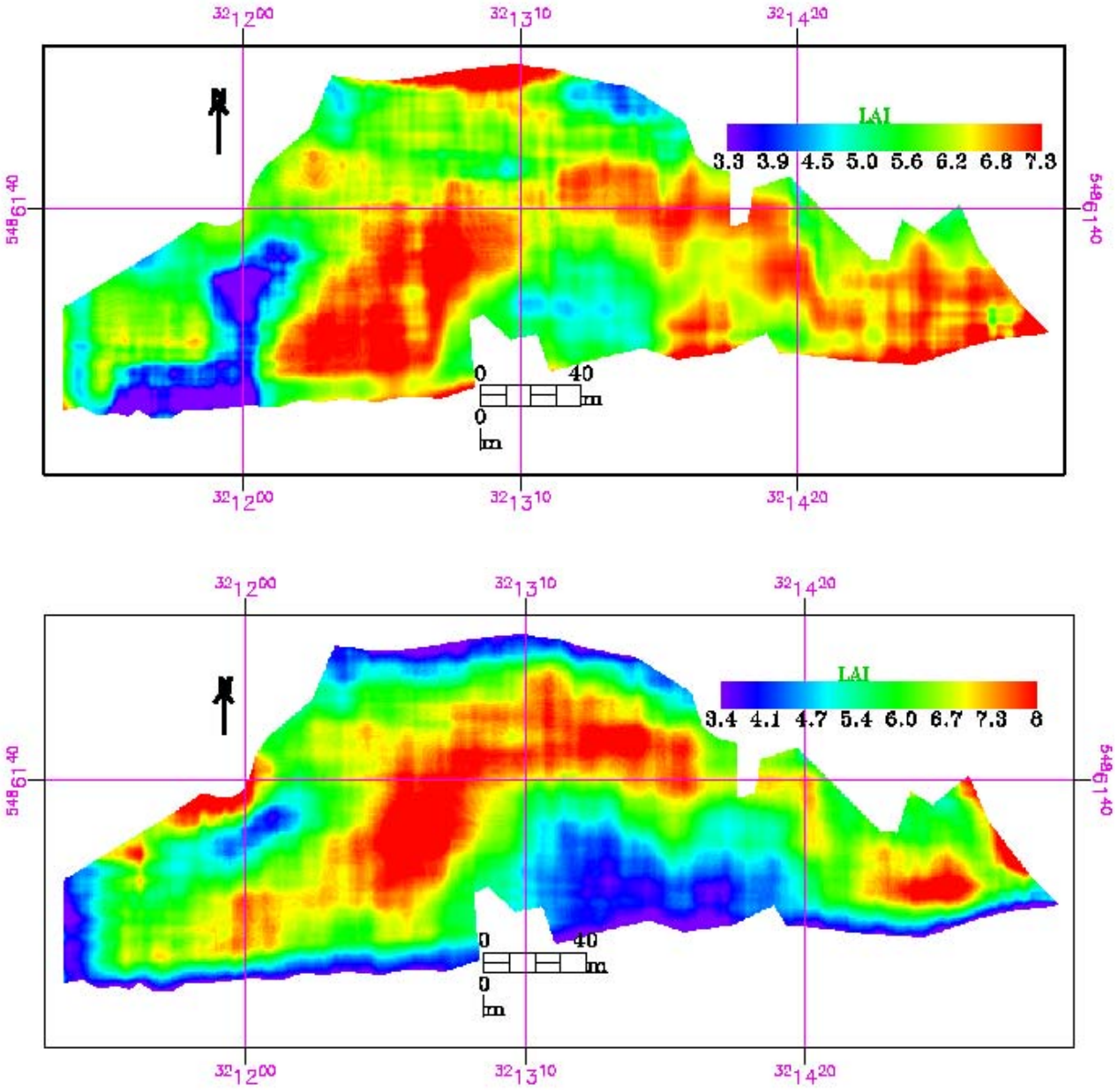

Figure 27. The LAI maps of the experimental Norway spruce stand retrieved by ANN trained without addition of the noise (upper) and by ANN trained using a noisy dataset (lower). The maps have the same resolution (0.4m) and the map projection as the AISA hyperspectral image. Each pixel represents LAI of the window 39.6 x 39.6 m around the pixel.

statistics of both cases. The mean leaf area index of the stand was inverted to be 5.52 and 5.62 with standard deviation of 0.6 and 0.77 in case 1 and case 2, respectively. The difference of the mean LAI of the two cases is minimal, but LAI spatial distributions were different, most probably due to the noise added to the training dataset in case 2. It should be noted that the aim of adding noise to the training dataset was to introduce real signal-to-noise ratio into the DART simulated spectral reflectance, which should eliminate radiometric difference between the simulated and real hyperspectral images.

4.6. Validation

The LAI computed from the effective LAI of hemispherical photography and clumping index (Ω_E) of the TRAC field measurements was used to validate the retrieved LAI. Since the LAI retrieval was made at the same resolution as the hemispherical photography processing, the LAI values could be compared per individual pixel of both LAI maps. However, many of the validation points lied on the pixel's border. Thus the average of four neighboring pixels was considered as the representative LAI to avoid the errors due to geo-referencing.

The ground truth and estimated LAI were compared by means of the Pearson correlation coefficient (Table 11) and the RMSE. The results of both cases showed a significant correlation with the ground truth LAI. Case 1 had better correlation (R = 0.73) than case 2 (R = 0.66). However, case 2 showed lower RMSE of 1.84 compared to case 1 (RMSE = 2.33). From the scatter plots in figure 28 one can observe that in both inversion cases the minimum LAI was about 5 while the ground truth LAI reached 3.6. Clearly, this one low LAI value was overestimated, while higher ground truth LAI values were underestimated. The maximum estimated LAI was below 8 while the ground truth LAI reached up to 11.2. The coefficient of determination indicated that LAI was slightly better determined in case 1 (r^2 = 0. 54) than in case 2 (r^2 = 0.44).

Table 11. Pearson correlation coefficient (R) computed between the LAI retrieved within the two cases and measured ground truth LAI.

Case	Samples mean	R	Sig.
1	5.7	0.734	0.000
2	6.5	0.664	0.000
Ground truth	7.6	NA	NA

Many studies revealed that the physical models represent the most appropriate way for biophysical variable estimation and can estimate LAI to a RMSE ≤ 1 (Gong *et al.* 1999; Kimes *et al.* 2002; Combal *et al.* 2003; Gascon *et al.* 2004). Although, we found a certain level of correlation between the estimated and the ground truth LAI measurements, it was not strong enough as we expected. This lower accuracy may be attributed to the number of following factors.

The accuracy of the estimation greatly depends on the computer representation of the forest stand (3D scene) in a radiative transfer model and on the inversion process itself. In order to obtain accurate inversion products, the canopy reflectance must be simulated within a wide range of the key model input parameters. Since our forest stand was very heterogeneous it should be simulated

with more than three representative trees, but due to the time and computer capacity constraints we simulated only very limited number of trees. Gastellu-Etchegorry *et al.* (2003) investigated the effect of the number of trees in a scene on simulated reflectance. He created two scenes, one with only one tree and the other one with four trees, keeping all other parameters same.

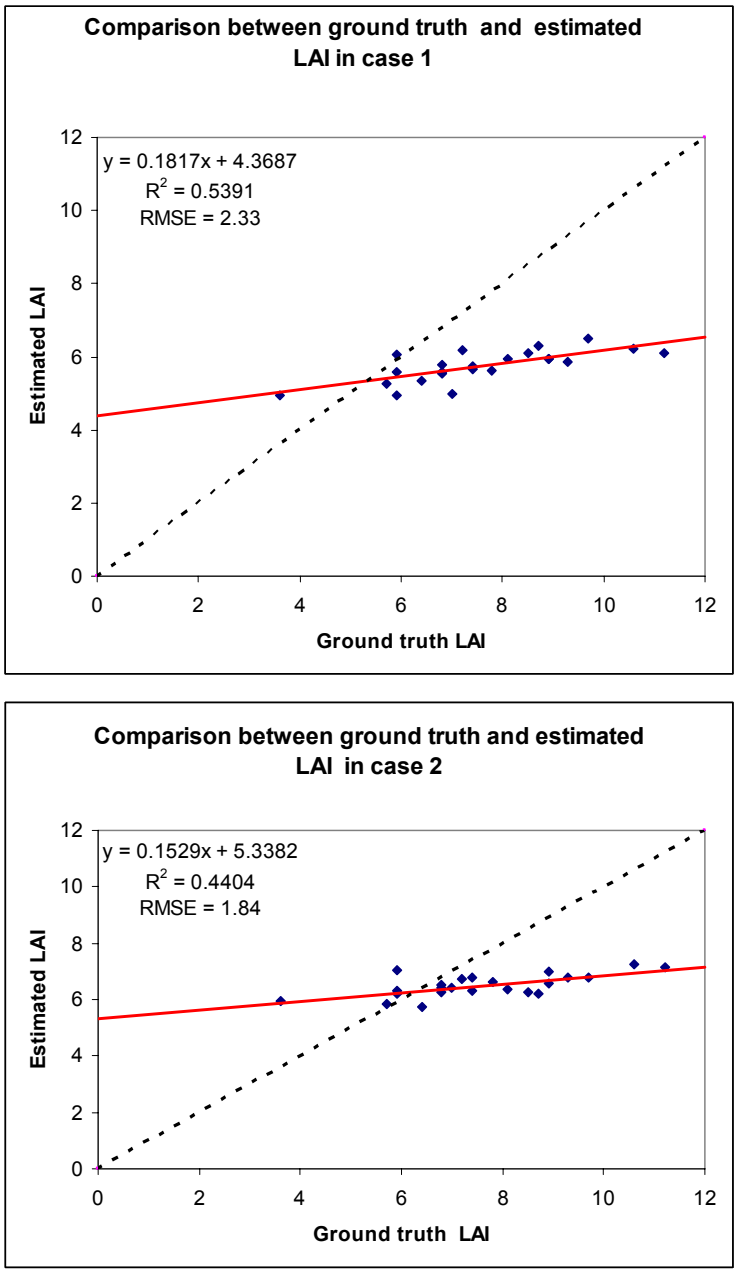

Figure 28. Comparison of the LAI estimated within two cases: i) without noise (upper) and ii) with noisy data (lower), compared against the ground truth LAI computed from the hemispherical photography and TRAC clumping measurements.

The results showed that the reflectance of the scene with only one tree fluctuated across different view angles, which was not the case in four tree scene, so he recommended using more trees. Variability in canopy structure has dominant influence on the canopy reflectance(Asner 1998). The

larger and more heterogeneous the vegetation element or stand, the more complicated measurement of scattering properties of it becomes. The reasons are the geometrical factors playing a major role in modifying forest stand reflectance and transmittance (Rautiainen 2004). Therefore, the forest stand should be simulated by more trees located according to their real distribution, so the simulated BRF would be more accurate.

The next source of uncertainty in our modeling approach was representation of crown shape. The shape of the crown determines the volume and spatial distribution of the needles within the crown. Rautiainen et al. (2004) studied the effect of crown shape on the reflectance of Norway spruce stand. For higher values of LAI, stands with conical crowns had much smaller reflectance than ellipsoid crowns. Gascon *et al.* (2004) indicated the importance of crown shape particularly when dealing with a very high spatial resolution images. In our case the adult trees had relatively wide surface at the top of crown and so the cone did not reproduce the crown shape credibly. Due to conical crown shape the needles were more clumped together increasing within shoot light scattering and influencing the canopy transmittance and reflectance. Better approximation of the crown shape of Norway spruce trees should be a combination of cone at the top with cylinder at the bottom.

The possible reason for overestimation of lower LAI values can also be the Understory vegetation. The model retrieval could mix spectral response of the Understory leaves with the Norway spruce needles. The contribution of Understory reflectance to coniferous stand reflectance was reported to be higher than for broadleaved forests, ranging from 0 to 95% for LAI values below 5 (Rautiainen and Stenberg 2005). In this study we observed that the reflectance of the crown decreases as the value of LAI increases. Therefore it is possible that the Understory represented by homogenous vegetation (one grass type) could undervalue the forest canopy reflectance, which would shift the estimated LAI to higher values. The effect of the Understory is highly important for open canopy. Hu *et al.* (2000) investigated the effect of Understory reflectance on the retrieval of canopy LAI from CASI hyperspectral image data in Canada using the FLIM model. Their results revealed that the correlation coefficient between the field-measured and retrieved LAI under the assumption of a uniform Understory reflectance was about 0.27, but it increased to 0.78 when the Understory reflectance was allowed to vary within the range of the mean value plus or minus its standard deviation obtained from field measurement.

As described in previous literature, the underestimation of higher LAI values could be related to saturation when reflectance remained constant or changed insignificantly for LAI value above 6 or 7 (Gastellu-Etchegorry *et al.* 1999). We have observed this problem particularly in the shaded crown parts. Excluding the information of the shaded crown parts or making the average or ratio of the sunlit and shaded crown may help to reduce the saturation problem.

Because of absence of information about the experimental Norway spruce stand we had to use some parameters collected from other spruce stand of similar age and status. The distribution of needle optical properties and determination of the holes within the crowns was based on data collected from a near by forest. Although, the stands were of the same age and species they could differ in site conditions. The DART simulations were also made without second order branches and twigs. As well there were other tree species in the forest stand which were not included in the

DART scene. As a result, the simulated forest stand reflectance may not reproduce the AISA image reflectance accurately and lead to a systematic error in the inversion process.

Another uncertainty source is represented by training of the ANN. Because our training data set was limited to 200 samples, in order to prevent the overfitting problem we used the early stopping mechanism. This could stop the training phase too early, before it generalizes the overall relation between the input and output data. Further more, the division of the input data into the training, validation and testing sets could cause failure of the training dataset to represent all the variability within the stand. Increase in the number of input samples and training without regularization algorithm could reduce this potential error.

Also the ground truth LAI data were not free of error. They might suffer from gap fraction saturation for LAI above 5 or 6 (Gower *et al.* 1999) . We used the combination of two optical instruments to reduce this problem and improve the accuracy. However, these measurements were taken in different time, so change of LAI throughout time, due to a disease and other environmental factor, may initiate the loss of needles and introduce certain error to the ground measurements.

The AISA image reflectance to certain extent is inaccurate due to the noise presence and errors in pre-processing (i.e. radiometric and atmospheric corrections, etc). We introduced a random artificial sensor noise into the DART simulated images as prior information, however, the uncertainty of the absolute sensor calibration and the correction procedures over the image could create systematic quantitative differences between the simulated and AISA acquired image reflectance.

Finally, the spectral bands used for retrieval also play important role. The number of spectral bands selected for the inversion may affect the output accuracy as shown by Weiss et al. (2000) Their results suggested 6 spectral bands as the optimum number for LAI retrieval (see figure 29). Too low and too high number of bands reduced the prediction accuracy. It is not only the number of bands but also their wavelength position that affects the variable prediction. Therefore, next time sensitivity analysis should be carried out to determine most appropriate combination of bands towards accurate LAI estimation.

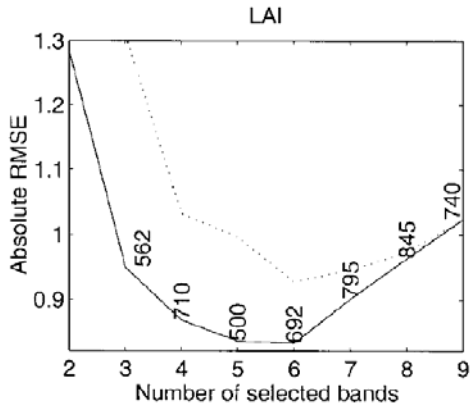

Figure 29**.** Effect of number of selected spectral bands on LAI retrieval accuracy according to Weiss *et al.* (2000): the solid line corresponds to the best band combination and the doted line to the worst combination.

5. Conclusion and recommendations

This study carried out LAI estimation of a mature Norway spruce stand from airborne hyperspectral image by inverting the 3D (DART) radiative transfer model using the Artificial Neural Network method. The overall performance of the retrieval method was validated using combined ground measurements of two optical instruments.

We demonstrated that the combination of the TRAC and hemispherical photography can be used for better ground based LAI estimation. The comparison of the two optical instruments suggested LAI underestimation by the TRAC instrument. However, the TRAC measurements were done over limited number of sampling transects, so this method needs further validation in the future. One of the main advantages of the combined LAI measurement method is reduction of the canopy gap fraction misestimating which is particularly important in dense canopy. The hemispherical photography was proven to be an appropriate method to measure effective LAI, while the TRAC device is more reliable in determining the clumping index of elements larger than foliage as also proved in previous studies (Chen and Chiller 1995; Chen *et al.* 1997).

An Artificial Neural Network of single hidden layer with 11 nodes and tan-sigmoid transfer function along with one out put layer with linear transfer function was found to be the best set-up for retrieval of the mature Norway spruce stand LAI. The LAI computed for the whole stand from the AISA hyperspectral image showed a good Pearson correlation with the ground measurements. However, spatial distribution of LAI values was not appropriately estimated which indicates necessity to improve the retrieval method. The results indicate that shaded crown parts carry less information for the retrieval than sunlit crown parts. Their reflectance was saturating for higher LAI values. Hence, avoiding the shaded crowns information or using their reflectance derivates could improve the accuracy of the method.

Choosing the appropriate artificial neural network architecture and optimization algorithms were time consuming and challenging tasks of this retrieval method. The study demonstrated the potential risk of a poorly trained network. The neural network approach needs to be further validated for its sensitivity to errors in remotely sensed optical data before its full potential can be exploited.

Finally, there were several problems concerning the parameterization and simulation with the Discrete Anisotropic Radiative Transfer model. The model requires a large set of input parameters, and it is quite difficult to measure reliably all the model inputs at the same time. The large amount of input parameters indicates how complex the relation between forest stand parameters and reflectance is. The inversion of the radiative transfer model to estimate forest parameters can effectively work only, if the simulated and measured reflectance does not have strong systematic differences. The effect of each input parameter should be investigated. Consequently, some inputs of less importance could be simplified and others with high influence (e.g. crown shape) should be incorporated in better of more detailed way.

6. References

Anonymous. (2004, October 2004). "MANUEL DART."

Asner, G. P. (1998). "Biophysical and Biochemical Sources of Variability in Canopy Reflectance." Remote Sensing of Environment **64**(3): 234-253.

Barclay, H. J., J. A. Trofymow and R. I. Leach (2000). "Assessing bias from boles in calculating leaf area index in immature Douglas-fir with the LI-COR canopy analyzer." Agricultural and Forest Meteorology **100**(2-3): 255.

Baret, F. and G. Guyot (1991). "Potentials and limits of vegetation indices for LAI and APAR assessment." Remote Sensing of Environment **35**(2-3): 161-173.

Baret, F. and M. Weiss (2004). CAN_EYE: Processing digital photographs for canopy structure characterization, INRA, Avignon, France.

Battaglia, M., M. L. Cherry, C. L. Beadle, P. J. Sands and A. Hingston (1998). "Prediction of leaf area index in eucalypt plantations: Effects of water stress and temperature." Tree Physiology **18**(8-9): 521.

Brand, D., G (1987). "Estimating the surface area of spruce and pine foliage from displaced volume and length." Can. J. For.Res **17**: 1305–1308.

Bruniquel-Pinel, V. and J. P. Gastellu-Etchegorry (1998). "Sensitivity of texture of high resolution images of forest to biophysical and acquisition parameters." Remote Sensing of Environment **65**(1): 61-85.

Chason, J. W., D. D. Baldocchi and M. A. Huston (1991). "A comparison of direct and indirect methods for estimating forest canopy leaf area." Agricultural and Forest Meteorology **57**(1-3): 107-128.

Chen, J. M. (1996). "Optically-based methods for measuring seasonal variation of leaf area index in boreal conifer stands." Agricultural and Forest Meteorology **80**(2-4): 135-163.

Chen, J. M. and T. A. Black (1991). "Measuring leaf area index of plant canopies with branch architecture." Agricultural and Forest Meteorology **57**(1-3): 1-12.

Chen, J. M. and T. A. Black (1992a). "Defining leaf area index for non-flat leaves." Plant, Cell & Environment **15**(4): 421-429.

Chen, J. M. and T. A. Black (1992b). "Foliage area and architecture of plant canopies from sunfleck size distributions." Agricultural and Forest Meteorology **60**(3-4): 249-266.

Chen, J. M. and J. Cihlar (1995). "Quantifying the effect of canopy architecture on optical measurements of leaf area index using two gap size analysis methods." IEEE Transactions on Geoscience and Remote Sensing **33**(3): 777.

Chen, J. M. and J. Cihlar (1996). "Retrieving leaf area index of boreal conifer forests using Landsat TM images." Remote Sensing of Environment **55**(2): 153-162.

Chen, J. M., C. H. Menges and S. G. Leblanc (2005). "Global mapping of foliage clumping index using multi-angular satellite data." Remote Sensing of Environment **97**(4): 447.

Chen, J. M., G. Pavlic, L. Brown, J. Cihlar, S. G. Leblanc, H. P. White, R. J. Hall, D. R. Peddle, D. J. King and J. A. Trofymow (2002). "Derivation and validation of Canada-wide coarse-resolution leaf area index maps using high-resolution satellite imagery and ground measurements." Remote Sensing of Environment **80**(1): 165.

Chen, J. M., P. M. Rich, S. T. Gower, J. M. Norman and S. E. Plummer (1997). "Leaf area index of boreal forests: Theory, techniques and measurements." Journal of Geophysical Research **102**(D24): 29,429-29,443.

Cohen, W. B. and C. O. Justice (1999). "Validating MODIS terrestrial ecology products: Linking in situ and satellite measurements." Remote Sensing of Environment **70**(1): 1-3.

Colombo, R., D. Bellingeri, C. M. Marino and D. Fasolini (2003). "Retrieval of leaf area index in different vegetation types using high resolution satellite data." Remote Sensing of Environment **86**(1): 120.

Combal, B., F. Baret and M. Weiss (2002). "Improving canopy variables estimation from remote sensing data by exploiting ancillary information. Case study on sugar beet canopies." Agronomie **22**(2): 205.

Combal, B., F. Baret, M. Weiss, A. Trubuil, D. Mace, A. Pragnere, R. Myneni, Y. Knyazikhin and L. Wang (2003). "Retrieval of canopy biophysical variables from bidirectional reflectance: Using prior information to solve the ill-posed inverse problem." Remote Sensing of Environment **84**(1): 1-15.

Coops, N. C., K. L. Jacobsen, M. L. Smith, M. Martin and S. Ollinger (2004). "Estimation of plant and leaf area index using three techniques in a mature native eucalypt canopy." Austral Ecology **29**(3): 332.

CSC_NOAA. (1999, April 30, 2001). "Remote Sensing: An Overview." Retrieved April 10, 2006.

Danson, F. M., C. S. Rowland and F. Baret (2003). "Training a neural network with a canopy reflectance model to estimate crop leaf area index." International Journal of Remote Sensing **24**(23): 4891.

Deblonde, G., M. Penner and A. Royer (1994). "Measuring leaf area index with the LI-COR LAI-2000 in pine stands." Ecology **75**(5): 1507.

Demarez, V. and J. P. Gastellu-Etchegorry (2000). "A Modeling Approach for Studying Forest Chlorophyll Content." Remote Sensing of Environment **71**(2): 226-238.

Demuth, H. and M. Beale (2005). Neural Network Toolbox.User's Guide. Version 4.

Di Girolamo, L. (2003). "Generalizing the definition of the bi-directional reflectance distribution function." Remote Sensing of Environment **88**(4): 479.

Erikssona, H., L. Eklundha, P. Perssona and E. and Perssona (2005). "Variation of satellite estimated LAI due to the impact of the ground vegetation cover."

Esteve, P., J. Fontes and J. P. Gastellu-Etchegorry (1998). "Tropical dry ecosystems modelling and monitoring from space." Ecological Modelling **108**(1-3): 175-188.

Fang, H. and S. Liang (2003). "Retrieving leaf area index with a neural network method: Simulation and validation." IEEE Transactions on Geoscience and Remote Sensing **41**(9 PART I): 2052.

Fang, H. and S. Liang (2005). "A hybrid inversion method for mapping leaf area index from MODIS data: experiments and application to broadleaf and needleleaf canopies." Remote Sensing of Environment **94**(3): 405-424.

Fang, H., S. Liang and A. Kuusk (2003). "Retrieving leaf area index using a genetic algorithm with a canopy radiative transfer model." Remote Sensing of Environment **85**(3): 257-270.

Fassnacht, K. S., S. T. Gower, J. M. Norman and R. E. McMurtric (1994). "A comparison of optical and direct methods for estimating foliage surface area index in forests." Agricultural and Forest Meteorology **71**(1-2): 183-207.

Ganapol, B. D., L. F. Johnson, C. A. Hlavka, D. L. Peterson and B. Bond (1999). "LCM2: A coupled leaf/canopy radiative transfer model." Remote Sensing of Environment **70**(2): 153-166.

Gardingen, P. R., G. E. Jackson, S. Hernandez-Daumas, G. Russell and L. Sharp (1999). "Leaf area index estimates obtained for clumped canopies using hemispherical photography." Agricultural and Forest Meteorology **94**(3-4): 243-257.

Gascon, F., J.-P. Gastellu-Etchegorry, M.-J. Lefevre-Fonollosa and E. Dufrene (2004). "Retrieval of forest biophysical variables by inverting a 3-D radiative transfer model and using high and very high resolution imagery." International Journal of Remote Sensing **25**(24): 5601-5616.

Gastellu-Etchegorry, J. P. and V. Bruniquel-Pinel (2001). "A modeling approach to assess the robustness of spectrometric predictive equations for canopy chemistry." Remote Sensing of Environment **76**(1): 1-15.

Gastellu-Etchegorry, J. P., V. Demarez, V. Pinel and F. Zagolski (1996). "Modeling radiative transfer in heterogeneous 3-D vegetation canopies." Remote Sensing of Environment **58**(2): 131-156.

Gastellu-Etchegorry, J. P., F. Gascon and P. Esteve (2003). "An interpolation procedure for generalizing a look-up table inversion method." Remote Sensing of Environment **87**(1): 55-71.

Gastellu-Etchegorry, J. P., P. Guillevic, F. Zagolski, V. Demarez, V. Trichon, D. Deering and M. Leroy (1999). "Modeling BRF and radiation regime of boreal and tropical forests: I. BRF." Remote Sensing of Environment **68**(3): 281-316.

Gastellu-Etchegorry, J. P., E. Martin and F. Gascon (2004). "DART: a 3D model for sumulating satellite images and studying surface radiation budget." Internation Journal of Remote Sensing **25**: 73-96.

Gobron, N., B. Pinty, M. M. Verstraete, Y. Govaerts and N. Gobron (1997). "A semidiscrete model for the scattering of light by vegetation." Journal of Geophysical Research D: Atmospheres **102**(8): 9431-9446.

Goel, N. S. and D. E. Strebel (1983). "Inversion of vegetation canopy reflectance models for estimating agronomic variables. 1. Problem definition and initial results using the Suits model." Remote Sensing of Environment **13**(6): 487.

Gong, P., R. Pu, G. S. Biging and M. R. Larrieu (2003). "Estimation of forest leaf area index using vegetation indices derived from Hyperion hyperspectral data." IEEE Transactions on Geoscience and Remote Sensing **41**(6 PART I): 1355.

Gong, P., D. X. Wang and S. Liang (1999). "Inverting a canopy reflectance model using a neural network." International Journal of Remote Sensing **20**(1): 111-122.

Gower, S. T., C. J. Kucharik and J. M. Norman (1999). "Direct and indirect estimation of leaf area index, fAPAR, and net primary production of terrestrial ecosystems." Remote Sensing of Environment **70**(1): 29-51.

Gower, S. T. and J. M. Norman (1991). "Rapid estimation of leaf area index in conifer and broad-leaved plantations." Ecology **72**: 1896-1900.

Hale, S. E. and C. Edwards (2002). "Comparison of film and digital hemispherical photography across a wide range of canopy densities." Agricultural and Forest Meteorology **112**(1): 51.

Homolová, L. (2005). Leaf area index estimation for Norway spruce forest stand by means of radiative transfer modeling and imaging spectroscopy. Laboratory of Geo-Information Science and Remote Sensing. Wageningen, Wageningen University and Research Centre**:** 62.

Hu, B., K. Inannen and J. R. Miller (2000). "Retrieval of leaf area index and canopy closure from CASI data over the BOREAS flux tower sites." Remote Sensing of Environment **74**(2): 255-274.

Iaquinta, J., B. Pinty and J. L. Privette (1997). "Inversion of a physically based bidirectional reflectance model of vegetation." IEEE Transactions on Geoscience and Remote Sensing **35**(3): 687.

Jacquemoud, S. and F. Baret (1990). "PROSPECT: A model of leaf optical properties spectra." Remote Sensing of Environment **34**(2): 75-91.

Jacquemoud, S., F. Baret, B. Andrieu, F. M. Danson and K. Jaggard (1995). "Extraction of vegetation biophysical parameters by inversion of the PROSPECT + SAIL models on sugar beet canopy reflectance data. Application to TM and AVIRIS sensors." Remote Sensing of Environment **52**(3): 163-172.

Jin, Y. Q. and Y. Wang (2001). "A genetic algorithm to simultaneously retrieve land surface roughness and soil wetness." International Journal of Remote Sensing **22**(16): 3093.

Jonckheere, I. (2004). "Review of mehtods for in situ leaf area index determination Part I. Theories, sensors and hemispherical pgotography." Agricultural and Forest Meteorology **121**(1-2): 19-35.

Jonckheere, I., K. Nackaerts, B. Muys and P. Coppin (2005). "Assessment of automatic gap fraction estimation of forests from digital hemispherical photography." Agricultural and Forest Meteorology **132**(1-2): 96.

Kavzoglu, T. and P. M. Mather (1999). "Pruning artificial neural networks: An example using land cover classification of multi-sensor images." International Journal of Remote Sensing **20**(14): 2787.

Kavzoglu, T. and P. M. Mather (2002). "The role of feature selection in artificial neural network applications." International Journal of Remote Sensing **23**(15): 2919.

Kavzoglu, T. and P. M. Mather (2003). "The use of backpropagating artificial neural networks in land cover classification." International Journal of Remote Sensing **24**(23): 4907.

Kimes, D., J. Gastellu-Etchegorry and P. Esteve (2002). "Recovery of forest canopy characteristics through inversion of a complex 3D model." Remote Sensing of Environment **79**(2-3): 320-328.

Kimes, D. S. and J. A. Kirchner (1982). "Radiative transfer model for heterogeneous 3-D scenes." Applied Optics **21**(22): 4119-4129.

Kimes, D. S., R. F. Nelson, M. T. Manry and A. K. Fung (1998). "Review article: Attributes of neural networks for extracting continuous vegetation variables from optical and radar measurements." International Journal of Remote Sensing **19**(14): 2639 - 2663.

Kimes, D. S., K. J. Ranson and G. Sun (1997). "Inversion of a forest backscatter model using neural networks." International Journal of Remote Sensing **18**(10): 2181-2199.

King, D., P. Walsh and F. Ciuffreda (1994). "Airborne digital frame camera imaging for elevation determination." Photogrammetric Engineering & Remote Sensing **60**(11): 1321.

Koetz, B., F. Baret, H. Poilve and J. Hill (2005). "Use of coupled canopy structure dynamic and radiative transfer models to estimate biophysical canopy characteristics." Remote Sensing of Environment **95**(1): 115-124.

Kucharik, C. J., J. M. Norman and S. T. Gower (1998). "Measurements of leaf orientation, light distribution and sunlit leaf area in a boreal aspen forest." Agricultural and Forest Meteorology **91**(1-2): 127-148.

Kuusk, A. (1995). "A Fast, Invertible Canopy Reflectance Model." Remote Sensing of Environment **51**(3): 342-350.

Leblanc, S. G. (2002). "Correction to the plant canopy gap-size analysis theory used by the Tracing Radiation and Architecture of Canopies instrument." Applied Optics **41**(36): 7667-7670.

Leblanc, S. G., J. M. Chen, R. Fernandes, D. W. Deering and A. Conley (2005). "Methodology comparison for canopy structure parameters extraction from digital hemispherical photography in boreal forests." Agricultural and Forest Meteorology **129**(3-4): 187-207.

Leblanc, S. G., R. Fernandes and J. M. Chen (2002). Recent advancements in optical field leaf area index, foliage heterogeneity, and foliage angular distribution measurements. International Geoscience and Remote Sensing Symposium (IGARSS).

Levy, P. E. and P. G. Jarvis (1999). "Direct and indirect measurements of LAI in millet and fallow vegetation in HAPEX-Sahel." Agricultural and Forest Meteorology **97**(3): 199.

LI-COR (1992). LAI-200 Plant Canopy Analyzer; Operating Manual.

Li, S. G., C. T. Lai, G. Lee, S. Shimoda, T. Yokoyama, A. Higuchi and T. Oikawa (2005). "Evapotranspiration from a wet temperate grassland and its sensitivity to microenvironmental variables." Hydrological Processes **19**(2): 517.

Liang, S. (2004). Quantitative remote sensing of land surfaces. Hoboken, New Jersey, John Wiley & Sons, Inc.

Lin, Y. and K. Sarabandi (1999). " Retrieval of forest parameters using a fractal-based coherent scattering model and a genetic algorithm." IEEE Transactions on Geoscience and Remote Sensing **37**(3): 1415–1424.

Martin, E., J.-P. Gastellu-Etchegorry, R. Dhalluin and F. Gascon (2003). "Model Intercomparison for validating the 2003 DART Model." International Geoscience and Remote Sensing Symposium (IGARSS) **5**: 3272-3274.

Meroni, M., R. Colombo and C. Panigada (2004). "Inversion of a radiative transfer model with hyperspectral observations for LAI mapping in poplar plantations." Remote Sensing of Environment **92**(2): 195-206.

Mesarch, M. A., E. A. Walter-Shea, G. P. Asner, E. M. Middleton and S. S. Chan (1999). "A Revised Measurement Methodology for Conifer Needles Spectral Optical Properties: Evaluating the Influence of Gaps between Elements." Remote Sensing of Environment **68**(2): 177-192.

Myneni, R. B. (1991). "Modeling Radiative-Transfer and Photosynthesis in 3-Dimensional Vegetation Canopies." Agricultural and Forest Meteorology **55**(3-4): 323-344.

NCTA. (1996). "Norway Spruce." Retrieved August 10, 2005, from http://www.realchristmastrees.org/treetype/nrwy_spr.html.

Neumann, H. H., G. Den Hartog and R. H. Shaw (1989). "Leaf area measurements based on hemispheric photographs and leaf- litter collection in a deciduous forest during autumn leaf-fall." Agricultural & Forest Meteorology **45**(3-4): 325.

Nilson, T., A. Kuusk, M. Lang and T. Lukk (2003a). "Forest Reflectance Modeling: Theoretical Aspects and Applications." AMBIO: A Journal of the Human Environment **32**(8): 535-541.

Pierce, L. L., S. W. Running and G. A. Riggs (1990). "Remote Detection of Canopy Water-Stress in Coniferous Forests Using the Ns001 Thematic Mapper Simulator and the Thermal Infrared Multispectral Scanner." Photogrammetric Engineering and Remote Sensing **56**(5): 579-586.

Pinty, B., N. Gobron, J.-L. Widlowski, S. A. W. Gerstl, M. M. Verstraete, M. Antunes, C. Bacour, F. Gascon, J.-P. Gastellu-Etchegorry, N. Goel, S. Jacquemoud, P. North, W. Qin and R. Thomson (2000). "The Radiation transfer Model Intercomparision (RAMI) Exercise." Journal of Geophysical Research **106**(IWMMM - 2 Special issue): 11937-11956.

Qi, J., Y. H. Kerr, M. S. Moran, M. Weltz, A. R. Huete, S. Sorooshian and R. Bryant (2000). "Leaf Area Index Estimates Using Remotely Sensed Data and BRDF Models in a Semiarid Region." Remote Sensing of Environment **73**(1): 18.

RAMI. (2005, February 22, 2006). Retrieved April 20, 2006, from http://rami-benchmark.jrc.it/HTML/Home.php.

Rautiainen, M. and P. Stenberg (2005). "Application of photon recollision probability in coniferous canopy reflectance simulations." Remote Sensing of Environment **96**(1): 98.

Rautiainena, M., Stenberga.P., T. Nilsonb and A. and Kuuskb (2004). " The Effect of Crown Shape on the Reflectance of Coniferous Stands." Remote Sensing of Environment **89**: 41–52.

RFS. (2001). "The Norway Spruce - Christmas tree." Retrieved August 10, 2005, from http://www.rfs.org.uk/thirdlevel.asp?ThirdLevel=64&SecondLevel=34.

Smolander, S. (2001). "Scattering properties of coniferous shoots in radiative transfer modeling." Retrieved April 23, 2006, from http://www.cs.helsinki.fi/combi/seminars/suitia_abs/smolander.html.

Smolandera, S. and P. Stenbergb (2003). "A method to account for shoot scale clumping in coniferous canopy reflectance models." Remote Sensing of Environment **88**: 363–373.

Soudani, K., J. Trautmann and J. M. N. Walter (2002). "Leaf area index and canopy stratification in Scots pine (Pinus sylvestris L.) stands." International Journal of Remote Sensing **23**(18): 3605-3618.

SPECIM. (2004). 2004, from http://www.specim.fi/products-aisa-eagle.html.

Tian, Y. H., C. E. Woodcock, Y. J. Wang, J. L. Privette, N. V. Shabanova, L. M. Zhou, Y. Zhang, W. Buermann, J. R. Dong, B. Veikkanen, T. Hame, K. Andersson, M. Ozdogan, Y. Knyazikhin and R. B. Myneni (2002). "Multiscale analysis and validation of the MODIS LAI product - II. Sampling strategy." Remote Sensing of Environment **83**(3): 431-441.

Treitz, P. and P. Howarth (1999). "Hyperspectral remote sensing for estimating biophysical parameters of forest ecosystems." Progress in Physical Geography **23**(3): 359-390.

Ufer, G., C. M. (2004). Comparison of scaling-up methods to retrive chlorophyll content in Norway spruce crowns from hyperspectral images simulated by the DART model. Laboratory of Geo-Information Science and Remote Sensing. Wageningen, Wageningen University and Research Centre**:** 73.

Walthall, C., W. Dulaney, M. Anderson, J. Norman, H. Fang and S. Liang (2004). "A comparison of empirical and neural network approaches for estimating corn and soybean leaf area index from Landsat ETM+ imagery." Remote Sensing of Environment **92**(4): 465.

Weiss, M. and F. Baret (1999). "Evaluation of canopy biophysical variable retrieval performances from the accumulation of large swath satellite data." Remote Sensing of Environment **70**(3): 293-306.

Weiss, M., F. Baret, M. Leroy, O. Hautec?ur, C. Bacour, L. Prévot and N. Bruguier (2002). "Validation of neural net techniques to estimate canopy biophysical variables from remote sensing data." Agronomie **22**(6): 547.

Weiss, M., F. Baret, R. B. Myneni, A. Pragne?re and Y. Knyazikhin (2000). "Investigation of a model inversion technique to estimate canopy biophysical variables from spectral and directional reflectance data." Agronomie **20**(1): 3.

Weiss, M., F. Baret, G. J. Smith, I. Jonckheere and P. Coppin (2004). "Review of methods for in situ leaf area index (LAI) determination Part II. Estimation of LAI, errors and sampling." Agricultural and Forest Meteorology **121**(1-2): 37-53.

Weiss, M., D. Troufleau, F. Baret, H. Chauki, L. Prévot, A. Olioso, N. Bruguier and N. Brisson (2001). "Coupling canopy functioning and radiative transfer models for remote sensing data assimilation." Agricultural and Forest Meteorology **108**(2): 113.

Weiss, S. B. (2000). "Vertical and temporal distribution of insolation in gaps in an old-growth coniferous forest." Canadian Journal of Forest Research **30**(12): 1953.

Welles, J., M and J. Norman, M (1991). "Instrument for indirect measurement of canopy architecture." Agric. J **83**: 818–825.

Welles, J. M. and S. Cohen (1996). "Canopy structure measurement by gap fraction analysis using commercial instrumentation." Journal of Experimental Botany **47**(302): 1335.

Williams, D. L. (1991). "A Comparison of Spectral Reflectance Properties at the Needle, Branch, and Canopy Level for Selected Conifer Species." Remote Sensing of Environment **35**(2-3): 79-93.

Yuhas, R. H., A. F. H. Goetz and J. W. Boardman (1992). "Discrimination among semiarid landscape endmembers using the spectral angle mapper (SAM) algorithm. In Summaries of the Third Annual JPL Airborne Geoscience Workshop." **1**: 147-149.

7. Appendices

Appendix 1. Conceptual model for LAI calculation from TRAC records in TRACWin 3.7.1 software

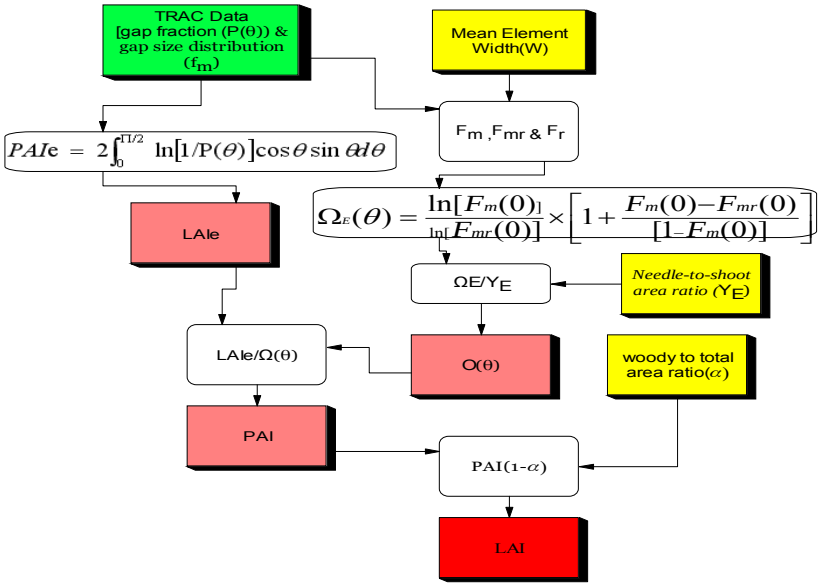

Appendix 2. Summary statistics of Vegetation indices as calculated from TRAC measurement

Transect	SZA	Ω_E	LAIe	LAI
A1	41.5	0.6094	2.89	6.01
A2	41.7	0.6583	3.89	7.53
A3	41.8	0.6321	2.50	5.06
A4	42.0	0.6474	2.70	5.24
A5	42.7	0.5697	3.01	6.56
A6	42.9	0.5891	3.18	6.79
A7	43.3	0.6686	2.84	5.32
B2	43.6	0.6754	1.55	2.99
B3	43.8	0.6909	1.93	3.525
B4	44.1	0.7048	2.29	4.14
B5	45.4	0.7082	2.58	4.65
B6	45.9	0.6571	3.40	6.59
B7	46.3	0.7417	3.20	5.485
B8	46.7	0.7786	3.84	6.14
B9	47.1	0.7253	3.96	6.91
C1	57.2	0.6624	3.59	9.17
C2	56.7	0.8174	3.44	7.27
C3	56.1	0.7584	2.72	6.4
C4	55.5	0.7288	3.2	7.97
C5	49.8	0.7630	2.32	4.88
C6	48.7	0.7378	1.97	4.36
C7	48.0	0.5834	2.89	6.85
C8	47.4	0.6841	3.32	7.96
C9	46.9	0.6829	2.6	7.87
Mean	46.9	0.6918	2.8	5.9
Std	4.92	0.06	0.63	1.54

Appendix 3. Summary statistics of vegetation indices of the mature Norway spruce forest stand as calculated from hemispherical photography

Subplot	LAIe	LAI	LAI combined	ALA(^{0})		Clumping factor		fcover
				Effective	TRUE	0^0	57.5^0	
1	3	6.9	6.4	76	80	0.58	0.37	0.538
2	2.7	6.3	5.7	76	80	0.6	0.37	0.515
3	1.7	3.7	3.6	58	56	0.49	0.38	0.566
4	2.8	4.9	5.9	80	80	0.52	0.35	0.406
5	3.3	5.6	7	80	80	0.55	0.39	0.467
6	2.8	5.2	5.9	80	80	0.51	0.39	0.406
7	3.2	5.5	6.8	80	80	0.56	0.39	0.466
8	3.2	5.8	6.8	80	80	0.49	0.39	0.442
11	3.5	6	7.4	80	80	0.54	0.39	0.468
12	3.7	6.2	7.8	80	80	0.55	0.42	0.513
13	3.5	6.2	7.4	80	80	0.5	0.39	0.479
14	4.4	7.3	9.3	80	80	0.55	0.39	0.568
15	3.2	7.1	6.8	74	78	0.58	0.35	0.578
16	3.8	7.6	8.1	78	80	0.55	0.38	0.512
17	4.2	6.9	8.9	80	80	0.55	0.4	0.522
18	2.8	4.8	5.9	80	80	0.52	0.39	0.484
19	3.4	5.6	7.2	80	80	0.54	0.42	0.525
20	4	7.9	8.5	78	80	0.6	0.35	0.55
21	4.2	7.2	8.9	80	80	0.52	0.37	0.515
22	5.3	8.3	11.2	80	80	0.58	0.42	0.615
23	5	7.8	10.6	80	80	0.56	0.45	0.612
24	4.6	7	9.7	80	80	0.6	0.48	0.587
25	4.1	6.6	8.7	80	80	0.6	0.4	0.545
Mean	3.6	6.4	7.6	78.26	78.87	0.55	0.39	0.52
Minimum	1.7	3.7	3.6	58	56	0.49	0.35	0.406
Maximum	5.3	8.3	11.2	80	80	0.6	0.48	0.615
Std	0.83	1.13	1.75	4.72	5.0	0.04	0.03	0.06

Appendix 4. Sunlit and shaded crown reflectance in band 27 (670.74nm) and band 48 (868.99nm)

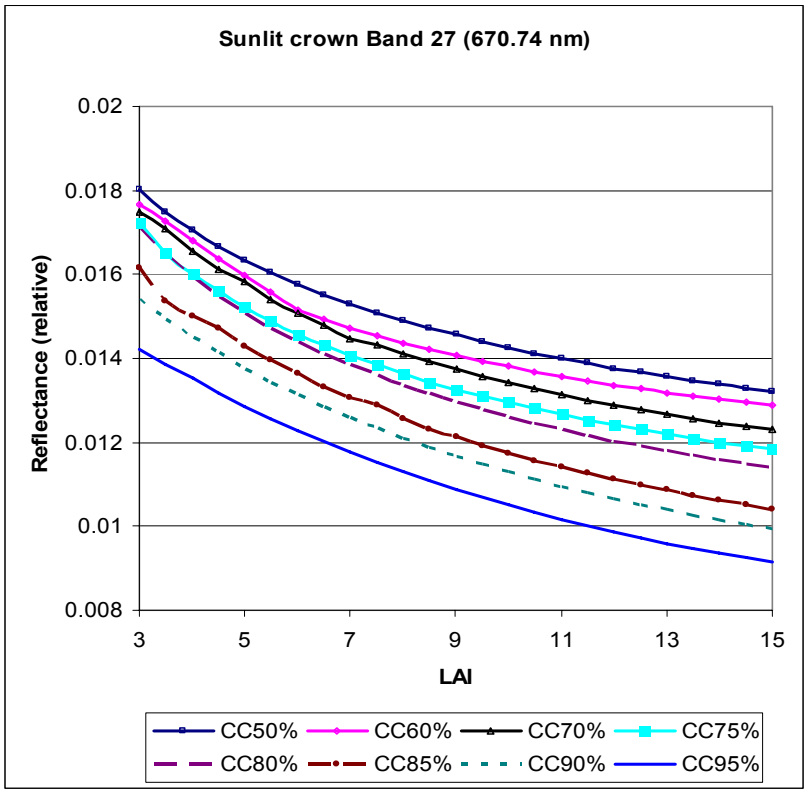

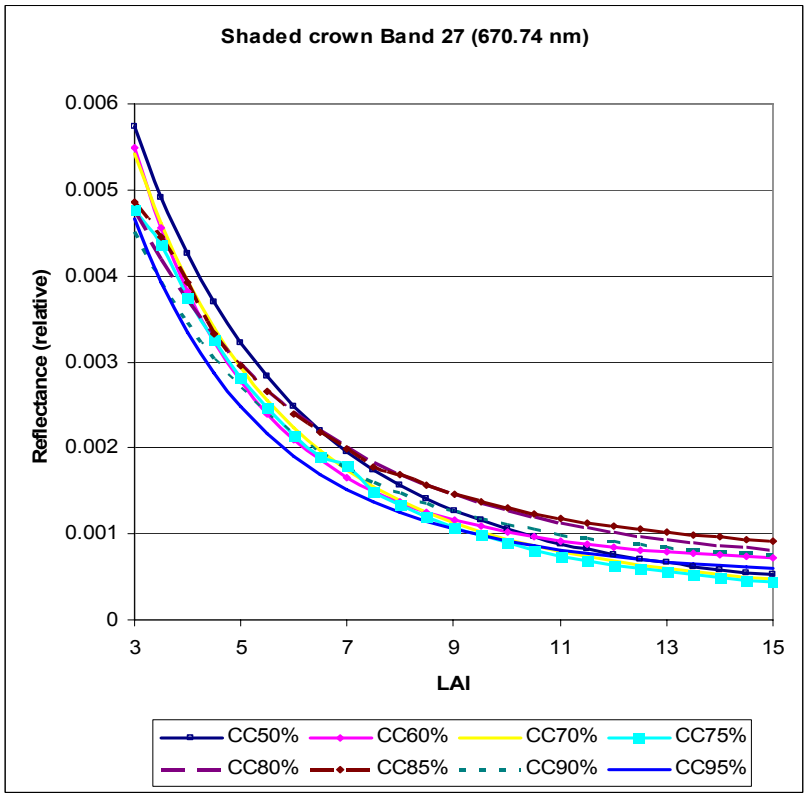

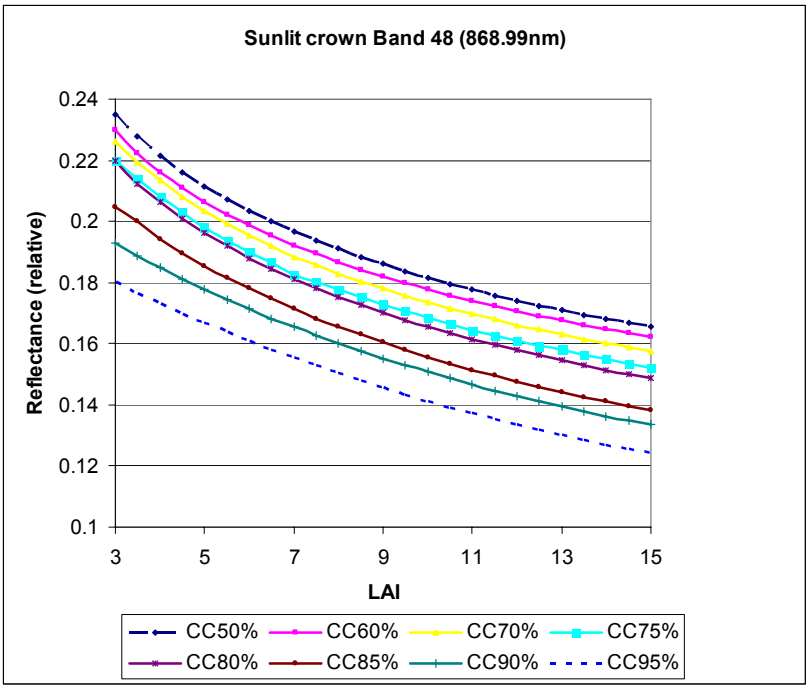
Sunlit crown Band 48 (868.99nm)
Reflectance (relative)
0.24
0.22
0.2
0.18
0.16
0.14
0.12
0.1
3
5
7
9
11
13
15
LAI
CC50%
CC60%
CC70%
CC75%
CC80%
CC85%
CC90%
CC95%

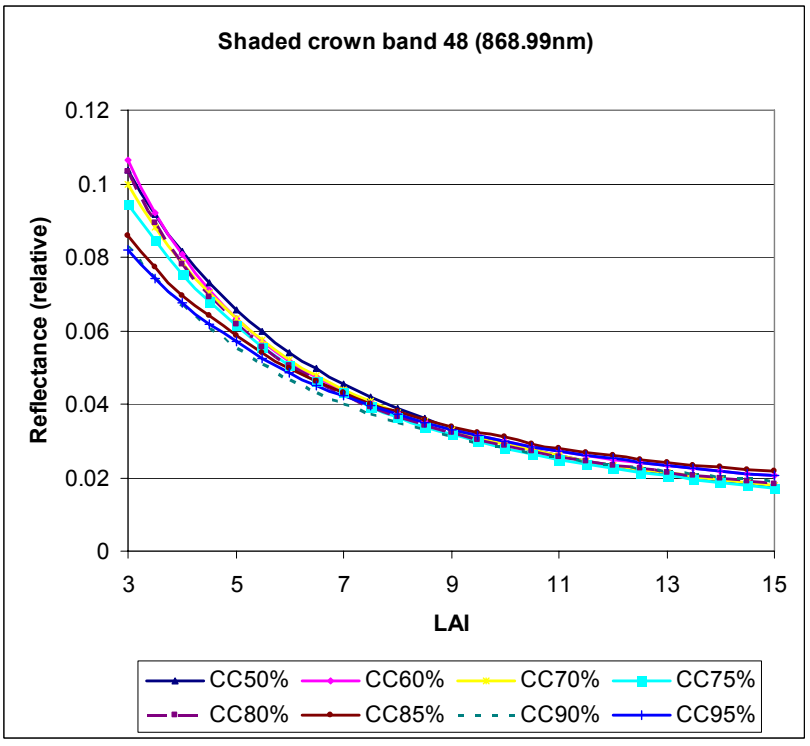
Shaded crown band 48 (868.99nm)
Reflectance (relative)
0.12
0.1
0.08
0.06
0.04
0.02
0
3
5
7
9
11
13
15
LAI
CC50%
CC60%
CC70%
CC75%
CC80%
CC85%
CC90%
CC95%